UNIVERSITY OF CALIFORNIA
Los Angeles

Learning and Neural Dynamics in Neocortical Microcircuits

A dissertation submitted in partial satisfaction of the
requirement for the degree Doctor of Philosophy in
Neuroscience

by

Benjamin Liu

2024

Abstract of the Dissertation

Learning and Neural Dynamics in Neocortical Microcircuits

by

Benjamin Liu
Doctor of Philosophy in Neuroscience
University of California, Los Angeles, 2024
Professor Dean Buonomano, Chair

Neural computations rely on the complex spatiotemporal dynamics that emerge from ensembles of interconnected neurons in neocortical microcircuits. It is widely accepted that experience—more precisely, previous patterns of neural activity—shapes neural circuits through activity-dependent modifications of synaptic strength. A key feature defining the behavior of any given neural circuit is the pattern of synaptic weights that connect the individual neurons that comprise the circuit. Yet it remains poorly understood how cortical microcircuits learn to perform different computations and how various interacting forms of plasticity contribute to this experience-dependent reorganization.

In the current dissertation, I examine some of the cellular, synaptic, and network mechanisms that underlie experience-dependent cortical reorganization. Combining, *in vitro* neural recordings, optogenetics, pharmacology, and computational modeling, the studies presented here describe various interacting forms of plasticity in isolated cortical microcircuits, as well as the associated changes that indicate learning. First, in Chapter

1, I review relevant background on neocortical organization, fundamental forms of neural plasticity, and examples of learning in cortical microcircuits, laying the groundwork for the original research presented in later chapters. Chapter 2 presents research examining the cellular and synaptic mechanisms underlying cortical ensemble formation by investigating how simple forms of chronic external input can reshape cortical microcircuits. Next, Chapter 3 investigates the ability of cortical circuits to learn different temporal intervals and generate timed predictions. Using organotypic slice cultures, this study demonstrates that timing is a computational primitive of neocortical microcircuits, specifically, that neural mechanisms are in place to allow isolated cortical circuits to autonomously learn the temporal structure of external stimuli and generate internal predictions. Finally, Chapter 4 presents a collaborative translational study led by Dr. Nazim Kourdougli and the Portera-Cailliau lab, utilizing a pharmacological rescue strategy for cortical network dysfunction in a mouse model of Fragile X Syndrome. Taken together, the results presented in this dissertation provide novel insights into the various mechanisms that cortical circuits engage to implement experience-dependent changes, perform temporal processing, and inform future studies linking neural dynamics with behavioral outcomes in normal and pathological conditions.

This dissertation of Benjamin Liu is approved.

Lindsay M. De Biase

Thomas J. O’dell

Carlos Portera-Cailliau

Dean V. Buonomano, Committee Chair

University of California, Los Angeles
2024

This dissertation is dedicated to my parents

Drs. Ling Jong and Jyanwei Liu

Table of Contents

Acknowledgments

I would like to thank my mentor Dr. Dean Buonomano for the time and effort he invested into my training, without his guidance this work would not have been possible. I greatly admire his character and brilliant ability to thoughtfully and creatively ask new scientific questions. My hope is that I will be able to carry forward all that I have learned during this time into my future career and life.

I would also like to thank my research family in the Buonomano Lab: Drs. Saray Soldado-Magraner, Michael Seay, Shanglin Zhou, Helen Motanis, as well as Jeffrey Yang, Kloey Reyes, Rachel Yu, and Jamie McDowell. Your camaraderie, hard work, patience in teaching me, and thoughtful discussions enabled this dissertation. I also thank our collaborators: Drs. Carlos Portera-Cailliau and Nazim Kourdougli for their guidance and for allowing me to contribute to the translational project that comprises Chapter 4 of this dissertation. Lastly, I thank the other members of my committee, Drs. Lindsay M. De Biase and Thomas J. O'dell, for their help and guidance in shaping my thesis research.

I thank the institutions at UCLA that supported my academic journey, including my graduate program (NSIDP), the Neurobiology Department, and the Brain Research Institute. Your interdisciplinary pursuit in advancing the field of neuroscience research inspired me throughout my graduate training. I also thank the UC Dissertation-Year Fellowship Program for supporting me during the last year of my graduate career.

Finally, I would like to acknowledge all the acquaintances and friends along the way, whose positive interactions shaped my journey into a memorable and happy time. I would not have been able to make it this far without you guys. Thank you.

Vita

Education

2016 B.A., Neuroscience, Boston University

2021 Ph.D. Candidate, Neuroscience, University of California Los Angeles

Research Experience

2019-2024 Buonomano Lab at UCLA
Advisor: Dr. Dean Buonomano

2019 Rotation in Mody Lab at UCLA
Advisor: Dr. Istvan Mody

2018 Rotation in Golshani Lab
Advisor: Dr. Peyman Golshani

2016-2018 Gladstone Institutes for Neurological Disease
Advisor: Dr. Jorge Palop

2014-2016 Lin Lab at Boston University
Advisor: Dr. Jen-Wei Lin

Publications

(Preprint) **Liu, B.,** Buonomano, D. V. (2024). Ex Vivo Cortical Circuits Learn to Predict and Spontaneously Replay Temporal Patterns.

Liu, B., Seay, M. J., & Buonomano, D. V. (2023). Creation of Neuronal Ensembles and Cell-Specific Homeostatic Plasticity through Chronic Sparse Optogenetic Stimulation. The Journal of Neuroscience.

Kourdougli, N., Suresh, A., **Liu, B.,** Juarez, P., Lin, A., Chung, D. T., Graven Sams, A., Gandal, M. J., Martínez-Cerdeño, V., Buonomano, D. V., Hall, B. J., Mombereau, C., &

Portera-Cailliau, C. (2023). Improvement of sensory deficits in fragile X mice by increasing cortical interneuron activity after the critical period. Neuron.

Molnár, L., Ferando, I., **Liu, B.,** Mokhtar, P., Domokos, J., & Mody, I. (2023). Capturing the power of seizures: an empirical mode decomposition analysis of epileptic activity in the mouse hippocampus. Frontiers in Molecular Neuroscience.

Hanson, J. E., Ma, K., Elstrott, J., Weber, M., Saillet, S., Khan, A. S., Simms, J., **Liu, B.,** Kim, T. A., Yu, G. Q., Chen, Y., Wang, T. M., Jiang, Z., Liederer, B. M., Deshmukh, G., Solanoy, H., Chan, C., Sellers, B. D., Volgraf, M., Schwarz, J. B., … Palop, J. J. (2020). GluN2A NMDA Receptor Enhancement Improves Brain Oscillations, Synchrony, and Cognitive Functions in Dravet Syndrome and Alzheimer's Disease Models. Cell reports.

Awards

University of California Dissertation Year Fellowship Program (2023 – 2024)

Eva Kavan Prize for Excellence in Research on the Brain – UCLA BRI (2023)

UCLA Brain Research Institute Research Travel Award (2021, 2022, 2023)

Notable Courses

35th Methods in Computational Neuroscience – Marine Biological Laboratory (2023)

Chapter 1: Introduction

It is intuitive to think of the brain as a versatile and flexible structure. Much of the development of our brain occurs postnatally and is heavily influenced by experience and learning [1-3]. In most cases, learning and developmental processes occur seamlessly, without altering the functional stability of brain circuits, indicating that neurons and their networks are versatile, flexible, but also resilient to unstable change. The mammalian neocortex is one of the most extensively studied brain areas to elucidate the neural mechanisms for plasticity and experience-dependent refinement. Experience-dependent changes in neocortical function and sensory representation have been demonstrated in a wide variety of brain areas at many different developmental ages[4, 5]. In humans, many complex faculties, such as language comprehension, arithmetical ability, and moral reasoning appear to be functionally localized to the neocortex. Indeed, it could be argued that a defining feature of the neocortex is plasticity—the ability to encode new information and to dynamically respond to experience to promote functional adaptation to an environment [6].

Understanding the mechanisms underlying cortical reorganization can, however, be difficult given the complex connectivity and dynamics of cortical networks. Each cortical area is composed of complex networks of various cell types, each with unique connectivity patterns[7]. Interestingly, the circuits of different cortical regions and species share striking commonalities in their constituent cell types, their intrinsic properties, and the incidence and properties of synaptic connections between them [8, 9]. These similarities suggest that there may be a set of general principles linking the common

characteristics of cortical circuitry to the nature of cortical processing in multiple areas. In recent years, there has been a great acceleration in progress towards uncovering these principles enabled by several newly developed experimental techniques. Advances in mouse genetics have provided tools to classify, identify and manipulate different classes of cortical neurons [8, 10, 11]. In addition, optical techniques now allow us to chronically stimulate and record from specific subpopulations of neurons within local cortical microcircuits [12]. An understanding of these principles enables us to consider how the neural dynamics in cortical circuits may translate to the diverse repertoire of computations that our brains perform.

In this chapter, I review relevant background on neocortical organization, fundamental forms of neural plasticity, and examples of learning in cortical microcircuits, laying the groundwork for the original research presented in later chapters. I provide insight into some of the plasticity mechanisms that neocortical microcircuits engage during learning as well as the long-lasting alterations that follow. In addition, I also discuss timing as an example neural computation and provide insight into how neural circuits can encode the temporal information necessary for timed behavior. Finally, I discuss *in vitro* examples of learning-associated cortical reorganization and build upon the idea that neural computations, temporal and otherwise, are computational primitives of neocortical microcircuits.

1.1 Neocortical Microcircuits

A major milestone in the evolution of the mammalian brain is the expansion of the

neocortex. This expansion is believed to be responsible for the emergence of higher cognitive abilities [13]. The neocortex plays an important role in many higher brain functions including cognition, sensory perception, goal-directed behavior, and associative-learning. The neocortex is organized in such a way that it is both highly specialized, with defined areas dedicated to specific functions or sensory modalities, and highly integrative, with each area receiving converging inputs from different thalamic nuclei, other cortical areas, and several neuromodulatory systems[14]. Converging inputs in different brain areas are integrated in local neocortical microcircuits generally considered to be composed of six layers and containing a richly interconnected array of diverse cell types, whose patterns of connectivity underlie the cortex's ability to perform various computations[15].

Cortical neurons can be divided into two major classes. Principal excitatory neurons that use the excitatory neurotransmitter glutamate. Usually pyramidal in shape, these cells respond selectively to specific features of sensory stimuli and contact local and distant targets through extensive axonal projections[16]. Principal cells comprise approximately 80% of cortical neurons in rodents and fall into multiple classes distributed across and within cortical layers. The remaining approximately 20% are interneurons that release the inhibitory neurotransmitter GABA and make mostly local connections[17]. Importantly, both principal cells and interneurons are integral in various forms of synaptic plasticity and comprise multiple subclasses with varying cellular properties.

Early investigations of neocortical function in cats revealed similar receptive field properties of visual area neurons aligned perpendicular to the brain surface in radial cortical columns[18-21]. Central to the idea of the canonical microcircuit is the notion that

a cortical column contains the necessary circuitry to perform requisite computations, and that these circuits can be replicated with minor variations throughout the cortex. In the core model, thalamic input drives activity in a feed-forward and sequential fashion from L4, to L2/3, to L5/L6 and out to other cortical and subcortical regions[22-25]. L4 neurons are thought to primarily target their local neighbors[22]. The principal neurons of L2/3 are intratelencephalic (IT) cells, meaning that their long-range axons project only to targets within the telencephalon, such as other cortical areas and striatum[26]. L5, sometimes called the primary cortical output layer, harbors IT cells as well as extratelencephalic (ET) cells, which send widely divergent projections to subcortical structures such as thalamus, striatum, and brainstem. L6 contains corticothalamic (CT) cells which provide a major feedback projection to thalamus, as well as IT cells that project back to L5[27]. There are putative discrepancies in the basic cortical circuitry between different mammalian species, however, despite their heterogeneity, existing data still indicate that cortical circuits across brain areas and species share some common functional principles that are key to understanding their function.

1.1.1 The organization of cortical connectivity

Which contributes more to the area of a rectangle, its length or its width? This was 20th century neuroscientist Donald Hebb's response when asked to weigh the importance of nature versus nurture in the development of the nervous system. Hebb's response conveys the point that these two forces are inseparable. Contemporary developmental neurobiologists and psychologists would agree that the division of nature and nurture is

overly simplistic and that there is a complex interplay of these two forces in the maturation of neural systems.

Despite agreement that the problem is complicated, there has been persistent interest in pinning down the forces that specify the anatomy and function of the cerebral cortex at different stages of development—studies that have alternatively shifted focus from deterministic to environmental factors. Almost 30 years ago, tissue transplantation studies showed that certain patterns of gene expression that were specific to somatosensory cortex could be preserved even when this embryonic tissue was moved to the visual cortex, indicating that specification was established in embryonic development[28]. Two decades ago, a provocative study suggested that larger-scale features of cortical organization such as ocular dominance columns could be established in the absence of sensory input[29]. More recently, the availability of genome sequencing has enabled a search for identifying genes whose expression defines cortical areas[30]. Defining patterns of gene expression that are linked to neural identity and function early in development are consistent with a deterministic process in circuit construction.

At the same time, it is incontrovertible that the environment—more precisely, neural activity—shapes neural circuits under normal conditions as well as under experimental conditions which can induce remarkable rewiring. Landmark studies in ferrets indicated that brain area identity could be modulated by inputs—where visual inputs could transform auditory cortex into a visually responsive area[31]. Sensory deprivation can induce remapping in neocortex, investigated perhaps most extensively as changes in ocular dominance in V1[32]. At the cellular level, neurotransmitter release can act as a trophic factor for guiding axons and establishing circuits, and neuron depolarization may

be critical for initiating patterns of gene expression that are required for circuit formation and stabilization[33-36]. Despite the diversity of approaches, all these studies suggest that cortical circuits are wired by a combination of molecular cues during early development and activity-dependent mechanisms that use patterned activation to adjust the strength and number of synaptic connections[37]. The focus of the next section will be on discussing fundamental forms of activity-dependent plasticity that contribute to cortical circuit refinement.

1.2 Fundamental Forms of Activity-Dependent Plasticity

Cortical circuits are dynamic networks that can be remodeled by behaviorally important experiences throughout life. It is now widely accepted that new information in cortical circuits is stored in the changes in the patterns of synaptic weights between neurons. This idea was put forward over 100 years ago by Santiago Ramon y Cajal and was further advanced in the late 1940s by Donald Hebb, who proposed that associative memories are formed in the brain by a process of synaptic modification that strengthens connections when presynaptic activity correlates with postsynaptic firing[38].

1.2.1 Hebbian plasticity

Although Hebb's rule was proposed in 1949, experimental support for the existence of such long-lasting, activity-dependent changes in synaptic strength was lacking until the early 1970s when experimenters reported that repetitive activation of

perforant pathway excitatory synapses onto granule cells in the dentate gyrus caused a potentiation of synaptic strength that could last for hours or even days[39, 40]. Over the last four decades, this phenomenon, eventually termed Long-term Potentiation (LTP), has been reliably reproduced in various experimental preparations [41-44]. This form of associative plasticity is an instantiation of Hebb's postulate—essentially, that correlated pre- and postsynaptic activity results in a strengthening of the synaptic connection. For neurons to implement Hebb's rule, they must possess a coincidence detector that records the co-concurrence of pre- and postsynaptic activity. A particular subtype of the glutamate receptor, the N-methyl-D-aspartate (NMDA) receptor (NMDARs), fulfills this role.

A major advance in the understanding of excitatory synaptic function and LTP was the demonstration that two major types of ionotropic glutamate receptors contribute to the postsynaptic response at glutamatergic synapses, *α*-amino-3-hydroxy-5-methyl-4-isoxazolepropionic acid (AMPA) receptors (AMPARs) and NMDARs. These two receptors are often found colocalized on individual dendritic spines. The AMPAR has a channel that is permeable to monovalent cations (Na^+ and K^+), and activation of AMPARs provides most of the inward current that generates the excitatory synaptic response near resting membrane potential[45]. In contrast to AMPARs, NMDARs exhibit a strong voltage dependence due to the block of its channel at negative membrane potentials by extracellular magnesium[46, 47]. As a result, NMDARs contribute little to the postsynaptic response during basal synaptic activity. However, when the cell is depolarized, magnesium dissociates from its binding site within the NMDAR channel, allowing both calcium as well as sodium to enter the postsynaptic dendritic spine. It is now firmly established that the induction of LTP in CA1 requires activation of NMDARs during strong

postsynaptic depolarization leading to an increase in postsynaptic calcium concentration, which activates the biochemical processes necessary for LTP[48, 49].

In NMDAR-dependent LTP, calcium from postsynaptic NMDA receptors activates kinases including αCaMKII, which drive AMPAR phosphorylation, leading to increased excitatory conductance, and insertion of additional GluA1-containing AMPARs within the postsynaptic density [50-54]. The basic principles of LTP can also be explained by the properties of NMDARs. Cooperativity and associativity occur because of the requirement for multiple synapses to be activated simultaneously to generate adequate postsynaptic depolarization to remove the magnesium block of the NMDARs. In addition, input specificity is attributed to the compartmentalized increase in calcium, which is limited to the postsynaptic dendritic spine and does not influence adjacent spines[55].

Although still considered prototypic, it is now clear that hippocampal LTP is only one of several different forms of long-term synaptic plasticity that exist in specific circuits in the mammalian brain. Importantly, it is well established that most synapses that exhibit LTP also express one or more forms of Long-term Depression (LTD)[56]. Thus, a key concept is that synaptic strength at synapses is bidirectionally modifiable by different patterns of activity[57-59]. Although the bulk of our knowledge on the molecular mechanisms of LTP and LTD have been derived from studies of excitatory synapses on CA1 pyramidal neurons in hippocampal slices, similar or identical forms of LTP and LTD have also been observed at synapses throughout the brain[60, 61]. Thus, the conclusions drawn from the study of LTP and LTD in CA1 are often applied to other brain areas.

Neocortical LTP has also been reliably demonstrated both in cortical slices and *in*

vivo [4, 62-66]. Where characterized, cortical LTP/LTD is most often classical NMDAR-dependent LTP/LTD[63, 67, 68]. A second form of neocortical LTP is expressed presynaptically by an increase in release probability, which alters short-term synaptic dynamics[64, 69-71].

Sensory receptive fields in the cortex are robustly modified by early postnatal experience. A strong connection between synaptic plasticity and experience-dependent plasticity has been established in the visual system during the shift in ocular dominance caused by monocular deprivation (MD)[72-74]. MD induces dephosphorylation of AMPAR subunit GluA1 in visual cortex, which serves as a molecular marker of NMDAR-dependent LTD[75]. In addition, visual cortical slices obtained from monocularly deprived animals show greatly reduced LTD, suggesting that LTD was elicited *in vivo*[75, 76]. Similar findings have been obtained in somatosensory barrel cortex. Sensory deprivation by whisker trimming or plucking causes a weakening of synaptic responses in L2/3 cells and an occlusion of LTD[77]. NMDA-LTP in neocortex can be blocked by viral expression of a GluA1 C-terminal tail construct (GluA1-ct) which prevents activity-dependent GluA1 (AMPA) insertion [78-80]. In mouse V1, daily visual stimulation with high contrast grating stimuli gradually increases visual responses to trained stimuli. This increased responsiveness is prevented by systemic injection of NMDAR antagonist and by viral expression of GluA1-ct, suggesting that responses are strengthened by LTP at cortical synapses[81].

1.2.2 Homeostatic plasticity

Without additional stabilizing mechanisms, associative forms of plasticity such as LTP and LTD could drive neural circuit activity towards epileptogenic excitation or complete quiescence. Synaptic scaling is considered a form of homeostatic plasticity that counters the potentially maladaptive effects of synapse-specific plasticity by globally adjusting the strength of all synapses on a given neuron to maintain mean cellular activity at a set point level[82]. Synaptic scaling was first discovered in dissociated cortical cultures, where chronic (>24 hours) pharmacological blockade of synaptic transmission with tetrodotoxin (TTX) caused an increase in the strength of all excitatory synapses onto excitatory neurons[83]. In addition, when activity was increased by partially blocking inhibitory transmission, excitatory synaptic strength was decreased [83]. Importantly, synaptic scaling appears to maintain the relative strengths of individual synapses. This allows neurons to stabilize activity while avoiding disruption of information storage or processing mechanisms that rely on the individual differences between synaptic weights. Synaptic scaling has now been shown in a variety of neuron types both *in vitro* and *in vivo*, including neocortical and hippocampal pyramidal neurons[83-89].

In neocortex, scaling of excitatory synapses onto principal neurons is expressed primarily by regulating AMPAR/NMDAR insertion, similar to NMDAR- dependent LTP and LTD[82, 90, 91]and in some cases, changes in presynaptic release[92, 93]. Perturbations in network activity can be detected by individual neurons as changes in their own firing, local changes in receptor activation, or changes in release of secreted factors. Although some forms of homeostatic plasticity appear to be triggered by local signaling or signaling through secreted factors, there is strong evidence that synaptic scaling is a cell-

autonomous process induced by changes in a neuron's own firing[94, 95]. Selectively blocking firing by micro-perfusion of TTX to the soma of individual neurons scales up synaptic strengths to the same degree as blockade of network activity, whereas local block of synaptic transmission does not induce a local enhancement of receptor accumulation[94]. Like scaling up, scaling down in response to elevated post-synaptic activity can also be induced by cell-autonomous changes in calcium influx and involves CaMKIV signaling and transcription[95].

In recent years, evidence has been presented supporting a role for secreted factors in the induction of homeostatic plasticity. Specifically, secretion of the proinflammatory cytokine tumor necrosis factor-α from glial cells appears to be important for the increase in synaptic AMPARs caused by extended periods of activity blockade[86, 96-98]. In addition, there is evidence suggesting a role for secreted BDNF in driving the decrease in synaptic strengths caused by extended periods of increased network activity[99, 100].

In addition to synaptic plasticity, activity-dependent changes in intrinsic properties including voltage gated conductance, length of the axon initial segment, and the distribution of spines on dendrites all contribute to shaping a neuron's input/output function[101-103]. Indeed, extensive experimental evidence demonstrates that plasticity of intrinsic excitability is an important homeostatic locus of control and is involved in various experience- and learning-dependent processes [104-109]. For example, it has been demonstrated that infralimbic prefrontal cortex intrinsic excitability plays a crucial role in memory extinction after fear conditioning training[110, 111]. Additionally, recent work has shown that there is significant plasticity at the axon initial segment (AIS), which

plays a crucial role in neuronal intrinsic excitability[112, 113]. Overall, studies of homeostatic plasticity are consistent in the hypothesis that parallel forms of plasticity cooperate in a synergistic and redundant manner to implement experience-dependent adjustments.

1.3 Neuronal Ensembles

Neuronal ensembles are defined as functional subgroups of coactive and interconnected neurons that underlie numerous neural computations from encoding memories to guiding behavior [114-117]. Ensembles represent an intermediate functional level between individual neurons and brain areas. The idea that neurons cooperate to form emergent functional units has a long history. Indeed, Cajal's drawings in 1899 already represented cortical circuits as repeated modules, with neurons linked by arrows that illustrated the flow of activity within. Sherrington proposed that groups or "ensembles" of neurons form scratch-reflex arcs in dogs, i.e., synaptic circuits linking sensory stimuli with motor responses[118]. The idea that cortical activity can be organized in functional subgroups of neurons was further developed by Hebb, who proposed that recurrently connected groups of neurons could form "assemblies" through the strengthening of connections following Hebbian learning rules[38].

The hippocampus is one of the first regions where experimental evidence for the existence of ensembles was observed. *In vivo* recordings revealed coordinated and repetitive firing within subgroups of pyramidal neurons, with neurons firing sequentially within the period of a theta cycle[119]. Recurring sequences of neuronal activity within

hippocampal ensembles can span from a few milliseconds to several seconds[120-123]. Furthermore, these hippocampal sequences were found to be reactivated offline during sharp-wave ripple (SWR) oscillations recorded during quiet rest or sleep, in a phenomenon now known as replay [124, 125]. The concept of replay supports the idea that neuronal ensembles may encode behaviorally relevant experiences or memories in the temporal relationship of coordinated neuronal activity[126]. Importantly, hippocampal ensembles can be causally linked to behavior. Activating or inhibiting neuronal ensembles associated with SWRs or theta sequences can impair spatial memory acquisition or recall[127-129]. Consistent with this, the same ensembles observed during behavior can be artificially activated through optogenetic activation of a subset of the participating neurons[130].

Findings from sensory areas in the neocortex parallel many of the findings from hippocampal ensembles. Coactive, or sequentially active, groups of neurons have been described in the neocortex both *in vitro* and *in vivo* using calcium imaging and electrophysiological recordings[114, 131-139]. Consistent with hippocampal replay, cortical ensembles evoked by sensory stimuli can also become spontaneously coactive in the absence of stimuli[135, 136, 140]. In addition, optogenetics have been used to manipulate behaviorally relevant ensembles in Go/No-Go visual discrimination tasks. In these experiments, inactivating visually evoked ensembles blocked visually guided behavior, whereas activation substituted for the presence of the visual stimulus in the behavioral task[141, 142].

We now know that the formation of functional neuronal ensembles can occur in an experience-dependent fashion. Since cortical ensembles can be generated by

simultaneous stimulation of groups of neurons[134, 143], it is assumed that Hebbian plasticity is involved in establishing cortical ensembles. Synaptic decoupling has been shown to occur when groups of neurons have chronically decorrelated activity[143]. In addition, changes in intrinsic excitability may also influence the formation of neuronal ensembles. For example, increases in intrinsic excitability can result in elevated neuronal firing, which increases total synaptic output, thus resulting in an effect analogous to synaptic strengthening. Several experiments have revealed cell-autonomous changes in the excitability of cortical neurons after behavioral training or exposure to novel sensory experiences[144, 145]. In summary, as experience-shaped, functional, units of neural circuits, neuronal ensembles could provide a mechanistic underpinning for fundamental neural computations such as timing.

1.4 Timing is a Computational Primitive of Neocortical Circuits

The ability to predict and prepare for external events is among the most important computations the brain performs. Timing is a critical component of prediction because it is often necessary to predict when future events will occur. An important question is whether this ability relies on innate, hardwired neural circuits, or emerges in an experience-dependent manner as a result of learning and plasticity. Given their critical role in perception, behavior, and cognition, it has been proposed that prediction and timing are computational primitives of neocortical microcircuits [146-149]. Specifically, that neural mechanisms are in place to allow local neocortical microcircuits to autonomously learn the temporal structure of external stimuli and generate internal

predictions of when subsequent stimuli will arrive.

Many forms of timing appear to rely on experience, for example, rodents can be trained to make timed behaviors in response to cues and discriminate between intervals of different durations[150, 151]. Experiments in primary visual cortex have demonstrated the learning-dependent emergence of timed neuronal responses that predict the timing of reward, as well as ramping neural activity that reflects the stimulus-reward pairing interval [152, 153]. In a subsequent study, the authors examined the contribution of neuromodulators to this form of reward-based associative learning task and demonstrated that changes in the temporal dynamics can also be observed in acute visual cortex slices[154]. Unsurprisingly, humans are also capable of robust interval specific temporal perceptual learning, repeated auditory interval discrimination training of a 100 ms interval leads to improved discrimination around this interval, but not to shorter or longer intervals[155-157].

For organisms to learn specific intervals and display timed behavior, changes must first occur in the synaptic and cellular properties of their neural circuits. State-dependent network (SDN) models propose that timing arises from the inherent time-varying properties of neurons and the emergent neural dynamics of recurrent circuits[146, 158-160]. More specifically, within this framework, time is naturally encoded in populations of neurons whose patterns of activity are dynamically changing in time. This model is an example of an intrinsic model of timing, in that it does not rely on specialized timing mechanisms, meaning that in theory any cortical network could have the capability to process temporal information.

Perhaps the most rigorous prediction of models that propose timing as an intrinsic computation is that timing can be observed *in vitro*. If cortical networks are indeed intrinsically capable of timing, it may be possible to not only observe examples of timing *in vitro*, but also to 'teach' *in vitro* circuits simple timing tasks. In the next section, I will discuss studies that have attempted to answer this question experimentally.

1.4.1 Examples of in vitro learning

In vitro whole-cell recordings in both acute and organotypic slices have demonstrated that external stimulation can elicit long-lasting polysynaptic responses. Polysynaptic activity reflects the internal dynamics of local cortical microcircuits. Figure 1 illustrates an example of evoked polysynaptic activity in simultaneously recorded neurons in an organotypic cortical slice. This illustrates that the intracellular activity recorded in single neurons serve as a measure of overall network activity—in that the subthreshold PSPs reflect a read-out of the subpopulation of neurons connected to the recorded cell. In this example, the two recorded neurons fire reliably at distinct timepoints across trials, this can be thought of as a direct readout of time. Specifically, if a neuron reliably fires during some time window after the stimulus, this neuron contains information about how much time has elapsed since the stimulus.

One demonstration of *in vitro* temporal learning came from organotypic slice cultures, researchers implanted a pair of electrodes in the cortex that were used to provide structured 'sensory' input into the cortical network. In the initial experiments, both electrodes were synchronously stimulated for 2 hours, whereas in the second group, both

electrodes were stimulated with a 100 ms interval difference. Thus, the pathways in both groups received the same amount of total stimulation but differed in the temporal pattern they were exposed to. After training, whole-cell recordings were made from L2/3 pyramidal neurons and demonstrated that, in the asynchronous group, there was clustering of evoked polysynaptic responses around the 100 ms interval. This was further tested by training slices with either a 100 or 500 ms interval, which revealed a significant difference in the timing of the evoked polysynaptic responses. Specifically, the temporal profile of the evoked polysynaptic activity reflected the interval used during training. One possible interpretation of this data is that the neurons learned to ‘anticipate’ or ‘predict’ the delivery of a stimulus around the trained interval[161].

In a subsequent study, the researchers further explored the ability of *in vitro* networks to ‘learn’ different experienced intervals by combining electrical and optogenetic stimulation. In these experiments, an electrical pulse was followed by optical stimulation of a subset of ChR2 neurons. In one group, the triggering of electrical and optical stimulation pathways was separated by 100 ms and 500 ms in the other group. After 4 hours of training, whole-cell recordings from the ChR2-positive neurons revealed that there was a significant difference in the timing of the distribution of polysynaptic events, specifically, there was a larger proportion of late events in the 500 ms group compared with the 100 ms group[162]. This demonstrates that the polysynaptic activity could encode multiple trained intervals and was specific to the trained interval, suggesting that the timing was learning-dependent. Moreover, the researchers demonstrated that timed cortical activity was generated by dynamic shifts in the balance of excitation and inhibition, supporting theoretical predictions about timing[163]. In line with theoretical

models of timing, these studies demonstrated that isolated cortical microcircuits can be trained to produce activity that represents a trained stimulus interval[161-163]. Together, these findings support that cortical circuit dynamics can be shaped by experience-dependent plasticity and that there are likely mechanisms in place that allow cortical circuits to 'learn' the temporal structure of the stimuli they are exposed to.

1.5 Summary and Overview of Following Chapters

In this chapter I have outlined a selection of key concepts that will serve as the foundation for the experiments described in the subsequent chapters. Of particular relevance are the observations of timed responses in *in vitro* cortical circuits, together with evidence that these circuits can adapt to the temporal structure of experienced stimuli. As these studies offer some of the best evidence that timing is a computational primitive. Thus, although the mechanisms underlying the diverse forms of temporal processing the brain performs remain to be elucidated, there is sufficient evidence to conclude that some forms of subsecond timing are a product of intrinsic mechanisms—that is, they are a general and inherent computation of neural circuits. Indeed, the notion that it is possible to study the neural mechanisms underlying simple forms of learning and computational primitives in neocortical circuits *in vitro* is a central tenet of this dissertation.

The original research I present in the following chapters examines some of the cellular, synaptic, and network mechanisms that underlie experience-dependent reorganization and temporal pattern learning in neocortical circuits. Chapter 2 presents research examining the cellular and synaptic mechanisms underlying cortical ensemble

formation by investigating how simple forms of chronic external input can reshape cortical microcircuits. Next, Chapter 3 investigates the ability of isolated cortical circuits to learn different temporal intervals and generate timed predictions. Finally, Chapter 4 presents a collaborative translational study led by Dr. Nazim Kourdougli and the Portera-Cailliau lab, utilizing a pharmacological rescue strategy for cortical network dysfunction in a mouse model of Fragile X Syndrome. Overall, this dissertation presents novel findings on the various mechanisms that neocortical circuits engage to implement experience-dependent changes, perform temporal processing, and inform future studies linking neural dynamics with behavioral outcomes in normal and pathological conditions.

1.6 Figures

Figure 1

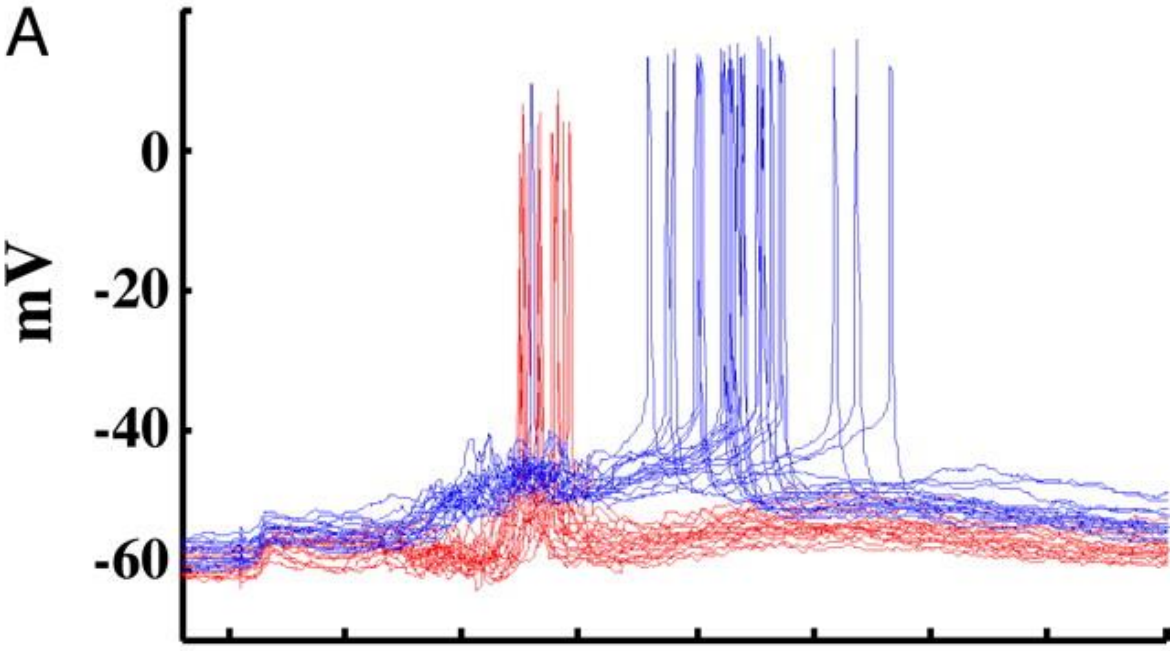

Paired recordings reveal different temporal profiles of polysynaptic activity. A. Twenty overlaid traces from two simultaneously recorded neurons (50 µm apart). Stimulation elicited complex excitatory/inhibitory profiles in both cells, however, the spike latency was different (129 vs. 205 ms). Both neurons received a short-latency monosynaptic input of approximately the same size. However, the red neuron consistently fired 65 ms before the blue neuron.

1.7 References Cited

1. André, M., et al., *Electroencephalography in premature and full-term infants. Developmental features and glossary.* Neurophysiol Clin, 2010. **40**(2): p. 59-124.

2. Ackman, J.B. and M.C. Crair, *Role of emergent neural activity in visual map development.* Curr Opin Neurobiol, 2014. **24**(1): p. 166-75.

3. Shen, J. and M.T. Colonnese, *Development of Activity in the Mouse Visual Cortex.* J Neurosci, 2016. **36**(48): p. 12259-12275.

4. Crair, M.C. and R.C. Malenka, *A critical period for long-term potentiation at thalamocortical synapses.* Nature, 1995. **375**(6529): p. 325-8.

5. Lu, H.C., E. Gonzalez, and M.C. Crair, *Barrel cortex critical period plasticity is independent of changes in NMDA receptor subunit composition.* Neuron, 2001. **32**(4): p. 619-34.

6. Barth, A.L., *Differential plasticity in neocortical networks.* Physiol Behav, 2002. **77**(4-5): p. 545-50.

7. Lodato, S. and P. Arlotta, *Generating neuronal diversity in the mammalian cerebral cortex.* Annu Rev Cell Dev Biol, 2015. **31**: p. 699-720.

8. Douglas, R.J. and K.A. Martin, *Neuronal circuits of the neocortex.* Annu Rev Neurosci, 2004. **27**: p. 419-51.

9. Thomson, A.M. and C. Lamy, *Functional maps of neocortical local circuitry.* Front Neurosci, 2007. **1**(1): p. 19-42.

10. Gong, S., et al., *A gene expression atlas of the central nervous system based on bacterial artificial chromosomes.* Nature, 2003. **425**(6961): p. 917-25.

11. Madisen, L., et al., *A robust and high-throughput Cre reporting and characterization system for the whole mouse brain.* Nat Neurosci, 2010. **13**(1): p. 133-40.

12. Hui, Y., et al., *Strategies for Targeting Neural Circuits: How to Manipulate Neurons Using Virus Vehicles.* Front Neural Circuits, 2022. **16**: p. 882366.

13. Lui, J.H., D.V. Hansen, and A.R. Kriegstein, *Development and evolution of the human neocortex.* Cell, 2011. **146**(1): p. 18-36.

14. Lee, S.H. and Y. Dan, *Neuromodulation of brain states.* Neuron, 2012. **76**(1): p. 209-22.

15. Kaas, J.H., *The evolution of neocortex in primates.* Prog Brain Res, 2012. **195**: p.

91-102.

16. Molyneaux, B.J., et al., *Neuronal subtype specification in the cerebral cortex.* Nature Reviews Neuroscience, 2007. **8**(6): p. 427-437.

17. Harris, K.D. and A. Zahavi, *The evolution of ACh and GABA as neurotransmitters: a hypothesis.* Med Hypotheses, 2013. **81**(5): p. 760-2.

18. Mountcastle, V.B., *Modality and topographic properties of single neurons of cat's somatic sensory cortex.* J Neurophysiol, 1957. **20**(4): p. 408-34.

19. Mountcastle, V.B., P.W. Davies, and A.L. Berman, *Response properties of neurons of cat's somatic sensory cortex to peripheral stimuli.* J Neurophysiol, 1957. **20**(4): p. 374-407.

20. Hubel, D.H. and T.N. Wiesel, *Receptive fields, binocular interaction and functional architecture in the cat's visual cortex.* J Physiol, 1962. **160**(1): p. 106-54.

21. Gilbert, C.D., *Microcircuitry of the visual cortex.* Annu Rev Neurosci, 1983. **6**: p. 217-47.

22. Binzegger, T., R.J. Douglas, and K.A. Martin, *A quantitative map of the circuit of cat primary visual cortex.* J Neurosci, 2004. **24**(39): p. 8441-53.

23. Armstrong-James, M., K. Fox, and A. Das-Gupta, *Flow of excitation within rat barrel cortex on striking a single vibrissa.* J Neurophysiol, 1992. **68**(4): p. 1345-58.

24. Douglas, R.J. and K.A. Martin, *A functional microcircuit for cat visual cortex.* J Physiol, 1991. **440**: p. 735-69.

25. Lefort, S., et al., *The excitatory neuronal network of the C2 barrel column in mouse primary somatosensory cortex.* Neuron, 2009. **61**(2): p. 301-16.

26. Petersen, C.C. and S. Crochet, *Synaptic computation and sensory processing in neocortical layer 2/3.* Neuron, 2013. **78**(1): p. 28-48.

27. Adesnik, H. and A. Naka, *Cracking the Function of Layers in the Sensory Cortex.* Neuron, 2018. **100**(5): p. 1028-1043.

28. Cohen-Tannoudji, M., C. Babinet, and M. Wassef, *Early determination of a mouse somatosensory cortex marker.* Nature, 1994. **368**(6470): p. 460-3.

29. Crowley, J.C. and L.C. Katz, *Early development of ocular dominance columns.* Science, 2000. **290**(5495): p. 1321-4.

30. Morris, J.A., et al., *Divergent and nonuniform gene expression patterns in mouse brain.* Proc Natl Acad Sci U S A, 2010. **107**(44): p. 19049-54.

31. Pallas, S.L., A.W. Roe, and M. Sur, *Visual projections induced into the auditory*

pathway of ferrets. I. Novel inputs to primary auditory cortex (AI) from the LP/pulvinar complex and the topography of the MGN-AI projection. J Comp Neurol, 1990. **298**(1): p. 50-68.

32. Levelt, C.N. and M. Hübener, *Critical-period plasticity in the visual cortex.* Annu Rev Neurosci, 2012. **35**: p. 309-30.

33. Lipton, S.A. and S.B. Kater, *Neurotransmitter regulation of neuronal outgrowth, plasticity and survival.* Trends Neurosci, 1989. **12**(7): p. 265-70.

34. Nguyen, L., et al., *Neurotransmitters as early signals for central nervous system development.* Cell Tissue Res, 2001. **305**(2): p. 187-202.

35. Mattson, M.P., *Neurotransmitters in the regulation of neuronal cytoarchitecture.* Brain Res, 1988. **472**(2): p. 179-212.

36. Lauder, J.M., *Neurotransmitters as growth regulatory signals: role of receptors and second messengers.* Trends Neurosci, 1993. **16**(6): p. 233-40.

37. Ruediger, T. and J. Bolz, *Neurotransmitters and the development of neuronal circuits.* Adv Exp Med Biol, 2007. **621**: p. 104-15.

38. Hebb, D.O., *Organization of behavior*. 1949, New York: Wiley.

39. Bliss, T.V. and T. Lomo, *Long-lasting potentiation of synaptic transmission in the dentate area of the anaesthetized rabbit following stimulation of the perforant path.* J Physiol, 1973. **232**(2): p. 331-56.

40. Bliss, T.V. and A.R. Gardner-Medwin, *Long-lasting potentiation of synaptic transmission in the dentate area of the unanaestetized rabbit following stimulation of the perforant path.* J Physiol, 1973. **232**(2): p. 357-74.

41. Kelso, S.R., A.H. Ganong, and T.H. Brown, *Hebbian synapses in hippocampus.* Proc Natl Acad Sci U S A, 1986. **83**(14): p. 5326-30.

42. Sastry, B.R., J.W. Goh, and A. Auyeung, *Associative induction of posttetanic and long-term potentiation in CA1 neurons of rat hippocampus.* Science, 1986. **232**(4753): p. 988-90.

43. Malinow, R. and J.P. Miller, *Postsynaptic hyperpolarization during conditioning reversibly blocks induction of long-term potentiation.* Nature, 1986. **320**(6062): p. 529-30.

44. Wigström, H. and B. Gustafsson, *Postsynaptic control of hippocampal long-term potentiation.* J Physiol (Paris), 1986. **81**(4): p. 228-36.

45. Citri, A. and R.C. Malenka, *Synaptic Plasticity: Multiple Forms, Functions, and Mechanisms.* Neuropsychopharmacology, 2008. **33**(1): p. 18-41.

46. Mayer, M.L., G.L. Westbrook, and P.B. Guthrie, *Voltage-dependent block by Mg2+ of NMDA responses in spinal cord neurones.* Nature, 1984. **309**(5965): p. 261-3.

47. Nowak, L., et al., *Magnesium gates glutamate-activated channels in mouse central neurones.* Nature, 1984. **307**(5950): p. 462-5.

48. Malenka, R.C. and R.A. Nicoll, *NMDA-receptor-dependent synaptic plasticity: multiple forms and mechanisms.* Trends Neurosci, 1993. **16**(12): p. 521-7.

49. Malenka, R.C., *Postsynaptic factors control the duration of synaptic enhancement in area CA1 of the hippocampus.* Neuron, 1991. **6**(1): p. 53-60.

50. Bredt, D.S. and R.A. Nicoll, *AMPA receptor trafficking at excitatory synapses.* Neuron, 2003. **40**(2): p. 361-79.

51. Derkach, V.A., et al., *Regulatory mechanisms of AMPA receptors in synaptic plasticity.* Nat Rev Neurosci, 2007. **8**(2): p. 101-13.

52. Malenka, R.C. and R.A. Nicoll, *Long-term potentiation--a decade of progress?* Science, 1999. **285**(5435): p. 1870-4.

53. Song, I. and R.L. Huganir, *Regulation of AMPA receptors during synaptic plasticity.* Trends Neurosci, 2002. **25**(11): p. 578-88.

54. Malinow, R. and R.C. Malenka, *AMPA receptor trafficking and synaptic plasticity.* Annu Rev Neurosci, 2002. **25**: p. 103-26.

55. Nicoll, R.A., J.A. Kauer, and R.C. Malenka, *The current excitement in long-term potentiation.* Neuron, 1988. **1**(2): p. 97-103.

56. Feldman, D.E., *Synaptic mechanisms for plasticity in neocortex.* Annu Rev Neurosci, 2009. **32**: p. 33-55.

57. Dudek, S.M. and M.F. Bear, *Homosynaptic long-term depression in area CA1 of hippocampus and effects of N-methyl-D-aspartate receptor blockade.* Proc Natl Acad Sci U S A, 1992. **89**(10): p. 4363-7.

58. Mulkey, R.M. and R.C. Malenka, *Mechanisms underlying induction of homosynaptic long-term depression in area CA1 of the hippocampus.* Neuron, 1992. **9**(5): p. 967-75.

59. Frégnac, Y., et al., *Temporal covariance of pre- and postsynaptic activity regulates functional connectivity in the visual cortex.* J Neurophysiol, 1994. **71**(4): p. 1403-21.

60. Kirkwood, A., et al., *Common forms of synaptic plasticity in the hippocampus and neocortex in vitro.* Science, 1993. **260**(5113): p. 1518-21.

61. Bear, M.F. and A. Kirkwood, *Neocortical long-term potentiation.* Curr Opin Neurobiol, 1993. **3**(2): p. 197-202.

62. Isaac, J.T., et al., *Silent synapses during development of thalamocortical inputs.* Neuron, 1997. **18**(2): p. 269-80.

63. Kirkwood, A. and M.F. Bear, *Hebbian synapses in visual cortex.* J Neurosci, 1994. **14**(3 Pt 2): p. 1634-45.

64. Buonomano, D.V., *Distinct functional types of associative long-term potentiation in neocortical and hippocampal pyramidal neurons.* J Neurosci, 1999. **19**(16): p. 6748-54.

65. Feldman, D.E., *Timing-based LTP and LTD at vertical inputs to layer II/III pyramidal cells in rat barrel cortex.* Neuron, 2000. **27**(1): p. 45-56.

66. Sjöström, P.J., G.G. Turrigiano, and S.B. Nelson, *Rate, timing, and cooperativity jointly determine cortical synaptic plasticity.* Neuron, 2001. **32**(6): p. 1149-64.

67. Castro-Alamancos, M.A., J.P. Donoghue, and B.W. Connors, *Different forms of synaptic plasticity in somatosensory and motor areas of the neocortex.* J Neurosci, 1995. **15**(7 Pt 2): p. 5324-33.

68. Markram, H., et al., *Regulation of synaptic efficacy by coincidence of postsynaptic APs and EPSPs.* Science, 1997. **275**(5297): p. 213-5.

69. Markram, H. and M. Tsodyks, *Redistribution of synaptic efficacy between neocortical pyramidal neurons.* Nature, 1996. **382**(6594): p. 807-10.

70. Markram, H. and M. Tsodyks, *Redistribution of synaptic efficacy: a mechanism to generate infinite synaptic input diversity from a homogeneous population of neurons without changing absolute synaptic efficacies.* J Physiol Paris, 1996. **90**(3-4): p. 229-32.

71. Eder, M., W. Zieglgänsberger, and H.U. Dodt, *Neocortical long-term potentiation and long-term depression: site of expression investigated by infrared-guided laser stimulation.* J Neurosci, 2002. **22**(17): p. 7558-68.

72. Foeller, E. and D.E. Feldman, *Synaptic basis for developmental plasticity in somatosensory cortex.* Curr Opin Neurobiol, 2004. **14**(1): p. 89-95.

73. Karmarkar, U.R. and Y. Dan, *Experience-dependent plasticity in adult visual cortex.* Neuron, 2006. **52**(4): p. 577-85.

74. Malenka, R.C. and M.F. Bear, *LTP and LTD: an embarrassment of riches.* Neuron, 2004. **44**(1): p. 5-21.

75. Heynen, A.J., et al., *Molecular mechanism for loss of visual cortical*

responsiveness following brief monocular deprivation. Nat Neurosci, 2003. **6**(8): p. 854-62.

76. Crozier, R.A., et al., *Deprivation-induced synaptic depression by distinct mechanisms in different layers of mouse visual cortex.* Proc Natl Acad Sci U S A, 2007. **104**(4): p. 1383-8.

77. Allen, C.B., T. Celikel, and D.E. Feldman, *Long-term depression induced by sensory deprivation during cortical map plasticity in vivo.* Nat Neurosci, 2003. **6**(3): p. 291-9.

78. Takahashi, Y., et al., *Autoantibodies to NMDA receptor in patients with chronic forms of epilepsia partialis continua.* Neurology, 2003. **61**(7): p. 891-6.

79. Hardingham, N. and K. Fox, *The role of nitric oxide and GluR1 in presynaptic and postsynaptic components of neocortical potentiation.* J Neurosci, 2006. **26**(28): p. 7395-404.

80. Toyoda, H., et al., *Time-dependent postsynaptic AMPA GluR1 receptor recruitment in the cingulate synaptic potentiation.* Dev Neurobiol, 2007. **67**(4): p. 498-509.

81. Frenkel, M.Y., et al., *Instructive effect of visual experience in mouse visual cortex.* Neuron, 2006. **51**(3): p. 339-49.

82. Turrigiano, G.G. and S.B. Nelson, *Homeostatic plasticity in the developing nervous system.* Nat Rev Neurosci, 2004. **5**(2): p. 97-107.

83. Turrigiano, G.G., et al., *Activity-dependent scaling of quantal amplitude in neocortical neurons.* Nature, 1998. **391**(6670): p. 892-6.

84. O'Brien, R.J., et al., *Activity-dependent modulation of synaptic AMPA receptor accumulation.* Neuron, 1998. **21**(5): p. 1067-78.

85. Desai, N.S., et al., *Critical periods for experience-dependent synaptic scaling in visual cortex.* Nature Neuroscience, 2002.

86. Stellwagen, D. and R.C. Malenka, *Synaptic scaling mediated by glial TNF-alpha.* Nature, 2006. **440**(7087): p. 1054-9.

87. Goel, A. and H.K. Lee, *Persistence of experience-induced homeostatic synaptic plasticity through adulthood in superficial layers of mouse visual cortex.* J Neurosci, 2007. **27**(25): p. 6692-700.

88. Kim, J. and R.W. Tsien, *Synapse-specific adaptations to inactivity in hippocampal circuits achieve homeostatic gain control while dampening network reverberation.* Neuron, 2008. **58**(6): p. 925-37.

89. Knogler, L.D., M. Liao, and P. Drapeau, *Synaptic scaling and the development of a motor network.* J Neurosci, 2010. **30**(26): p. 8871-81.

90. Pérez-Otaño, I. and M.D. Ehlers, *Homeostatic plasticity and NMDA receptor trafficking.* Trends Neurosci, 2005. **28**(5): p. 229-38.

91. Watt, A.J. and N.S. Desai, *Homeostatic Plasticity and STDP: Keeping a Neuron's Cool in a Fluctuating World.* Front Synaptic Neurosci, 2010. **2**: p. 5.

92. Burrone, J., M. O'Byrne, and V.N. Murthy, *Multiple forms of synaptic plasticity triggered by selective suppression of activity in individual neurons.* Nature, 2002. **420**(6914): p. 414-8.

93. Burrone, J. and V.N. Murthy, *Synaptic gain control and homeostasis.* Curr Opin Neurobiol, 2003. **13**(5): p. 560-7.

94. Ibata, K., Q. Sun, and G.G. Turrigiano, *Rapid Synaptic Scaling Induced by Changes in Postsynaptic Firing.* Neuron 2008.

95. Goold, C.P. and R.A. Nicoll, *Single-cell optogenetic excitation drives homeostatic synaptic depression.* Neuron, 2010.

96. Beattie, E.C., et al., *Control of synaptic strength by glial TNFalpha.* Science, 2002. **295**(5563): p. 2282-5.

97. Stellwagen, D., et al., *Differential regulation of AMPA receptor and GABA receptor trafficking by tumor necrosis factor-alpha.* J Neurosci, 2005. **25**(12): p. 3219-28.

98. Kaneko, M., et al., *Tumor necrosis factor-alpha mediates one component of competitive, experience-dependent plasticity in developing visual cortex.* Neuron, 2008. **58**(5): p. 673-80.

99. Rutherford, L.C., S.B. Nelson, and G.G. Turrigiano, *BDNF has opposite effects on the quantal amplitude of pyramidal neuron and interneuron excitatory synapses.* Neuron, 1998. **21**(3): p. 521-30.

100. Turrigiano, G.G., *More than a sidekick: glia and homeostatic synaptic plasticity.* Trends Mol Med, 2006. **12**(10): p. 458-60.

101. Desai, N.S., *Homeostatic plasticity in the CNS: synaptic and intrinsic forms.* Journal of Physiology Paris 2003.

102. Desai, N.S., L.C. Rutherford, and G.G. Turrigiano, *Plasticity in the intrinsic excitability of cortical pyramidal neurons.* Nat Neurosci, 1999. **2**(6): p. 515-20.

103. Remy, S., H. Beck, and Y. Yaari, *Plasticity of voltage-gated ion channels in pyramidal cell dendrites.* Curr Opin Neurobiol, 2010. **20**(4): p. 503-9.

104. Bekisz, M., et al., *Increased excitability of cortical neurons induced by associative learning: an ex vivo study.* Eur J Neurosci, 2010. **32**(10): p. 1715-25.

105. Cohen-Matsliah, S.I., K. Rosenblum, and E. Barkai, *Olfactory-learning abilities are correlated with the rate by which intrinsic neuronal excitability is modulated in the piriform cortex.* Eur J Neurosci, 2009. **30**(7): p. 1339-48.

106. Hayton, S.J., M.C. Olmstead, and C. Dumont É, *Shift in the intrinsic excitability of medial prefrontal cortex neurons following training in impulse control and cued-responding tasks.* PLoS One, 2011. **6**(8): p. e23885.

107. Kida, H., et al., *Motor Training Promotes Both Synaptic and Intrinsic Plasticity of Layer II/III Pyramidal Neurons in the Primary Motor Cortex.* Cereb Cortex, 2016. **26**(8): p. 3494-507.

108. Maffei, A. and G.G. Turrigiano, *Multiple modes of network homeostasis in visual cortical layer 2/3.* J Neurosci, 2008. **28**(17): p. 4377-84.

109. Yan, J., et al., *Short-term sleep deprivation increases intrinsic excitability of prefrontal cortical neurons.* Brain Res, 2011. **1401**: p. 52-8.

110. Santini, E., G.J. Quirk, and J.T. Porter, *Fear conditioning and extinction differentially modify the intrinsic excitability of infralimbic neurons.* J Neurosci, 2008. **28**(15): p. 4028-36.

111. Song, C., V.L. Ehlers, and J.R. Moyer, Jr., *Trace Fear Conditioning Differentially Modulates Intrinsic Excitability of Medial Prefrontal Cortex-Basolateral Complex of Amygdala Projection Neurons in Infralimbic and Prelimbic Cortices.* J Neurosci, 2015. **35**(39): p. 13511-24.

112. Grubb, M.S. and J. Burrone, *Activity-dependent relocation of the axon initial segment fine-tunes neuronal excitability.* Nature, 2010. **465**(7301): p. 1070-1074.

113. Grubb, M.S., et al., *Short- and long-term plasticity at the axon initial segment.* J Neurosci, 2011. **31**(45): p. 16049-55.

114. Cossart, R., D. Aronov, and R. Yuste, *Attractor dynamics of network UP states in the neocortex.* Nature, 2003. **423**(6937): p. 283-288.

115. Gerstein, G.L., P. Bedenbaugh, and A.M.H.J. Aertsen, *Neuronal assemblies.* IEEE Transactions on Biomedical Engineering, 1989. **36**(1): p. 4-14.

116. Carrillo-Reid, L. and R. Yuste, *What Is a Neuronal Ensemble?* Oxford Research Encyclopedia of Neuroscience, 2020.

117. Buzsáki, G., *Neural Syntax: Cell Assemblies, Synapsembles, and Readers.* Neuron, 2010. **68**(3): p. 362-385.

118. Sherrington, C.S., *Observations on the scratch-reflex in the spinal dog.* J Physiol, 1906. **34**(1-2): p. 1-50.

119. Harris, K.D., et al., *Organization of cell assemblies in the hippocampus.* Nature, 2003. **424**(6948): p. 552-6.

120. Pastalkova, E., et al., *Internally generated cell assembly sequences in the rat hippocampus.* Science, 2008. **321**(5894): p. 1322-7.

121. Aery Jones, E.A. and L.M. Giocomo, *Neural ensembles in navigation: From single cells to population codes.* Curr Opin Neurobiol, 2023. **78**: p. 102665.

122. Drieu, C., R. Todorova, and M. Zugaro, *Nested sequences of hippocampal assemblies during behavior support subsequent sleep replay.* Science, 2018. **362**(6415): p. 675-679.

123. Villette, V., et al., *Internally Recurring Hippocampal Sequences as a Population Template of Spatiotemporal Information.* Neuron, 2015. **88**(2): p. 357-66.

124. Lee, A.K. and M.A. Wilson, *Memory of sequential experience in the hippocampus during slow wave sleep.* Neuron, 2002. **36**(6): p. 1183-94.

125. Skaggs, W.E. and B.L. McNaughton, *Replay of neuronal firing sequences in rat hippocampus during sleep following spatial experience.* Science, 1996. **271**(5257): p. 1870-3.

126. El-Gaby, M., et al., *An emergent neural coactivity code for dynamic memory.* Nat Neurosci, 2021. **24**(5): p. 694-704.

127. Gridchyn, I., et al., *Assembly-Specific Disruption of Hippocampal Replay Leads to Selective Memory Deficit.* Neuron, 2020. **106**(2): p. 291-300.e6.

128. Girardeau, G., et al., *Selective suppression of hippocampal ripples impairs spatial memory.* Nat Neurosci, 2009. **12**(10): p. 1222-3.

129. Fernández-Ruiz, A., et al., *Entorhinal-CA3 Dual-Input Control of Spike Timing in the Hippocampus by Theta-Gamma Coupling.* Neuron, 2017. **93**(5): p. 1213-1226.e5.

130. Stark, E., et al., *Local generation of multineuronal spike sequences in the hippocampal CA1 region.* Proc Natl Acad Sci U S A, 2015. **112**(33): p. 10521-6.

131. Grewe, B.F. and F. Helmchen, *Optical probing of neuronal ensemble activity.* Curr Opin Neurobiol, 2009. **19**(5): p. 520-9.

132. Ikegaya, Y., et al., *Synfire chains and cortical songs: temporal modules of cortical activity.* Science, 2004. **304**(5670): p. 559-64.

133. Carrillo-Reid, L., et al., *Controlling Visually Guided Behavior by Holographic Recalling of Cortical Ensembles.* Cell, 2019.

134. Carrillo-Reid, L., et al., *Imprinting and recalling cortical ensembles.* Science, 2016. **353**(6300): p. 691-4.

135. Miller, J.E., et al., *Visual stimuli recruit intrinsically generated cortical ensembles.* Proc Natl Acad Sci U S A, 2014. **111**(38): p. E4053-61.

136. MacLean, J.N., et al., *Internal Dynamics Determine the Cortical Response to Thalamic Stimulation.* Neuron, 2005. **48**(5): p. 811-823.

137. Luczak, A., P. Barthó, and K.D. Harris, *Spontaneous Events Outline the Realm of Possible Sensory Responses in Neocortical Populations.* Neuron, 2009. **62**(3): p. 413-425.

138. Luczak, A., et al., *Sequential structure of neocortical spontaneous activity in vivo.* PNAS, 2007. **104**(1): p. 347-52.

139. Hemberger, M., et al., *Reliable Sequential Activation of Neural Assemblies by Single Pyramidal Cells in a Three-Layered Cortex.* Neuron, 2019. **104**(2): p. 353-369.e5.

140. Arieli, A., et al., *Dynamics of ongoing activity: explanation of the large variability in evoked cortical responses.* Science, 1996. **273**(5283): p. 1868-71.

141. Lloyd, E.R., et al., *The influence of visual cortex on perception is modulated by behavioural state.* bioRxiv, 2019: p. 706010.

142. Marshel, J.H., et al., *Cortical layer-specific critical dynamics triggering perception.* Science, 2019. **365**(6453): p. eaaw5202.

143. Liu, B., M.J. Seay, and D.V. Buonomano, *Creation of Neuronal Ensembles and Cell-Specific Homeostatic Plasticity through Chronic Sparse Optogenetic Stimulation.* The Journal of Neuroscience, 2023. **43**(1): p. 82-92.

144. Ryan, T.J., et al., *Memory. Engram cells retain memory under retrograde amnesia.* Science, 2015. **348**(6238): p. 1007-13.

145. Pignatelli, M., et al., *Engram Cell Excitability State Determines the Efficacy of Memory Retrieval.* Neuron, 2019. **101**(2): p. 274-284.e5.

146. Mauk, M.D. and D.V. Buonomano, *The Neural Basis of Temporal Processing.* Ann. Rev. Neurosci., 2004. **27**: p. 307-340.

147. Paton, J.J. and D.V. Buonomano, *The Neural Basis of Timing: Distributed Mechanisms for Diverse Functions.* Neuron, 2018. **98**(4): p. 687-705.

148. Keller, G.B. and T.D. Mrsic-Flogel, *Predictive Processing: A Canonical Cortical Computation.* Neuron, 2018. **100**(2): p. 424-435.

149. Rao, R.P. and D.H. Ballard, *Predictive coding in the visual cortex: a functional interpretation of some extra-classical receptive-field effects.* Nat Neurosci, 1999. **2**(1): p. 79-87.

150. Gouvêa, T.S., et al., *Striatal dynamics explain duration judgments.* Elife, 2015. **4**.

151. Pai, S., et al., *Minimal impairment in a rat model of duration discrimination following excitotoxic lesions of primary auditory and prefrontal cortices.* Front Syst Neurosci, 2011. **5**: p. 74.

152. Shuler, M.G. and M.F. Bear, *Reward timing in the primary visual cortex.* Science, 2006. **311**(5767): p. 1606-9.

153. Namboodiri, V., et al., *Visually Cued Action Timing in the Primary Visual Cortex.* Neuron, 2015. **86**(1): p. 319-330.

154. Chubykin, A.A., et al., *A Cholinergic Mechanism for Reward Timing within Primary Visual Cortex.* Neuron, 2013. **77**(4): p. 723-735.

155. Wright, B.A., et al., *Learning and generalization of auditory temporal-interval discrimination in humans.* J Neurosci, 1997. **17**(10): p. 3956-63.

156. Karmarkar, U.R. and D.V. Buonomano, *Temporal specificity of perceptual learning in an auditory discrimination task.* Learn Mem, 2003. **10**(2): p. 141-7.

157. Bratzke, D., T. Seifried, and R. Ulrich, *Perceptual learning in temporal discrimination: asymmetric cross-modal transfer from audition to vision.* Exp Brain Res, 2012. **221**(2): p. 205-10.

158. Buonomano, D.V. and M.M. Merzenich, *Temporal information transformed into a spatial code by a neural network with realistic properties.* Science, 1995. **267**: p. 1028–30.

159. Buonomano, D.V. and M.D. Mauk, *Neural Network Model of the Cerebellum: Temporal Discrimination and the Timing of Motor Responses.* Neural Computation, 1994. **6**(1): p. 38-55.

160. Buonomano, D.V., *Decoding temporal information: A model based on short-term synaptic plasticity.* J Neurosci, 2000. **20**(3): p. 1129-41.

161. Johnson, H.A., A. Goel, and D.V. Buonomano, *Neural dynamics of in vitro cortical networks reflects experienced temporal patterns.* Nat Neurosci, 2010. **13**(8): p. 917-919.

162. Goel, A. and D.V. Buonomano, *Temporal Interval Learning in Cortical Cultures Is*

Encoded in Intrinsic Network Dynamics. Neuron, 2016. **91**: p. 320-327.

163. Buonomano, D.V. and W. Maass, *State-dependent computations: spatiotemporal processing in cortical networks.* Nat Rev Neurosci, 2009. **10**(2): p. 113-25.

Chapter 2: Creation of Neuronal Ensembles and Cell-Specific Homeostatic Plasticity through Chronic Sparse Optogenetic Stimulation

Published as: **Liu, B.**, Seay, M. J., & Buonomano, D. V. (2023). Creation of Neuronal Ensembles and Cell-Specific Homeostatic Plasticity through Chronic Sparse Optogenetic Stimulation. *The Journal of Neuroscience.*

2.1 Abstract

Cortical computations emerge from the dynamics of neurons embedded in complex cortical circuits. Within these circuits, neuronal ensembles, which represent subnetworks with shared functional connectivity, emerge in an experience-dependent manner. Here we induced ensembles in *ex vivo* cortical circuits from mice of either sex by differentially activating subpopulations through chronic optogenetic stimulation. We observed a decrease in voltage correlation, and importantly a synaptic decoupling between the stimulated and non-stimulated populations. We also observed a decrease in firing rate during Up-states in the stimulated population. These ensemble-specific changes were accompanied by decreases in intrinsic excitability in the stimulated population, and a decrease in connectivity between stimulated and non-stimulated pyramidal neurons. By incorporating the empirically observed changes in intrinsic excitability and connectivity into a spiking neural network model, we were able to demonstrate that changes in both intrinsic excitability and connectivity accounted for the decreased firing rate, but only

changes in connectivity accounted for the observed decorrelation. Our findings help ascertain the mechanisms underlying the ability of chronic patterned stimulation to create ensembles within cortical circuits. And, importantly, show that while Up-states are a global network-wide phenomenon, functionally distinct ensembles can preserve their identity during Up-states through differential firing rates and correlations.

SIGNIFICANCE STATEMENT

The connectivity and activity patterns of local cortical circuits are shaped by experience. This experience-dependent reorganization of cortical circuits is driven by complex interactions between different local learning rules, external input, and reciprocal feedback between many distinct brain areas. Here we used an ex vivo approach to demonstrate how simple forms of chronic external stimulation can shape local cortical circuits in terms of their correlated activity and functional connectivity. The absence of feedback between different brain areas and full control of external input allowed for a tractable system to study the underlying mechanisms and development of a computational model. Results show that differential stimulation of subpopulations of neurons significantly reshapes cortical circuits and forms subnetworks referred to as neuronal ensembles.

KEYWORDS

Neuronal ensembles, Up-states, neural dynamics, computational model, homeostatic plasticity

2.2 Introduction

Cortical computations rely on the neural dynamics that emerge from local cortical microcircuits [164-166]. While it is not known how the appropriate connectivity between the tens of thousands of neurons within local circuits emerges through development, it is known that experience and patterned activity shape cortical circuits into functional neuronal ensembles [38, 115-117]. Neuronal ensembles are often defined as subgroups of coactive and interconnected neurons that underlie numerous neural computations, from encoding memories to guiding behavior [114, 167, 168]. It has been shown that patterned stimulation of subpopulations of neurons alters the functional connectivity of local microcircuits and leads to the formation of neuronal ensembles [134, 169-172].

Neuronal ensembles are often identified based on high degrees of correlated activity between neurons within an ensemble, and decorrelated activity between ensembles. This neural signature, however, appears to be at odds with other dynamic regimes which are characterized by network-wide or global patterns of activity. The best-studied example of such global activity regimes is Up-states, in which highly correlated transitions from a quiescent state to a depolarized state occur simultaneously in all neurons within a local microcircuit [173-175]. Up-states seem to comprise a fundamental and intrinsic cortical dynamic regime because they are observed during anesthesia, slow-wave sleep, quiet wakefulness [176-179], as well as in acute slices [173-175, 180-184]. Indeed, Up-states even emerge over the course of *ex vivo* development [185-189]. While Up-states have been reported to have some spatiotemporal structure [136, 184, 189], a defining property of Up-states is that they are characterized by a global shift in activity, in

which virtually all excitatory and inhibitory neurons become depolarized and increase their firing rate simultaneously. The global nature of Up-states poses a paradox regarding how distinct functional connections within ensembles of neurons are maintained and whether the identity of the ensembles can be preserved during Up-states. Here we examined both the ability for patterned stimulation to shape local microcircuits and induce ensembles, as well as whether the induced ensemble identities are preserved during network-wide Up-states.

Our approach was to chronically optogenetically stimulate sparse populations of pyramidal neurons and record spontaneous Up-states. The use of *ex vivo* cortical cultures allowed us to preserve the defining microcircuitry of local cortical networks while unambiguously ascertaining that the observed dynamics emerge locally within the circuit being studied—i.e., in the absence of influences from down- or up-stream circuits. This approach also allowed us to develop a spike-based computational model of network dynamics that captures the "stand-alone" results of an isolated cortical circuit.

We first show that, consistent with previous results, chronic global stimulation induces a dramatic homeostatic decrease in Up-state frequency [190]. In contrast, the same amount of optical stimulation to a sparse subpopulation of neurons did not abolish spontaneous Up-states, but induced intrinsic homeostatic plasticity of the optogenetically stimulated neurons. Critically, these units formed a local ensemble, and during Up-states the identity of this ensemble was preserved through differences in firing rate and pairwise correlations. Mechanistically, these alterations were associated with subpopulation specific changes in connectivity and intrinsic excitability. When incorporated into a spiking neural network model, these mechanistic changes were able to account for the differential

ensemble activity during simulated Up-states.

2.3 Results

2.3.1 Homeostatic regulation of Up-states following chronic optical stimulation

To confirm the effectiveness of chronic optogenetic stimulation *ex vivo*, we first densely expressed channelrhodopsin-2 (ChR) using AAV9-CamKIIa-ChR2-mCherry in excitatory neurons of mouse cortical organotypic slices. We stimulated the transduced slices at 0.2 Hz with 50 ms pulses of 465 nm blue light in the incubator for 24- or 48-hrs (**Fig. 1A**). Using whole-cell patch clamp recordings we confirmed that each 50 ms pulse of light was sufficient to elicit 1-2 action potentials in ChR^+ pyramidal neurons, and consistent with previous results observed that optical stimulation often triggered Up-states. We quantified spontaneous Up-state activity using three measures: standard deviation of the membrane potential (STD_{Vm}), Up-state frequency, and Up-state duration (**Fig. 1B**, see Methods). There was a significant decrease in both STD_{Vm} (**Fig. 1C**) at 24-hrs (t_{70}=5.6, p=<10^{-4}, unpaired t-test) and 48-hrs (t_{78}=5.9, p=<10^{-4}). We also observed a decrease in spontaneous Up-state frequency following both 24-hrs (t_{69}=5.8, p=<10^{-4}) and 48-hrs (t_{77}=6.6, p=<10^{-4}) of light stimulation (**Fig. 1D**). There was no change in the observed Up-state duration (**Fig. 1E**).

These data demonstrate that chronic stimulation of excitatory neurons produced a pronounced homeostatic down-regulation of Up-states—consistent with the notion that neural circuits seek out “setpoint” levels of activity [191-194]), which in control slices are achieved through internally generated spontaneous Up-states. But in the stimulated

slices, these setpoints are achieved through external inputs, resulting in the internal activity being down-regulated.

2.3.2 Chronic stimulation of a sparse subpopulation of pyramidal neurons generates a decorrelation of activity between stimulated and non-stimulated populations

To determine if we could induce distinct ensembles or “clustering” through differential stimulation of neurons, we next expressed ChR in a sparse population of pyramidal neurons using a Cre-dependent ChR and a diluted Cre expressing AAV (see Methods). This approach led to sparse (~10%) transduction of cortical pyramidal neurons (Fig. 2A). We next used the same 48-hr chronic stimulation protocol used above. In contrast to the effect of stimulation on densely transduced circuits, robust spontaneous Up-states were present in the sparsely transduced slices.

Up-states correspond to global changes in network activity which are believed to recruit all excitatory neurons in a circuit. Thus, as expected, there was no difference in Up-state frequency between ChR+ and ChR- subpopulations. Interestingly, however, there were differences in the voltage dynamics during the Up-state between the ChR+ and ChR- subpopulations. First, the amplitude of Up-states was significantly reduced ($t_{18}=6.3$, $p=<10\ 4$, paired t-test) in the ChR+ compared to the ChR- neurons (Fig. 2B). To control for the possibility that the amplitude differences could be driven by the changes in the intrinsic properties of ChR+ and ChR- neurons (see below), such as resting membrane potential, we also compared Up-state amplitude of simultaneously recorded ChR- pairs grouped by lowest and highest membrane potential. These analyses revealed

that Up-state amplitude was not affected by baseline Vm (Fig. 2B, right). The average firing rate during Up-states was also significantly lower ($t_{13}=3.1$, $p=0.008$, paired t-test) in ChR+ neurons (Fig. 2C), although there was no difference in the firing rate between ChR- pairs with low and high membrane potential ($t_{15}=0.2$, $p=0.85$). Importantly, the pairwise correlation of Up-state activity between simultaneously recorded ChR /ChR pairs was significantly greater ($U=41$, $n1 = n2 = 14$, $p=0.008$, Mann-Whitney test) than in ChR+/ChR pairs (Fig. 2D). These findings suggest that chronic patterned stimulation of a sparse population of pyramidal neurons in a cortical network led to the formation of distinct clusters or neuronal ensembles, whereby the ChR+ is decoupled from ChR- subpopulation as indicated by the differences in firing rate and correlations during Up-states.

2.3.3 Differential input-output functions between stimulated and non-stimulated neurons

The differential activity during Up-states is somewhat surprising given that Up-states are a global network-wide phenomena. To begin to understand whether this decoupling may be accounted for by intrinsic and/or network properties we analyzed the intrinsic neuronal properties of the ChR^+ and ChR^- subpopulations including the F-I curve, that is, the input-output function as defined by the relationship between spike frequency and injected current (**Fig. 3A**). Consistent with previous studies of intrinsic homeostatic plasticity [102, 195], chronic stimulation of the ChR^+ neurons resulted in significantly different F-I curves ($F_{1,86}=20.5$, $p<10^{-4}$**; Fig. 3B**). To quantify the source of these differences, and to incorporate the differences in intrinsic excitability in a

neurocomputational model (see below) we fit the F-I curve of each neuron to a rectified linear function defined by a threshold and gain [196]. Results revealed that the differences in F-I curve could be accounted for by a significant increase (t_{109}=2.8, p=0.006, paired t-test) in the threshold from θ=0.10±0.06 nA in the ChR^- population to θ=0.13±0.04 nA in ChR^+ neurons (**Fig. 3C**). There was also a trend (t_{109}=1.8, p=0.07) for an accompanying decrease in the gain (the slope of the F-I curve) in the ChR^+ subpopulation. Additionally, there was a small difference in resting Vm between ChR^+ and ChR^- cells (-65.6±5.3 and -67.5±3.2 mV, respectively; p=0.05), and input resistance (236±54 and 202±63 MΩ, respectively; p=0.01). Overall these results establish that there are significant changes in intrinsic excitability that could contribute to the subpopulation differences. Specifically, the intrinsic plasticity may account for the observed decrease in Up-state firing rate observed in the ChR^+ neurons (**Fig. 2C**), however it is less clear if the changes in intrinsic excitability could account for the decoupling of the correlation in activity (**Fig. 2D**).

2.3.4 Synaptic decoupling between stimulated and non-stimulated pyramidal neurons

To examine whether network-level changes contribute to the observed differential effects in firing rate and activity correlation we next asked if there is a synaptic decoupling between the ChR^+ and ChR^- subpopulations. We assessed the connection probability and strength of the connections between ChR^+ and ChR^-. Connectivity between nearby pyramidal neurons (<50 um) was measured through paired whole-cell current clamp recordings. Trains of action potentials were alternatively elicited in one cell while measuring any corresponding excitatory post-synaptic potentials (EPSPs) in the other

(**Fig. 4A**). We recorded from ChR^+/ChR^- and ChR^-/ChR^- pairs. Because of the sparseness of the ChR expression it was not feasible to record from nearby ChR^+/ChR^+ pairs—and recording from distant pairs dramatically decreased the connectivity likelihood.

Among the connected pairs both the unitary EPSP amplitudes (U=20, n_1=8, n_2=19, p=<0.002, Mann-Whitney test) and slopes (U=24, n_1=8, n_2=19, p=<0.004) were dramatically smaller in ChR^+/ChR^-compared to ChR^-/ChR^- pairs (**Fig. 4B**). In addition to weaker synaptic connections between the subpopulations, there was a significant difference in connection probability ($\chi^2_{1,158} = 5.1$, p=0.02, Chi-square) between pairs of ChR^-/ChR^- (0.24) compared with ChR^+/ChR^- (0.10) (**Fig. 4C**). There was not a significant difference in the likelihood in the proportion of reciprocal connections ($\chi^2_{1,21} = 1.1$, p=0.31) between the ChR^-/ChR^- (4/15 pairs) and the ChR^+/ChR^- (3/6 pairs), nor was there any detectable asymmetry in the direction of the $ChR^+ \leftrightarrow ChR^-$ connections. Together these results establish that chronic stimulation of sparsely transduced pyramidal neurons resulted in a rewiring of the local cortical circuit in the form of a synaptic decoupling between ChR^+ and ChR^- subpopulations.

2.3.5 Synaptic decoupling between subpopulations accounts for the experimental observations.

In order to determine if either, or both, the empirically observed changes in intrinsic excitability and synaptic decoupling, could account for the observed changes in Up-state firing rate we next implemented an empirically informed spike-based computational model of Up-states (see Methods). Previous computational and mathematical models of Up-

states and inhibition-stabilized networks have carefully characterized the constraints that must be met in order for networks to exhibit transiently stable Up- and Down-states [197-201]. Key among these, is the appropriate balance of excitation and inhibition in both the excitatory and inhibitory populations. The model was composed of 1600 excitatory (Ex) and 400 inhibitory (Inh) integrate-and-fire units. We first established that in the baseline network, in which all Ex units had the same input-output function and a uniform connection probability, the network exhibited global transitions between a quiescent Down-state and depolarized Up-states (Fig 5A). This provided the opportunity to directly model and evaluate the influence of the empirically observed cell-specific and connectivity changes to account for the observed changes in firing rates during Up-states. Our approach allowed us to independently adjust both the input-output function as well as the connection probability between populations in the spiking neural network model to approximately match the empirically observed changes following chronic optogenetic stimulation.

We first created two subpopulations of excitatory units (Ex+ and Ex-), as defined by the F-I curves of the ChR^+ and ChR^- neurons (**Fig. 3**), respectively. Simply adjusting the input-output function of the Ex+ population to match the empirically derived F-I curves was sufficient to account for the population-specific changes in Up-state firing rate (**Fig 5B-E**). Specifically, we modified the intrinsic parameters of 200 (12.5%) Ex units so that they had a higher spike threshold and lower gain (Ex+) while leaving the intrinsic parameters of the remaining 1400 Ex units untouched (Ex-). We then ran ten 60-second simulations with the manipulated intrinsic parameters and shuffled the weights within each weight class for each simulation. Across simulations, the Up-state median firing rate

of the Ex+ population was significantly reduced to 1.9 Hz compared to the Ex- population's median of 4.2 Hz (t_9 = 100.2, $p < 10^{-10}$). To determine whether changes in intrinsic excitability could account for the decrease in voltage correlation during Up-states between the ChR^+ and ChR^- populations (**Fig. 2D**), we also measured the pairwise correlation of model units' voltage during Up-states using the same methodology used to quantify the experimental data. We found that across simulations there was no significant difference in the median pairwise correlations during Up-states between or within ChR^+ and ChR^- populations (**Fig 5F**): (Ex-/Ex-) vs. (Ex-/Ex+) (n = 10, W = 29, p = 0.16), (Ex-/Ex+) vs. (Ex+/Ex+) (n = 10, W = 33, p = 0.10), (Ex-/Ex-) vs. (Ex+/Ex+) (n = 10, W = 35, p = 0.08).

We next modified the model to incorporate only the empirically observed changes in connectivity, while leaving the intrinsic excitability unchanged (i.e., as in the baseline model all Ex units in this simulation have the same input-output function) (**Fig. 6**). According to our observation that the connection probability between ChR^+ and ChR^- neurons decreased (symmetrically) from 24% to 10% (**Fig. 4C**), we deleted half of the connections between Ex+ (200 units) and Ex- (1400 units) populations (reciprocally), decreasing their probability of connection from 25% to 12.5%. However, due to the model's sensitivity to the balance of excitation and inhibition, we found that deleting a portion of excitatory connections without an accompanying decrease in inhibition resulted in unbalanced dynamics and implausible behavior in the model. We thus made an additional assumption that there was an excitatory/inhibitory rebalancing—implemented by decreasing the inhibitory connections onto each of the two populations (**Fig. 6A**). Across simulations, the Up-state median firing rate of the Ex+ population was significantly

reduced compared to the Ex- population (**Fig. 6B**; $t_9 = 8.5$, $p < 10^{-4}$). Importantly, we also observed a marked decrease in the voltage correlation between Ex+/Ex- pairs during Up-states (**Fig 6C**), compared to the Ex-/Ex- (n = 10, W = 55, p = 0.002) and the Ex+/Ex+ populations (n = 10, W = 55, p = 0.002).

These findings indicate that either decreases in the intrinsic excitability of the ChR^+ subpopulation or synaptic decoupling of the ChR^+ and ChR^- subpopulations can account for the observed decreases in firing rate during Up-states, but only the manipulation of synaptic connectivity accounted for the decrease in Up-state voltage correlations. Our results are consistent with the hypothesis that parallel forms of plasticity cooperate in a synergistic and redundant manner to implement homeostatic adjustments and experience-dependent neuronal ensembles, and that each plasticity loci can produce distinct or shared phenotypes [92, 108, 192, 193, 202-204].

2.4 Discussion

Cortical circuits must carefully balance opposing neuronal and circuit properties, including the balance of excitation and inhibition [205, 206], and overall levels of neuronal activity so that cells are neither under- or over-active [95, 194, 207]. Additionally, cortical circuits must balance the degree to which interconnected neurons function as independent groups or as globally co-active networks. On one hand distinct neuronal ensembles must operate independently during cortical processing, but also remain a part of a larger network during global dynamic regimes including Up-states and sleep states. Here we have begun to address this balance between local versus global dynamic

regimes by showing that while chronic stimulation of subsets of neurons induces a decoupling from other neurons in the circuit, it remains the case that both populations of neurons participate in global Up-state dynamics. Critically, however, in contrast to the prevailing view in computational models of Up-states in which all neurons participate equally in Up-state dynamics [197, 200], we observed that functionally distinct ensembles can preserve their identity during Up-states through differential firing rates and decreased cross-ensemble correlations.

2.4.1 Homeostatic plasticity of Up-states

Up-states have been proposed to have multiple functional roles, including memory consolidation and synaptic homeostasis [208-212]. Consistent with previous studies, our results suggest that Up-states also play a role in the homeostatic regulation of neural activity [190, 213]. Specifically, in densely-transduced cortical circuits, chronic optical stimulation dramatically reduced the frequency of spontaneous Up-states—in many cases no Up-states were observed in stimulated slices—suggesting that in the presence of an external source of neural activity, networks down-regulated spontaneous network-wide Up-states to adjust their activity setpoints. We note that while the concept of an activity setpoint is generally interpreted as an ontogenetically determined target level of activity as measured by the mean levels of Ca^{2+}, the existence and potential mechanisms of these hypothesized setpoints remains an open question [194, 207, 214].

In sparsely transduced slices, network-wide Up-states were observed in both ChR^- and ChR^+ neurons; however, the firing rate during Up-states was significantly reduced in

the directly stimulated population. This indicates that all neurons participated in Up-states at the same time, but that ChR^+ neurons down-regulated their spiking—again consistent with the notion that they reached their activity setpoints through direct optical stimulation and down-regulated their activity during Up-states to achieve activity homeostasis. To the best of our knowledge this is the first result suggesting that, based on activation history, different subpopulations of the same neuron class may have distinct activity signatures during Up-states.

2.4.2 Ensembles maintain identity within Up-states

It is widely accepted that the formation of functionally distinct sub-circuits embedded within larger local cortical networks is of fundamental importance to cortical computations [38, 116, 165, 172]. This functional specialization has been observed in many *in vivo* and *in vitro* studies [133, 142, 215-217]. Furthermore, *in vivo* studies have shown that it is possible to artificially induce the formation of ensembles by direct co-activation of cortical neurons [134, 170], consistent with the theory that Hebbian plasticity contributes to this functional specialization. Here, we demonstrate that the co-activation of a subset of pyramidal neurons also reconfigures cortical circuits *ex vivo*, resulting in a synaptic decoupling between directly activated ChR^+ neurons and the ChR^- subpopulation, and the formation of neuronal ensembles.

One might have predicted that our stimulation protocol would have resulted in ChR^+ neurons becoming hubs of a rich-club network architecture, in which ChR^+ neurons asymmetrically drive ChR^- neurons—a prediction that might be expected based on STDP

or reports of rich-club networks in the cortex [218]. We did not observe any enhanced connectivity from ChR^+ to ChR^- neurons, however, given the relatively low inter-population connectivity it is possible that a small degree of $ChR^+ \leftrightarrow$ChR- asymmetry could have been missed. Nevertheless, our results suggest that the differential stimulation of different subpopulations of neurons favors the formation of neural ensembles rather than rich-club networks.

While neuronal ensembles refer to functionally interconnected subpopulations of neurons, it is recognized that they are not fully isolated functional units. Ensembles are composed of overlapping subpopulations of neurons, but during some cortical regimes most, if not all, neurons within a local circuit undergo synchronous shifts between inactive Down-states to depolarized Up-states. This tension between compartmentalized and global activity regimes raises the question of if, and how, ensemble identity is maintained during Up-states. Here we show that ensemble identity is preserved during Up-states. Specifically, in addition to the lower firing rates during Up-states, the cross-ensemble correlations are weaker. At the mechanistic level this is likely to be a result of the decreased cross-ensemble connectivity.

2.4.3 Mechanisms underlying the formation of neuronal ensembles and homeostasis

The experience-dependent reconfiguration of cortical subnetworks observed here must be mediated through specific learning rules and plasticity mechanisms. Part of the observed changes are attributed to well-defined homeostatic mechanisms: activity-dependent up- and down-regulation of intrinsic excitability [102, 112, 204, 219-221].

Homeostatic plasticity by itself, however, cannot fully account for our results as it would not account for the selective decrease in cross-ensemble connectivity (e.g., the decrease in ChR^+ to ChR^- connectivity). Thus, associative Hebbian mechanisms that capture the correlational structure of neuron pairs are likely to operate in parallel with homeostatic plasticity [222-225].

A limitation of our study was that we were not able to specifically contrast the connectivity between ChR^+ pairs and ChR^- pairs because of the challenges in performing paired ChR^+ recordings in sparsely transduced slices in which the ChR^+ neurons were distant from each other. Thus, future studies should specifically determine if the connectivity within ChR^+ pairs is the same, or perhaps higher, than between ChR^- pairs. However, our computational model allowed us to demonstrate that synaptic decoupling was sufficient to account for the observed cross-ensemble decreases in correlations, as well as for the lower firing rates in ChR^+ neurons. Overall, our experimental and computational results support the notion that the nervous system engages multiple synergistically operating plasticity loci in parallel in order to robustly implement experience-dependent cortical reorganization.

2.5 Materials and Methods

Organotypic Cultures

Cortical organotypic slices were prepared and transduced as described previously [162, 190]. Slices were obtained from postnatal day 6-7 wildtype FVB mice of either sex. Organotypic cultures were prepared using the interface method [226]. Coronal slices (400

μm thickness) containing primary somatosensory and auditory cortex were sliced using a vibratome (Leica VT1200) and bisected before being placed on filters (Millipore) with 1 mL of culture media. Culture media was changed at 1 and 24 hours after cutting and every 2-3 days thereafter. Cutting media consisted of MEM (Corning 15-010-CV) plus (final concentration in mM): MgCl2, 3; glucose, 10; HEPES, 25; and Tris-base, 10. Culture media consisted of MEM (Corning 15-010-CV) plus (final concentration in mM): glutamine, 1; CaCl2, 2.6; MgSO4, 2.6; glucose, 30; HEPES, 30; ascorbic acid, 0.5; 20% horse serum, 10 units/L penicillin, and 10 μg/L streptomycin. Slices were incubated in 5% CO2 at 35°C.

Viral Transduction

For the dense transduction optogenetic experiments, slices were transduced with AAV9-CamKIIa-hChR2(H134R)-mCherry [$1x10^{13}$], whereas for the sparse experiments, slices were transduced with diluted AAV9-CamKIIa-Cre [$1x10^{9}$] and non-diluted AAV9-DIO-ChR2-mCherry [$5x10^{12}$]. Each slice received a total of 1 uL of viral solution gently delivered via a sterilized pipette above the cortex. All viral transductions were performed at day-in-vitro (DIV) 7 and recordings were performed between DIV 21 – 30 to allow sufficient time for viral expression.

Chronic optogenetic stimulation

To reduce variability, experiments relied on “sister” slices, i.e. experimental groups were derived from the same batch of animals (littermates), maintained with the same culture medium and serum, placed in the same incubator, and virally transduced in the same session. For the fully transduced slices, both stimulated and unstimulated sister

slices were simultaneously placed into the stimulation incubator to ensure identical culture environments and experimental conditions. The optical stimulation protocol consisted of 50 ms pulses of blue light (465 nm) delivered every 5 seconds for either 24- or 48-hours. The sparsely transduced slices underwent an identical stimulation protocol for 48-hours.

Electrophysiology

Culture filters were transferred to the recording rig and perfused with oxygenated ACSF composed of (mM): 125 NaCl, 5 KCl, 2.5 $MgSO_4$, 25 $NaHCO_3$, 1 NaH_2PO_4, 25 glucose, 2.5 $CaCl_2$ (ACSF was formulated to match the standard culture media). Temperature was maintained at 32-33°C and perfused at 5 mL/min. Whole-cell solution was be composed of (mM): 100 K-gluconate, 20 KCl, 4 ATP-Mg, 10 phosphocreatine, 0.3 GTP, 10 HEPES (adjusted to pH 7.3 and 300 mOsm). For the dense transduction experiments, whole-cell current-clamp recordings were performed on pyramidal neurons in both stimulated and non-stimulated slices. For the sparse transfection experiments, simultaneous whole-cell current-clamp recordings were performed on one ChR^- and one ChR^+ pyramidal neuron or two ChR^- neurons. In both paradigms, transduced cells were identified by the presence of mCherry expression and additionally confirmed by the presence of a direct light-evoked response.

Intrinsic excitability was measured as the number of action potentials evoked during a 250 ms current step at intensities of (0.05, 0.1, 0.15, 0.2, 0.25, 0.3 nA). For each neuron, a minimum of 5 minutes of spontaneous activity was recorded. Connectivity between stimulated and non-stimulated pyramidal neurons was assessed through simultaneous current clamp recordings where alternating trains of current were applied

to each cell. A connection was considered to exist if the average excitatory post-synaptic potential (EPSP) amplitude was at least 3 times the baseline standard deviation.

In the sparse transduction experiments, we fit the mean spike frequency x intensity (F-I) curve to a threshold-linear activation function.

Up-state Quantification/Analysis

A minimum of 5 min of spontaneous activity was recorded for each neuron. Recordings were sampled at 10 kHz. Spontaneous network events and Up-states were quantified based on previously defined criteria (Johnson & Buonomano, 2007; Goel & Buonomano, 2013). The first criterion for Up-states was voltage deflections of 5 mV above the resting membrane potential. However, during network events, the membrane potential would often make multiple crossings above and below the 5 mV threshold before returning to the resting potential. Thus, we defined Up-states as events that remained above threshold for at least 500 ms, allowing for drops below threshold that lasted less than 100 ms. We also calculated the standard deviation of the voltage during spontaneous activity (vSTD) to provide an assumption-independent measure of overall spontaneous activity.

Up-state pairwise correlations were calculated with median-filtered traces (25 ms window) to remove the spikes during Up-states. For each Up-state the median-filtered voltage was taken from 50 ms after its detected onset to 50 ms before its detected offset in order to exclude the transitions between Down- and Up-states. The set of resulting Up-state voltage segments (representing the same time indices in each cell's recording) were then concatenated for each cell in a paired recording, and the two concatenated voltage

time series were correlated in order to yield a single correlation coefficient for each simultaneously recorded pair of cells, either (ChR^- /ChR^-) or (ChR^+ /ChR^-).

Statistics

Comparisons between stimulated and unstimulated slices were performed with unpaired two-tailed t-tests, comparisons that used paired recordings of ChR^+ and ChR^- cells in the same slice were performed with paired two-tailed t-tests. To compare the F-I curve results, we used a two-way repeated measures ANOVA with factors of Cell (ChR^-, ChR^+) and Intensity (0.05, 0.1, 0.15, 0.2, 0.25, 0.3 nA). Mann-Whitney tests were used to compare the experimental Up-state voltage correlations, EPSP amplitudes, and EPSP slopes because the data were not normally distributed. To compare the proportion of connected vs. unconnected pairs of pyramidal neurons, a Chi-squared test was used. Wilcoxon Signed Rank Tests were used to compare the model units' mean pairwise Up-state voltage correlations across simulations.

Computational model

Elaborating on previous work [197] we modeled a network of 2000 units (1600 Ex and 400 Inh) that were sparsely connected (25%) by current-based synapses. Units in the model were leaky integrate-and-fire (IAF) neurons with an adaptation current whose membrane potential was governed by the following equations:

$$C_m \frac{dV(t)}{dt} = g_L(E_L - V(t)) + I^{Syn}(t) - I^{Ad}(t) + \sigma\sqrt{\tau_m}\eta(t)$$

$$\frac{dI^{Ad}(t)}{dt} = \frac{-I^{Ad}(t)}{\tau_{Ad}}$$

The noise term $\sigma\sqrt{\tau_m}\eta(t)$ represents an Ornstein-Uhlenbeck process with zero mean, standard deviation σ, and a time constant equal to the membrane time constant $\tau_m = C_m/g_L$. When $V(t) \geq V_{thresh}$, the unit emitted a spike, its voltage was reset to V_{reset}, and its adaptation current I^{Ad} was incremented by β/τ_{Ad}. After spiking, the unit entered an absolute refractory period $\tau_{refractory}$, during which time it could not emit spikes. In some simulations (Figure 5), the unit parameters for 200 of the 1600 Ex units were modified based on empirical observations to create a subpopulation we refer to as Ex+. Default values for unit parameters based on their type can be found in Table 1.

Total synaptic current $I_{syn}(t)$ was summed across each unit's incoming synapses with distinct synaptic weights determined by matrices J^{EE}, J^{EI}, J^{IE}, and J^{II}. Thus, for example, the total synaptic current to the i^{th} excitatory unit was given by:

$$I_i^{Syn}(t) = \sum_{j=1}^{N_{exc}} J_{ij}^{EE}\, s_{ij}(t) + \sum_{j=1}^{N_{inh}} J_{ij}^{EI}\, s_{ij}(t), \qquad i \in N_{exc}$$

Note that we use "post-pre" notation for the weight matrices J^{XY} such that the weights from presynaptic population Y onto postsynaptic population X. The kinetics of synaptic currents were determined by the function $s_{syn}(x, y, t)$ for each presynaptic unit y and postsynaptic unit x. When a presynaptic spike occurred in unit y at time t^*, $s_{syn}(x, y, t)$ was incremented by an amount described by a delayed difference of exponentials equation [227]:

$$\Delta s_{ij}(t) = \frac{\tau_m}{\tau_d - \tau_r}\left[\exp\left(-\frac{t - \tau_l - t^*}{\tau_d}\right) - \exp\left(-\frac{t - \tau_l - t^*}{\tau_r}\right)\right]$$

where τ_m indicated the postsynaptic membrane time constant. Thus, the temporal envelope of a synaptic current was determined by the synaptic delay τ_l, the synaptic rise time τ_r, and the synaptic decay time τ_d, which differed for excitatory and inhibitory synapses (see Table 2). Normalization constants were chosen so that varying synaptic time constants would not affect the time integral of the synaptic current. The synaptic delay τ_l was uniformly distributed between 0 and 1 ms (0 and 0.5 ms) across all excitatory (inhibitory) synapses. Default values for synaptic parameters can be found in Table 2. Weight matrices JEE, JEI, JIE, and JII were pre-defined to contain normally-distributed weights that were capable of supporting stable Up-states with empirically observed firing rates [228]. The average value of the non-zero elements of JEE, JEI, JIE, and JII are shown in Table 2. Neither JEE nor JII had non-zero diagonal elements; in other words, there were no autapses (self-connections). In some simulations (Figure 6), the weight matrix JEE was modified based on empirical observations. Specifically, E units were first divided into two populations (Ex- and Ex+) consisting of 1400 and 200 units respectively, and 50% of the mutual connections between the Ex- and Ex+ units were randomly deleted, which reduced the probability of connection between the Ex- and Ex+ populations from 25% to 12.5%. In order to prevent a large imbalance of excitation and inhibition from causing spurious model behavior, J^{EI} was also modified by deleting a number of inhibitory connections equivalent to the deleted excitatory connections of that same postsynaptic population.

In order to model the stochastic process by which Up-states are initiated, we simulated 60 second trials in which external “kicks” [197, 229] were applied to a subpopulation of 100 Ex units (these units were always Ex- units for simulations with

subpopulations of Ex+ units). To do so, we first defined kick times by randomly generating a Poisson process with the mean parameter $\lambda = 0.2\,Hz$ over the 60 second trial period. At each kick time, the subpopulation of 100 kicked Ex units each received a large excitatory synaptic current with an equivalent synaptic weight of 960 pA, which typically caused exactly one spike. Spike times of all Inh units were used to construct a post-stimulus time histogram (PSTH) with a bin size of 10 ms. Up-states were detected as contiguous periods of time in which the population FR of inhibitory neurons exceeded 0.2 Hz for at least 500 ms, and fluctuations beneath the 0.2 Hz threshold that were shorter than 100 ms were considered interruptions of an Up-state. For each Up-state, the FR of each unit was calculated as the number of spikes it fired during that Up state divided by that Up state's duration. Each unit's average FR during the Up state was then calculated as the mean FR across all Up-states in the 60 s trial, yielding distinct values for each unit. Up-state voltage correlation among all pairwise units was calculated using identical methodology to what was used for the experimental data. Pairwise correlations between units in different populations were then separated. A total of 10 60-second simulations were run for each manipulation (control, intrinsic excitability, or connectivity) where the initial weight matrix would undergo a random shuffling of weights within each weight class. The average Up-state firing rate of each population per simulation was used as the unit of observation for analyses in Figures 5E and 6C. The average pairwise Up-state voltage correlation within each population of neurons per simulation was used as the unit of observation for analyses in Figures 5F and 6D. Simulations were implemented in the Brian 2 library [230] on Python 3.7 using forward Euler integration with a time step of 0.1 ms. Code is available at: https://github.com/BuonoLab/spiking-upstates/tree/liu-et-al

Cell Parameter	Symbol	Ex-	Ex+	Inh	Unit
Resting potential	E_L	-65	-65	-65	mV
Reset potential	V_{reset}	-58	-58	-58	mV
Spike threshold	V_{thresh}	-52	-46	-43	mV
Refractory period	$\tau_{refractory}$	2.5	2.5	1	ms
Membrane capacitance	C_m	200	240	120	pF
Leak conductance	g_L	10	8	8	nS
Membrane time constant	τ	20	30	15	ms
Adaptation strength	β	10	10	1	nA·ms
Adaptation time constant	τ_a	500	500	500	ms
Noise standard deviation	σ	1	1	1	mV

Table 1. Unit parameters.

Synaptic Parameter	Value	Unit
Average E-to-E weight	252	pA
Average E-to-I weight	264	pA
Average I-to-E weight	308	pA
Average I-to-I weight	282	pA
Excitatory rise time	8	ms
Excitatory fall time	23	ms
Inhibitory rise time	1	ms
Inhibitory fall time	1	ms
Mean excitatory synaptic delay	1	ms
Mean inhibitory synaptic delay	0.5	ms

Table 2. Synaptic parameters.

2.6 Figures

Figure 1

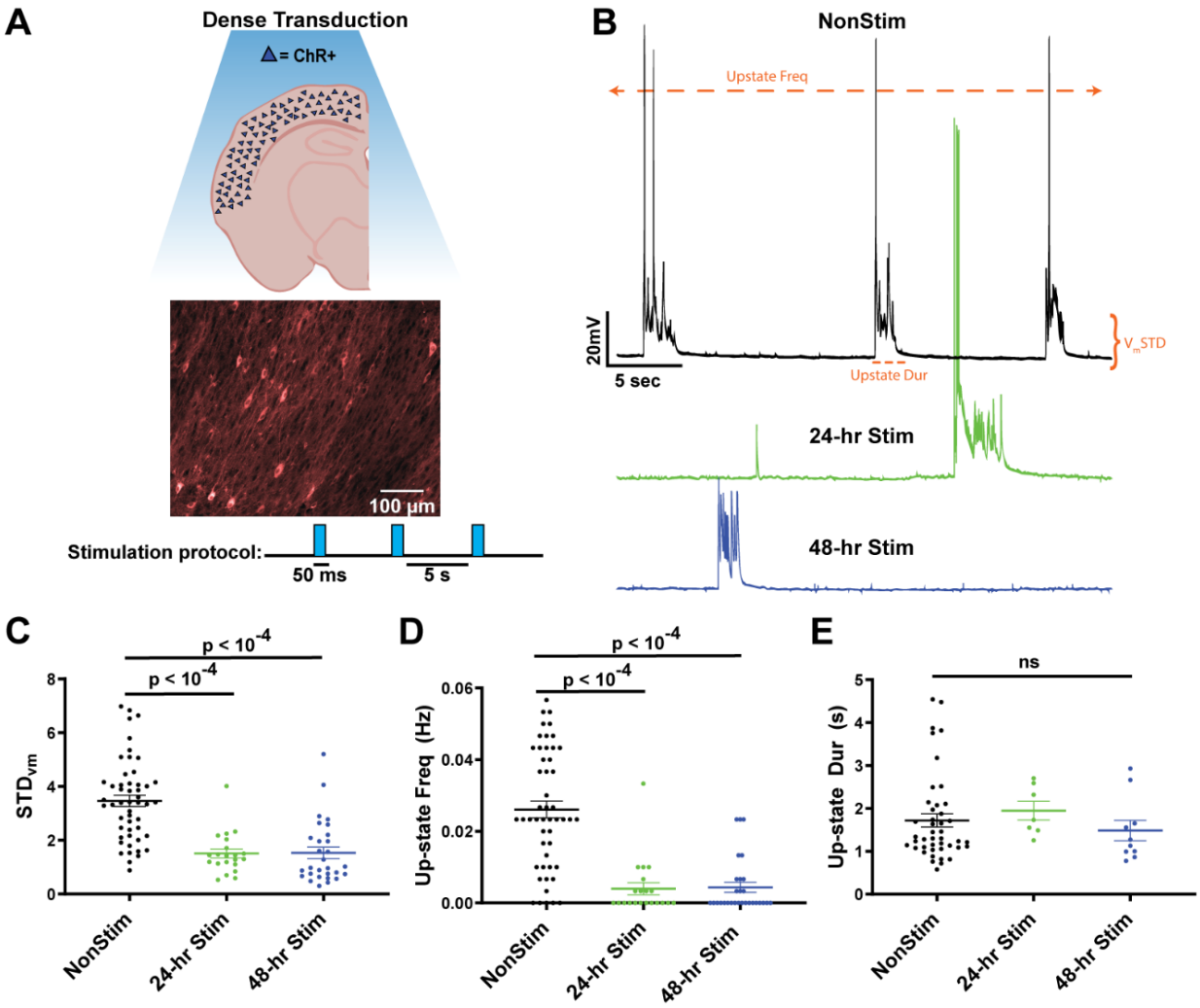

Spontaneous Up-state frequency is reduced in densely transduced cortical slices following 24- or 48-hrs of stimulation. A, Schematic of densely transduced cortical circuits in organotypic slice cultures (top) and image from auditory cortex densely transduced with AAV9-CaMKIIa-hChR2(H134R)-mCherry and chronic optogenetic stimulation paradigm (bottom). **B,** Example traces of spontaneous Up-states in Pyramidal neurons from unstimulated (black), 24-hr stimulated (green), and 48-hr stimulated (blue) slices. Up-states were rarely observed in the 24- and 48-hr stimulated slices. Orange annotations represent the three quantitative measures of spontaneous activity shown in panels C-E. **C,** The standard deviation of membrane voltage was significantly decreased by both 24- and 48-hrs of stimulation. STDVm was calculated over a 5-minute period of spontaneous activity in Pyr neurons. **D,** Spontaneous Up-state frequency was significantly decreased by both 24- and 48-hrs of stimulation. **E,** Although Up-state frequency was decreased by stimulation, when Up-states occurred, on average they were of the same duration.

Figure 2

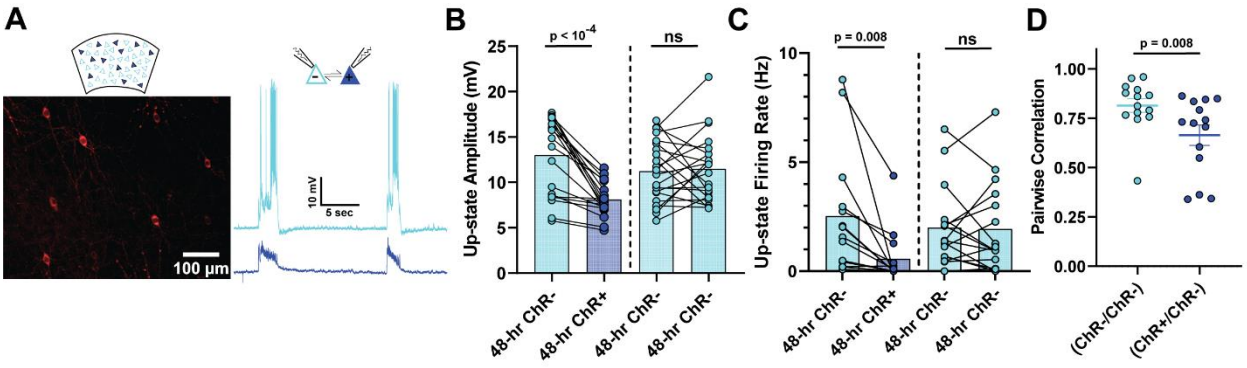

Pairwise differences in Up-state amplitude, firing rate, and voltage correlation between stimulated and non-stimulated pyramidal neurons in sparsely transduced slices. A, Example of cortical pyramidal neurons sparsely transduced with AAV9-CaMKIIa-Cre and EF1a-DIO-hChR2(H134R)-mCherry (left), and sample paired recordings of ChR^+ and ChR^- neurons (right). **B,** Spontaneous Up-state amplitude was significantly reduced in ChR^+ compared to ChR^- pyramidal neurons. Up-state amplitude was not significantly different between simultaneously recorded ChR^+ pyramidal neurons grouped according to their resting membrane potential (ChR^- pyramidal neurons with the lower resting membrane potential of the pair was plotted on the left). **C,** Spontaneous Up-state firing rate was significantly reduced in ChR^+ vs ChR^- pyramidal neurons. Up-state firing rate was not significantly different between simultaneously recorded ChR^- pyramidal neurons grouped according to their resting membrane potential. **D,** The correlation between the Up-state voltage dynamics of ChR^+ and ChR^- neurons was significantly less than ChR^- and ChR^- pairs, indicating a decorrelation between the shared inputs to the ChR^+ and ChR^- subpopulations.

Figure 3

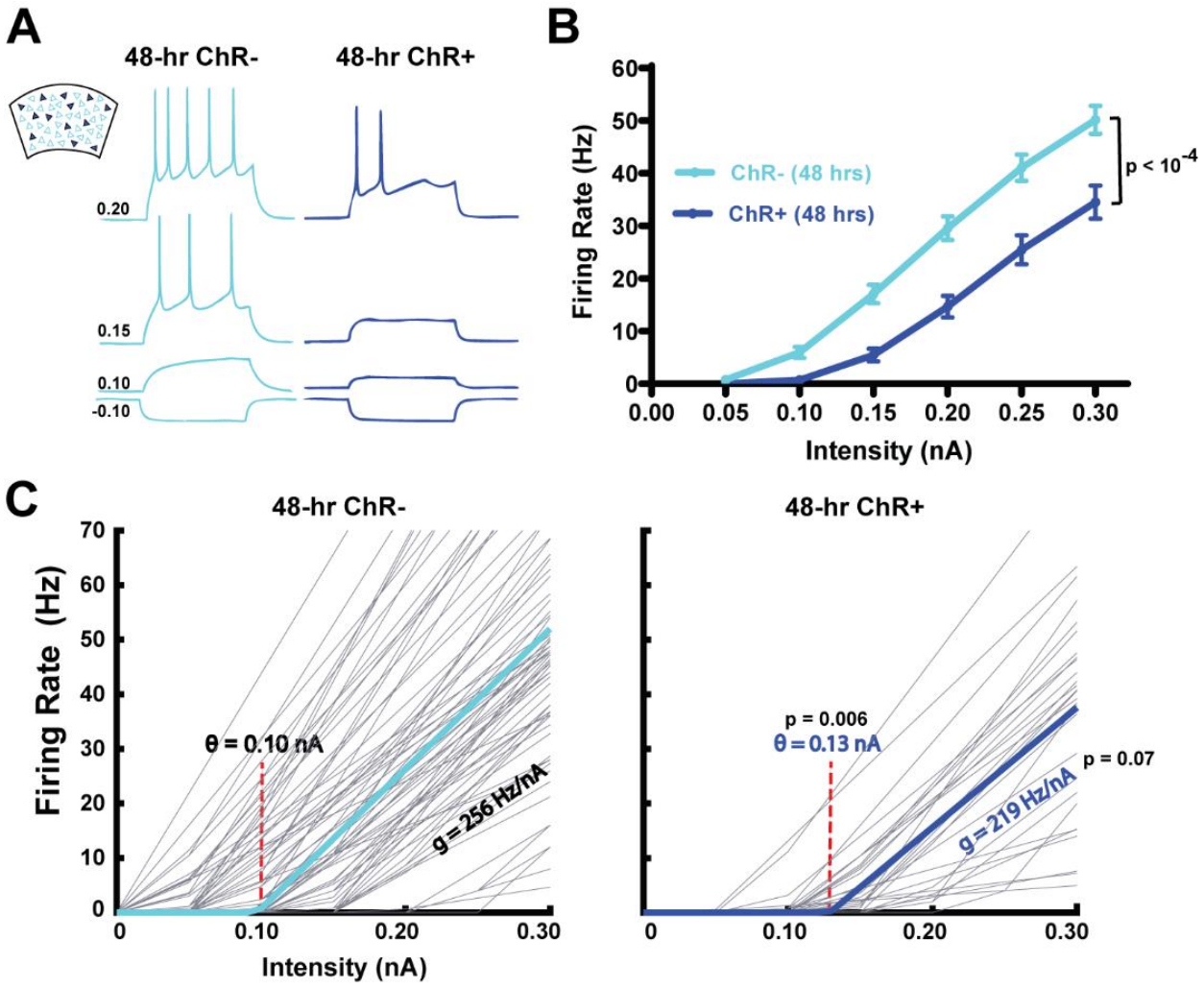

Cell-autonomous decreases in the intrinsic input-output function of ChR$^+$ compared with ChR$^-$ pyramidal neurons in sparsely transduced slices. A, Sample intrinsic excitability traces simultaneously recorded from ChR$^-$ and ChR$^+$ pyramidal neurons from sparsely transduced cortical circuits stimulated for 48-hrs (250 ms current steps ranged from -0.10 to 0.3 nA). **B,** F-I curves of the average input-output functions from ChR$^-$ and ChR$^+$ pyramidal neurons from sparsely transduced cortical slices stimulated for 48-hrs. **C,** Threshold-linear fits of the F-I curves of the ChR$^-$ and ChR$^+$ populations. Light gray lines are the fits of the F-I curves of individual neurons, and solid cyan or blue lines are the mean threshold-linear fit. The threshold (θ=0.10nA) of the ChR$^-$ Pyr neurons was significantly lower than the ChR$^+$ Pyr neurons (θ=0.13nA).

Figure 4

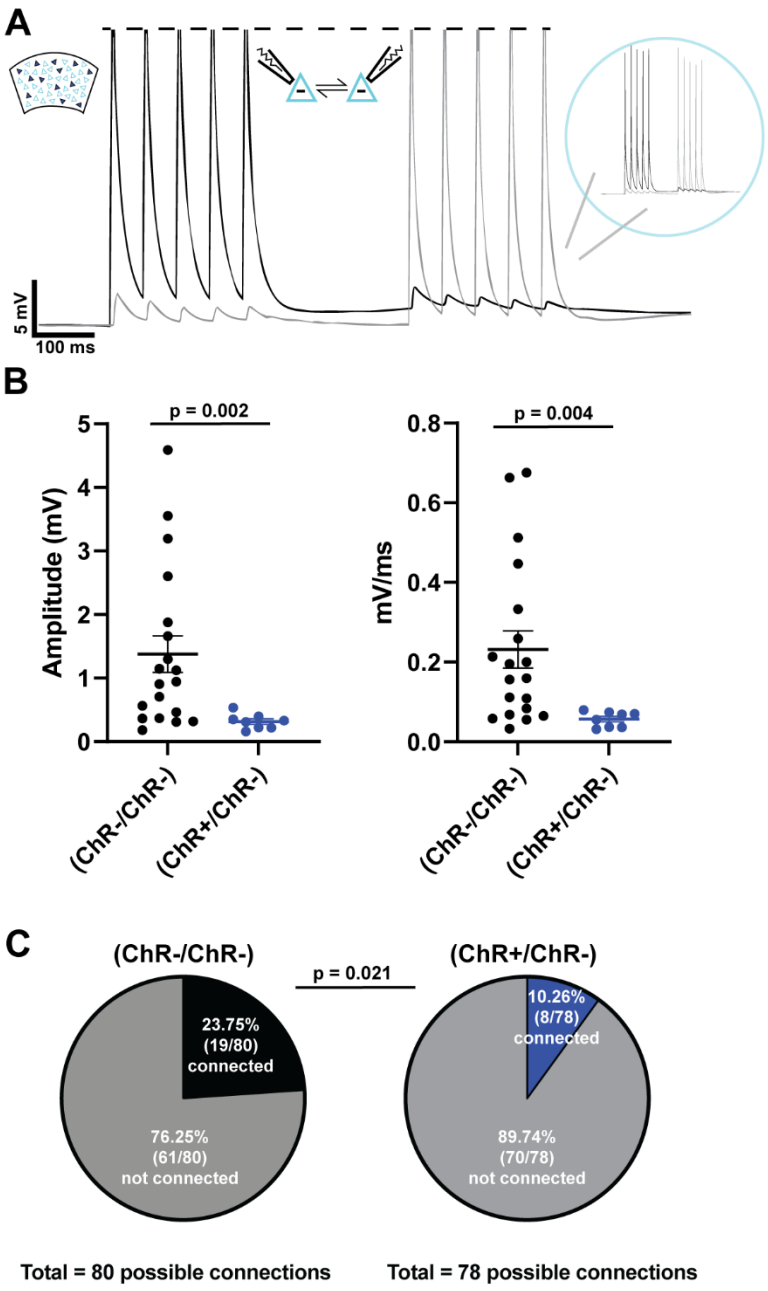

Synaptic decoupling between ChR$^+$ and ChR$^-$ pyramidal neurons. A, Example traces of a paired recording between reciprocally connected ChR$^-$ and ChR$^-$ pyramidal neurons (<50 um apart). **B,** EPSP amplitude and slope were significantly reduced between connected pairs of ChR$^+$ and ChR$^-$ pyramidal neurons compared to connected pairs of ChR$^-$ pyramidal neurons following 48-hrs of stimulation. **C,** Connectivity ratio was higher between pairs of ChR$^-$ pyramidal neurons compared to pairs of ChR$^+$ and ChR$^-$ pyramidal neurons.

Figure 5

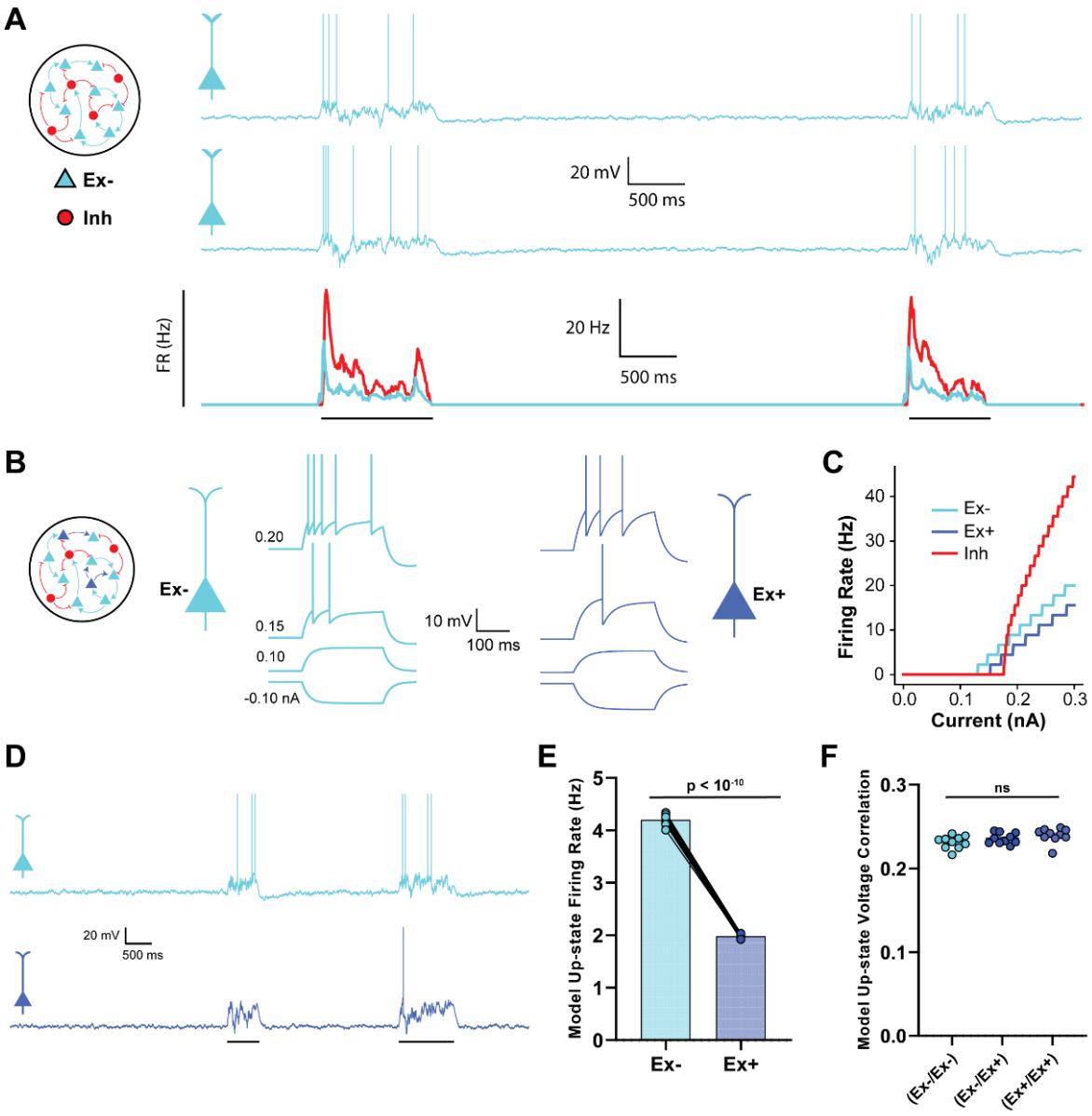

Empirically observed changes in intrinsic excitability is sufficient to account for cluster-specific changes in firing rate. A, The neural network model was composed of 2000 adaptive IAF units (1600 Ex, 400 Inh). Traces show two example Up-states in two sample Ex units in the baseline model. Average firing rate of all excitatory and inhibitory neurons during an Up-state is shown below. **B,** In the experimental network there were two populations of Ex units (Ex+ and Ex-) with different intrinsic excitability. Spike threshold, leak conductance, and membrane capacitance parameters differed between the Ex- and Ex+ units. Traces show the response to 250 ms square waves of injected current. **C,** F-I curves comparing the spiking output of the Ex+, Ex-, and Inh units. The difference in spike threshold and slope for the Ex- and Ex+ units qualitatively match empirical findings. **D,** Sample Up-states in the experimental neural network. **E,** Average firing rates of Ex- and Ex+ units during Up-states were significantly different. **F,** the mean pairwise correlations between the Ex-/Ex-, Ex-/Ex+, and Ex+/Ex+ pairs were not significantly different (data from ten simulations).

Figure 6

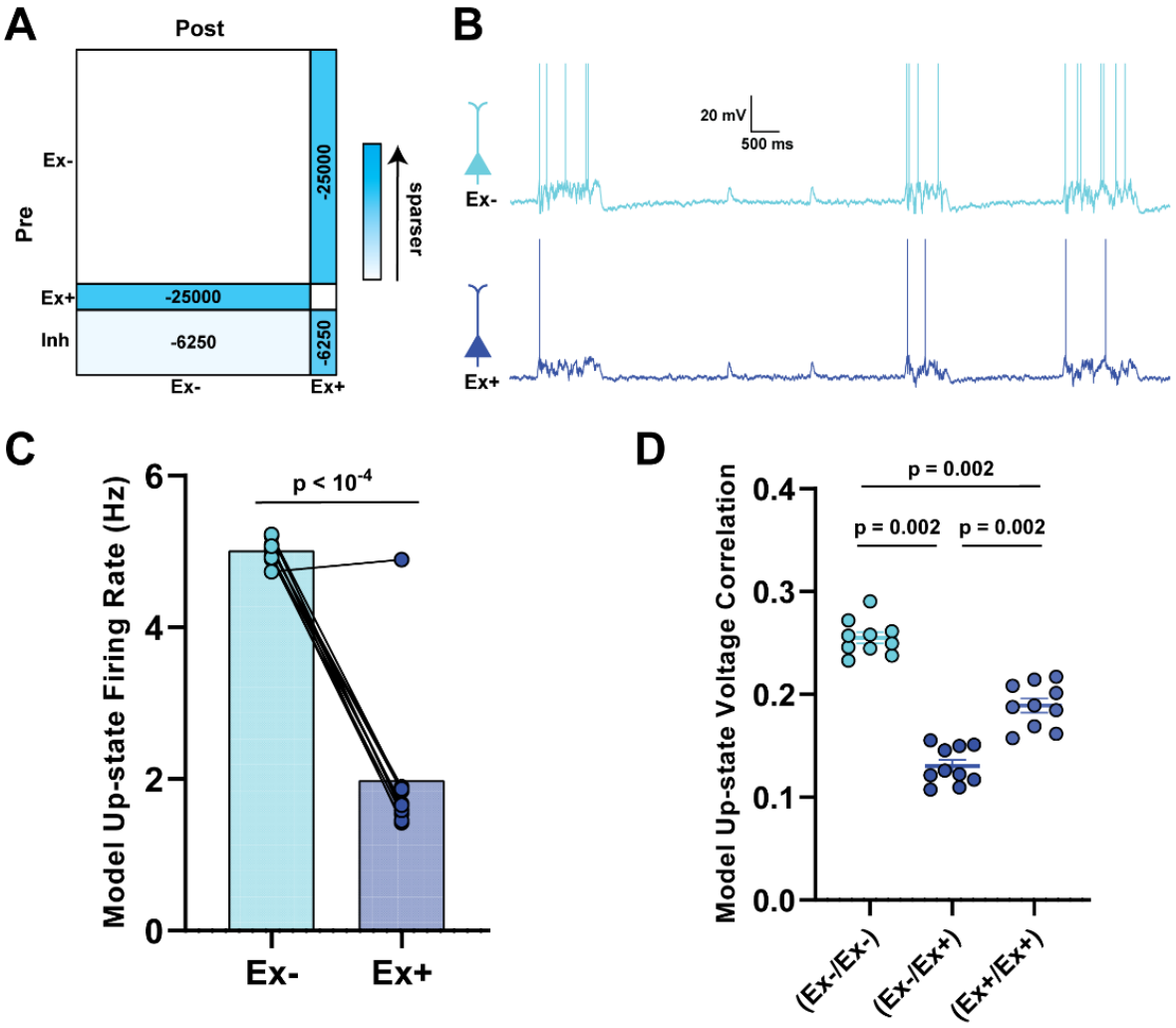

Empirically observed changes in probability of connection is sufficient to account for cluster-specific differences in firing rates and correlations. A, Schematic of the changes made to the weight matrix in comparison with the baseline network in Figure 5a. **B,** Sample Up-states following manipulation of the synaptic coupling between Ex+ and Ex- populations. **C,** Average firing rates of Ex- and Ex+ units during Up-states were significantly different. **D,** There was a significant decrease in the mean pairwise Ex-/Ex+ correlations compared to the Ex-/Ex- and Ex+/Ex+ correlations, as well as a weaker correlation in the Ex+/Ex+ compared to Ex-/Ex- pairs. Note that because the correlations are bounded between -1 and 1, we are using nonparametric sign-rank statistics, thus all p values can be the same despite the differences in the group values.

2.7 References Cited

38. Hebb, D.O., *Organization of behavior*. 1949, New York: Wiley.

92. Burrone, J., M. O'Byrne, and V.N. Murthy, *Multiple forms of synaptic plasticity triggered by selective suppression of activity in individual neurons.* Nature, 2002. **420**(6914): p. 414-8.

95. Goold, C.P. and R.A. Nicoll, *Single-cell optogenetic excitation drives homeostatic synaptic depression.* Neuron, 2010.

102. Desai, N.S., L.C. Rutherford, and G.G. Turrigiano, *Plasticity in the intrinsic excitability of cortical pyramidal neurons.* Nat Neurosci, 1999. **2**(6): p. 515-20.

108. Maffei, A. and G.G. Turrigiano, *Multiple modes of network homeostasis in visual cortical layer 2/3.* J Neurosci, 2008. **28**(17): p. 4377-84.

112. Grubb, M.S. and J. Burrone, *Activity-dependent relocation of the axon initial segment fine-tunes neuronal excitability.* Nature, 2010. **465**(7301): p. 1070-1074.

114. Cossart, R., D. Aronov, and R. Yuste, *Attractor dynamics of network UP states in the neocortex.* Nature, 2003. **423**(6937): p. 283-288.

115. Gerstein, G.L., P. Bedenbaugh, and A.M.H.J. Aertsen, *Neuronal assemblies.* IEEE Transactions on Biomedical Engineering, 1989. **36**(1): p. 4-14.

116. Carrillo-Reid, L. and R. Yuste, *What Is a Neuronal Ensemble?* Oxford Research Encyclopedia of Neuroscience, 2020.

117. Buzsáki, G., *Neural Syntax: Cell Assemblies, Synapsembles, and Readers.* Neuron, 2010. **68**(3): p. 362-385.

133. Carrillo-Reid, L., et al., *Controlling Visually Guided Behavior by Holographic Recalling of Cortical Ensembles.* Cell, 2019.

134. Carrillo-Reid, L., et al., *Imprinting and recalling cortical ensembles.* Science, 2016. **353**(6300): p. 691-4.

136. MacLean, J.N., et al., *Internal Dynamics Determine the Cortical Response to Thalamic Stimulation.* Neuron, 2005. **48**(5): p. 811-823.

142. Marshel, J.H., et al., *Cortical layer-specific critical dynamics triggering perception.* Science, 2019. **365**(6453): p. eaaw5202.

162. Goel, A. and D.V. Buonomano, *Temporal Interval Learning in Cortical Cultures Is Encoded in Intrinsic Network Dynamics.* Neuron, 2016. **91**: p. 320-327.

164. Douglas, R.J., et al., *Recurrent excitation in neocortical circuits.* Science, 1995.

269(5226): p. 981-5.

165. Yuste, R., *From the neuron doctrine to neural networks.* Nat Rev Neurosci, 2015. **16**(8): p. 487-497.

166. Barack, D.L. and J.W. Krakauer, *Two views on the cognitive brain.* Nature Reviews Neuroscience, 2021.

167. Stringer, C., et al., *High-dimensional geometry of population responses in visual cortex.* Nature, 2019. **571**(7765): p. 361-365.

168. Perez-Ortega, J., T. Alejandre-Garcia, and R. Yuste, *Long-term stability of cortical ensembles.* 2021.

169. Johansen, J.P., et al., *Optical activation of lateral amygdala pyramidal cells instructs associative fear learning.* Proceedings of the National Academy of Sciences, 2010. **107**(28): p. 12692-12697.

170. Kim, T., et al., *Emergence of functional subnetworks in layer 2/3 cortex induced by sequential spikes in vivo.* Proceedings of the National Academy of Sciences, 2016. **113**(10): p. E1372-E1381.

171. Mendez, P., et al., *Homeostatic Plasticity in the Hippocampus Facilitates Memory Extinction.* Cell Reports, 2018. **22**(6): p. 1451-1461.

172. Sadeh, S. and C. Clopath, *Excitatory-inhibitory balance modulates the formation and dynamics of neuronal assemblies in cortical networks.* Science Advances, 2021. **7**(45): p. eabg8411.

173. Sanchez-Vives, M.V. and D.A. McCormick, *Cellular and network mechanisms of rhythmic recurrent activity in neocortex.* Nat Neurosci, 2000. **3**(10): p. 1027-34.

174. Neske, G.T., S.L. Patrick, and B.W. Connors, *Contributions of Diverse Excitatory and Inhibitory Neurons to Recurrent Network Activity in Cerebral Cortex.* The Journal of Neuroscience, 2015. **35**(3): p. 1089-1105.

175. Bartram, J., et al., *Cortical Up states induce the selective weakening of subthreshold synaptic inputs.* Nature Communications, 2017. **8**(1): p. 665.

176. Steriade, M., D. McCormick, and T. Sejnowski, *Thalamocortical oscillations in the sleeping and aroused brain.* Science, 1993. **262**(5134): p. 679-685.

177. Timofeev, I., et al., *Origin of slow cortical oscillations in deafferented cortical slabs.* Cereb Cortex, 2000. **10**(12): p. 1185-99.

178. Beltramo, R., et al., *Layer-specific excitatory circuits differentially control recurrent network dynamics in the neocortex.* Nat Neurosci, 2013. **16**(2): p. 227-234.

179. Hromádka, T., A.M. Zador, and M.R. DeWeese, *Up states are rare in awake auditory cortex.* Journal of Neurophysiology, 2013. **109**(8): p. 1989-1995.

180. Shu, Y., A. Hasenstaub, and D.A. McCormick, *Turning on and off recurrent balanced cortical activity.* Nature, 2003. **423**: p. 288-293.

181. Fanselow, E.E. and B.W. Connors, *The Roles of Somatostatin-Expressing (GIN) and Fast-Spiking Inhibitory Interneurons in up-down States of Mouse Neocortex.* Journal of Neurophysiology, 2010. **104**(2): p. 596-606.

182. Sippy, T. and R. Yuste, *Decorrelating Action of Inhibition in Neocortical Networks.* The Journal of Neuroscience, 2013. **33**(23): p. 9813-9830.

183. Xu, H., et al., *Neocortical Somatostatin-Expressing GABAergic Interneurons Disinhibit the Thalamorecipient Layer 4.* Neuron, 2013. **77**(1): p. 155-167.

184. Sadovsky, A.J. and J.N. MacLean, *Mouse Visual Neocortex Supports Multiple Stereotyped Patterns of Microcircuit Activity.* The Journal of Neuroscience, 2014. **34**(23): p. 7769-7777.

185. Plenz, D. and S.T. Kitai, *Up and down states in striatal medium spiny neurons simultaneously recorded with spontaneous activity in fast-spiking interneurons studied in cortex-striatum-substantia nigra organotypic cultures.* J Neurosci, 1998. **18**(1): p. 266-83.

186. Seamans, J.K., L. Nogueira, and A. Lavin, *Synaptic Basis of Persistent Activity in Prefrontal Cortex In Vivo and in Organotypic Cultures.* Cerebral Cortex, 2003. **13**(11): p. 1242-1250.

187. Johnson, H.A. and D.V. Buonomano, *Development and Plasticity of Spontaneous Activity and Up States in Cortical Organotypic Slices.* J. Neurosci., 2007. **27**(22): p. 5915-5925.

188. Kroener, S., et al., *Dopamine Modulates Persistent Synaptic Activity and Enhances the Signal-to-Noise Ratio in the Prefrontal Cortex.* PLoS ONE, 2009. **4**(8): p. e6507.

189. Motanis, H. and D. Buonomano, *Decreased reproducibility and abnormal experience-dependent plasticity of network dynamics in Fragile X circuits.* Scientific Reports, 2020. **10**(1): p. 14535.

190. Motanis, H. and D.V. Buonomano, *Delayed in vitro development of Up states but normal network plasticity in Fragile X circuits.* European Journal of Neuroscience, 2015.

191. Hengen, Keith B., et al., *Neuronal Firing Rate Homeostasis Is Inhibited by Sleep and Promoted by Wake.* Cell, 2016. **165**(1): p. 180-191.

192. Slomowitz, E., et al., *Interplay between population firing stability and single neuron dynamics in hippocampal networks.* eLife, 2015. **4**: p. e04378.

193. Turrigiano, G., *Homeostatic synaptic plasticity: local and global mechanisms for stabilizing neuronal function.* Cold Spring Harbor perspectives in biology, 2012. **4**(1): p. a005736-a005736.

194. Turrigiano, G.G., *The Self-Tuning Neuron: Synaptic Scaling of Excitatory Synapses.* Cell 2008.

195. Karmarkar, U.R. and D.V. Buonomano, *Different forms of homeostatic plasticity are engaged with distinct temporal profiles.* European Journal of Neuroscience, 2006.

196. Romero-Sosa, J.L., H. Motanis, and D.V. Buonomano, *Differential Excitability of PV and SST Neurons Results in Distinct Functional Roles in Inhibition Stabilization of Up States.* The Journal of Neuroscience, 2021. **41**(34): p. 7182-7196.

197. Jercog, D., et al., *UP-DOWN cortical dynamics reflect state transitions in a bistable network.* eLife, 2017. **6**: p. e22425.

198. Tsodyks, M.V., et al., *Paradoxical Effects of External Modulation of Inhibitory Interneurons.* The Journal of Neuroscience, 1997. **17**(11): p. 4382-4388.

199. Ozeki, H., et al., *Inhibitory Stabilization of the Cortical Network Underlies Visual Surround Suppression.* Neuron, 2009. **62**(4): p. 578-592.

200. Destexhe, A., *Self-sustained asynchronous irregular states and Up–Down states in thalamic, cortical and thalamocortical networks of nonlinear integrate-and-fire neurons.* Journal of Computational Neuroscience, 2009. **27**(3): p. 493.

201. Maes, A., M. Barahona, and C. Clopath, *Learning spatiotemporal signals using a recurrent spiking network that discretizes time.* PLOS Computational Biology, 2020. **16**(1): p. e1007606.

202. Gainey, M.A. and D.E. Feldman, *Multiple shared mechanisms for homeostatic plasticity in rodent somatosensory and visual cortex.* Philos Trans R Soc Lond B Biol Sci, 2017. **372**(1715).

203. Tetzlaff, C., et al., *Synaptic Scaling in Combination with Many Generic Plasticity Mechanisms Stabilizes Circuit Connectivity.* Frontiers in Computational Neuroscience, 2011. **5**.

204. Wefelmeyer, W., C.J. Puhl, and J. Burrone, *Homeostatic Plasticity of Subcellular Neuronal Structures: From Inputs to Outputs.* Trends in neurosciences, 2016. **39**(10): p. 656-667.

205. Hennequin, G., E.J. Agnes, and T.P. Vogels, *Inhibitory Plasticity: Balance, Control,*

and Codependence. Annual Review of Neuroscience 2017.

206. Froemke, R.C., *Plasticity of cortical excitatory-inhibitory balance.* Annu Rev Neurosci., 2015.

207. Pozo, K. and Y. Goda, *Unraveling mechanisms of homeostatic synaptic plasticity.* Neuron, 2010. **66**(3): p. 337-51.

208. Tononi, G. and C. Cirelli, *Sleep and synaptic homeostasis: a hypothesis.* Brain Research Bulletin, 2003. **62**(2): p. 143-150.

209. Diekelmann, S. and J. Born, *The memory function of sleep.* Nature Reviews Neuroscience, 2010. **11**: p. 114.

210. Marshall, L., et al., *Boosting slow oscillations during sleep potentiates memory.* Nature, 2006. **444**: p. 610.

211. Vyazovskiy, V.V., et al., *Molecular and electrophysiological evidence for net synaptic potentiation in wake and depression in sleep.* Nature Neuroscience, 2008. **11**: p. 200.

212. Sirota, A. and G. Buzsáki, *Interaction between neocortical and hippocampal networks via slow oscillations.* Thalamus & Related Systems, 2007. **3**(4): p. 245-259.

213. Goel, A. and D.V. Buonomano, *Chronic electrical stimulation homeostatically decreases spontaneous activity, but paradoxically increases evoked network activity.* Journal of Neurophysiology, 2013. **109**(7): p. 1824-1836.

214. Trojanowski, N.F., J. Bottorff, and G.G. Turrigiano, *Activity labeling in vivo using CaMPARI2 reveals intrinsic and synaptic differences between neurons with high and low firing rate set points.* Neuron, 2021. **109**(4): p. 663-676.e5.

215. Sugden, A.U., et al., *Cortical reactivations of recent sensory experiences predict bidirectional network changes during learning.* Nature Neuroscience, 2020. **23**(8): p. 981-991.

216. Dechery, J.B. and J.N. MacLean, *Emergent cortical circuit dynamics contain dense, interwoven ensembles of spike sequences.* Journal of Neurophysiology, 2017. **118**(3): p. 1914-1925.

217. DeNardo, L.A., et al., *Temporal evolution of cortical ensembles promoting remote memory retrieval.* Nature Neuroscience, 2019. **22**(3): p. 460-469.

218. Nigam, S., et al., *Rich-Club Organization in Effective Connectivity among Cortical Neurons.* The Journal of Neuroscience, 2016. **36**(3): p. 670-684.

219. Karmarkar, U.R. and D.V. Buonomano, *Different forms of homeostatic plasticity*

are engaged with distinct temporal profiles. Eur J Neurosci, 2006. **23**(6): p. 1575-84.

220. Debanne, D., Y. Inglebert, and M. Russier, *Plasticity of intrinsic neuronal excitability.* Current Opinion in Neurobiology, 2019. **54**: p. 73-82.

221. Maffei, A., S.B. Nelson, and G.G. Turrigiano, *Selective reconfiguration of layer 4 visual cortical circuitry by visual deprivation.* Nat Neurosci, 2004. **7**(12): p. 1353-9.

222. Zbili, M., et al., *Homeostatic regulation of axonal Kv1.1 channels accounts for both synaptic and intrinsic modifications in the hippocampal CA3 circuit.* Proceedings of the National Academy of Sciences, 2021. **118**(47): p. e2110601118.

223. Walcott, E.C., E.A. Higgins, and N.S. Desai, *Synaptic and Intrinsic Balancing during Postnatal Development in Rat Pups Exposed to Valproic Acid in Utero.* The Journal of Neuroscience, 2011. **31**(37): p. 13097-13109.

224. Watt, A. and N. Desai, *Homeostatic plasticity and STDP: keeping a neuron's cool in a fluctuating world.* Frontiers in Synaptic Neuroscience, 2010. **2**.

225. Turrigiano, G.G., *Too Many Cooks? Intrinsic and Synaptic Homeostatic Mechanisms in Cortical Circuit Refinement.* Annual Review of Neuroscience, 2011.

226. Stoppini, L., P.A. Buchs, and D. Muller, *A simple method for organotypic cultures of nervous tissue.* J Neurosci Methods, 1991. **37**(2): p. 173-82.

227. Brunel, N. and X.J. Wang, *What determines the frequency of fast network oscillations with irregular neural discharges? I. Synaptic dynamics and excitation-inhibition balance.* J Neurophysiol, 2003. **90**(1): p. 415-30.

228. Soldado-Magraner, S., et al., *Orchestrated Excitatory and Inhibitory Learning Rules Lead to the Unsupervised Emergence of Up-states and Balanced Network Dynamics.* bioRxiv, 2021: p. 2020.12.30.424888.

229. DeWeese, M.R. and A.M. Zador, *Non-Gaussian Membrane Potential Dynamics Imply Sparse, Synchronous Activity in Auditory Cortex.* J. Neurosci., 2006. **26**(47): p. 12206-12218.

230. Stimberg, M., R. Brette, and D.F. Goodman, *Brian 2, an intuitive and efficient neural simulator.* Elife, 2019. **8**.

Chapter 3: Ex Vivo Cortical Circuits Learn to Predict and Spontaneously Replay Temporal Patterns

3.1 Summary

It has been proposed that prediction and timing are computational primitives of neocortical microcircuits, specifically, that neural mechanisms are in place to allow neocortical circuits to autonomously learn the temporal structure of external stimuli and generate internal predictions. To test this hypothesis, we differentially trained cortical organotypic slices on two specific temporal patterns using dual-optical stimulation. After 24-hours of training, whole-cell recordings revealed network dynamics consistent with training-specific timed prediction. Unexpectedly, there was replay of the learned temporal structure during spontaneous activity. Furthermore, some neurons exhibited timed prediction errors. Mechanistically our results indicate that learning relied in part on asymmetric connectivity between distinct neuronal ensembles with temporally-ordered activation. These findings further suggest that local cortical microcircuits are intrinsically capable of learning temporal information and generating predictions, and that the learning rules underlying temporal learning and spontaneous replay are intrinsic to local cortical microcircuits and not necessarily dependent on top-down interactions.

3.2 Introduction

The ability to predict and prepare for external events is among the most important

computations the brain performs. Timing is a critical component of prediction because it is often necessary to predict when future events will occur. Given their critical role in perception, behavior, and cognition, it has been proposed that prediction and timing are computational primitives of neocortical microcircuits [146-149]. Specifically, that neural mechanisms are in place to allow local neocortical microcircuits to autonomously learn the temporal structure of external stimuli and generate internal predictions of when subsequent stimuli will arrive. Testing this hypothesis *in vivo* is challenging because local cortical microcircuits are difficult to study in the presence of upstream and downstream influences. The view that cortical microcircuits are, in effect, programmed to learn and perform certain types of computations leads to the hypothesis that some simple computations can be observed and studied in reduced preparations. Indeed, prior studies have shown that *in vitro* (here defined as dissociated cultures or acute slices) and *ex vivo* (cortical organotypic cultures or organoids) circuits have the ability to perform simple forms of pattern recognition and learning [154, 161, 162, 231-234]. These reduced model systems provide insight into the extent to which local cortical circuits, independent of broader brain systems, can perform and learn simple computations.

Here we used cortical organotypic cultures as an *ex vivo* approach to determine whether neocortical circuits can autonomously learn to predict the temporal structure of chronically presented stimuli and study the underlying mechanisms. Cortical organotypic cultures are well-suited to bridge conventional *in vitro* and *in vivo* approaches as they preserve much of the local *in vivo* neocortical microarchitecture [187, 235-240]. Additionally, the synaptic learning rules observed in acute slices and *in vivo* are present in organotypic slices, indeed a number of early studies of synaptic plasticity were

performed in organotypic cultures [241-248]. Furthermore, and critical to our goals, organotypic slices provide a tractable way to fully control “sensory” experience and to study forms of learning that may take hours or days to develop.

Importantly, organotypic cultures also exhibit internally generated activity, consistent with the balanced regimes of inhibition stabilized networks [185, 196, 249, 250]. This form of activity is characterized by spontaneous, self-sustained, neural dynamics driven by recurrent excitation and held in check by inhibition [198, 199, 251]. Thus, providing a unique opportunity to study emergent dynamic regimes that are generally only studied in vivo, including prediction, timing, and replay. Replay is generally defined as the spontaneous reactivation of activity patterns during resting or sleep states that mirror the spatiotemporal structure of activity that occurred during prior learning or behavior [215, 252-258]. These “offline” spontaneous reactivations of patterned activity observed during recent waking experience is in itself a form of network level learning and may serve a purpose in the consolidation of memories or information by further engaging neural plasticity and synaptic restructuring mechanisms.

To study the learning of network-level computations, *ex vivo* cortical pyramidal neurons were sparsely transduced with either Channelrhodopsin2 or ChrimsonR. Training consisted of the presentation of trains of red and blue light pulses separated by either a short (10 ms) or long (370 ms) interval for 24-hours. Following training, we observed robust differential dynamics evoked by red light alone that was consistent with prediction and learned timing. Unexpectedly, we also observed spontaneous replay of the learned temporal patterns. Such structured spontaneous activity [136-138] and replay [253, 255, 259-261] parallels *in vivo* studies. Overall, our results provide the first

demonstration that neocortical circuits are autonomously able to learn to generate timed prediction errors and replay. Consistent with the hypothesis that prediction, timing, and replay are computational primitives of neocortical microcircuits.

3.3 Results

We first established a dual-optical stimulation approach that leveraged sparse expression of Channelrhodopsin2 (ChR2) and ChrimsonR (Chrim) in cortical pyramidal neurons (**Fig. 1**). To achieve sparse and differential expression of both ChR2 and Chrim we utilized four different adeno-associated viruses (AAVs): [AAV9-CamKII(0.4)-Cre], [AAV9-CamKII(0.4)-FLPo], [AAV9-EF1a-DIO-hChR2(H134R)-EYFP], and [AAV8-CAG-FLPX-ChrimsonR-tdTomato]. Approximately 10-15% of total neurons expressed ChR2 or Chrim with no detectable overlap. Using whole-cell patch-clamp recordings, we confirmed that 5 ms pulses of blue light reliably induced single action potentials in ChR2-expressing ($ChR2^+$) neurons (see Methods). Similarly, 5 ms pulses of red light reliably induced single action potentials in Chrim-expressing ($Chrim^+$) neurons. As expected, red light did not produce detectable depolarization of $ChR2^+$ neurons, but blue light could produce mild subthreshold depolarization of $Chrim^+$ neurons [262, 263] in the presence of glutamate receptor antagonists (**Fig 1B**). As described below, our experimental design relies on the ability to differentially stimulate two subpopulations of neurons, thus the potential subthreshold crosstalk or co-expression of opsins does not influence our experimental protocol, which was designed with these potential constraints in mind.

Training protocols mirrored behavioral delay conditioning paradigms. A long train

of red light pulses (440 ms, 25 Hz) represented the “conditioned stimulus” (CS), and a shorter but higher frequency train of blue light pulses (80 ms, 50 Hz) represented the “unconditioned stimulus” (US). Mirroring the CS-US interstimulus intervals (ISIs) of behavioral studies, we used two red-blue light (CS-US) ISIs. In the Early condition, both stimuli were activated with similar onset times (10 ms ISI), while in the Late condition the ISI was 370 ms, with similar offset times (**Fig. 1C**). Our primary goal was to test the hypothesis that following 24-hours of chronic training, isolated neural circuits have the ability to learn to “predict” the presentation of the blue light at the appropriate time.

3.3.1 Cortical circuits learn the temporal structure of experienced patterns

To test whether the cortical circuits were able to successfully learn the trained intervals, we initially recorded the responses of opsin-negative ($Opsin^-$) and $ChR2^+$ pyramidal neurons to presentation of just the red light pulses alone (red-alone). Following 24-hours of training, recordings revealed differentially timed network dynamics in response to the red light pulses, which closely aligned with the corresponding training interval to which the slice was exposed. Specifically, in the Late, but not in the Early condition, presentation of red-alone generally elicited a marked late peak in network activity, suggesting the prediction of an expected (but absent) arrival of blue light stimulation (**Fig. 2A**). Qualitatively, both the averaged (**Fig. 2B**) and individual traces (**Fig. 2C**) revealed a large difference in temporal structure between the Early- and Late-training groups. These differences were confirmed by quantification of the temporal distribution of the evoked polysynaptic peak times between Early- and Late-trained slices (Kolmogorov-

Smirnov test, $p < 0.0001$; **Fig. 2D**). The mean times of the detected polysynaptic events were also significantly different (150 ± 26 ms and 479 ± 32 ms for Early and Late, respectively; $U = 97$, $n_{Early} = 30$, $n_{Late} = 35$, $p < 0.0001$, Mann–Whitney test; **Fig. 2E**). Similarly, the time of peak postsynaptic potential was significantly different between the Early and Late groups, with median latencies of 203 ± 40 ms and 648 ± 27 ms respectively ($U = 77$, $n_{Early} = 30$, $n_{Late} = 35$, $p < 0.0001$, Mann–Whitney test; **Fig. 2F**). Lastly, the time of the center of gravity of the mean response of each cell was also significantly different between neurons in Early- vs Late-trained slices ($U = 61$, $n_{Early} = 30$, $n_{Late} = 35$, $p < 0.0001$, Mann–Whitney test; **Fig. 2G**). Together, these results demonstrate that the temporal profile of evoked neural activity was differentially shaped in a training-dependent manner. This finding suggests that isolated cortical circuits are intrinsically capable of learning and predicting the temporal structure of experienced stimuli.

3.3.2 Cortical circuits spontaneously replay learned dynamics

In addition to the training-specific differences in the evoked neural dynamics, we also unexpectedly observed group-dependent differences in the spontaneous network activity. Indeed, the temporal structure of the spontaneous activity closely mirrored the learned, training-dependent, evoked network dynamics (**Fig. 3A**). Group averaged data revealed a robust training-dependent difference in the temporal structure of spontaneous events (**Fig 3B**). To quantify these differences, we isolated bouts of spontaneous activity and analyzed the temporal structure time-locked to the onset of each bout (see Methods). This was confirmed by multiple measures: differences in the distribution of spontaneous

event peak times (Kolmogorov-Smirnov test, $p < 0.0001$; **Fig 3C, D**), the median time of the detected polysynaptic events ($U = 36$, $n_{Early} = 24$, $n_{Late} = 21$, $p < 0.0001$, Mann–Whitney test; **Fig 3E**), the time of the spontaneous peak of the postsynaptic potential ($U = 11$, $n_{Early} = 24$, $n_{Late} = 21$, $p < 0.0001$, Mann–Whitney test; **Fig 3F**), and the mean center of gravity of spontaneous events ($U = 3$, $n_{Early} = 24$, $n_{Late} = 21$, $p < 0.0001$, Mann–Whitney test; **Fig 3G**).

In order to establish, on a cell-by-cell case, that the training-specific temporal profile of evoked and spontaneous activity were correlated, we directly compared the evoked and spontaneous activity dynamics (**Fig. 4**). As shown in the comparison of two different sample neurons from each training group, the averaged evoked and spontaneous activity was qualitatively similar (**Fig. 4A**), and consistent with the notion that the same circuits and neural trajectories activated by red light were being spontaneously replayed “offline”. This was confirmed by the similarity between the distributions of spontaneous and evoked peak times across cells within one training condition, and the significant difference between the timing of evoked Early vs Late events (Kolmogorov-Smirnov test, *Early Evoked vs Late Spont*: $p < 0.0001$) and spontaneous Early vs Late events ($p < 0.0001$)(**Fig. 4B**). To further quantify the similarity between spontaneous and evoked activity within training conditions, we computed the correlation coefficients between mean evoked and mean spontaneous activity across all recorded neurons within a training group, excluding within cell comparisons (**Fig. 4C**, top row). Furthermore, we also computed the correlation coefficients between the mean evoked and mean spontaneous activity across all recorded neurons between training groups (**Fig. 4C**, bottom row). Interestingly, the correlation coefficients of mean evoked and mean

spontaneous activity was much higher across neurons within one training condition compared to across training conditions (U = 19342, *Early Evoked vs Early Spont* = 552, *Early Evoked vs Late Spont* = 504, $p < 0.0001$, Mann–Whitney test) (U = 45680, *Late Evoked vs Late Spont* = 504 *Late Evoked vs Early Spont* = 420, $p < 0.0001$, Mann–Whitney test; **Fig. 4D**). The striking similarity between the evoked and spontaneous dynamics likely results from common cortical circuits being active in both forms of activity. Thus, even across cortical circuits from different slices, the temporal structure of the evoked and spontaneous activity appeared to be highly shaped by the training paradigm to which the circuits were exposed, suggestive of longer-lasting changes at the synaptic level.

3.3.3 Distinct neuronal ensembles with temporally-ordered activation

The above results reveal that the internal network dynamics of local cortical microcircuits learn to reproduce the temporal structure of the patterned stimulation they experience during training. To elucidate the network-level mechanisms that underlie the learned temporal dynamics we reasoned that potential connectivity differences between subpopulations of neurons may be revealed by the cross-correlation structure between pairs of neurons during spontaneous activity. In the Late group, during training in the incubator, Chrim$^+$ neurons were consistently activated hundreds of milliseconds before ChR2$^+$ neurons. We thus asked if this was also true during spontaneous replay by performing simultaneous whole-cell recordings of Chrim$^+$ and ChR2$^+$ expressing neurons (**Fig. 5**). In Untrained circuits, spontaneous activity in Chrim$^+$ and ChR2$^+$ neurons was

highly correlated, but in late-trained circuits this correlation was significantly weaker, suggesting that the Chrim$^+$ and ChR2$^+$ populations may be forming into distinct neuronal ensembles as a result of experience (r2= Untrained: 0.71, Late: 0.55; U = 13, $n_{Untrained}$ = *13,* n_{Late} = 22, $p < 0.007$, Mann–Whitney test; **Fig 5A, B**). In addition, cross-correlation analyses revealed a temporal lag in the peak cross-correlation of spontaneous activity dynamics between Chrim$^+$ and ChR2$^+$ neurons (31 ± 11 ms; **Fig 5C**), with the Chrim$^+$ neurons leading the ChR2$^+$ (**Fig 5A**, right). In contrast, in the Untrained group the peak cross-correlation lag between ChR2$^+$ and Chrim$^+$ neurons was approximately zero (U = 65, $n_{Untrained}$ = *13,* n_{Late} = 22, $p < 0.007$, Mann–Whitney test; **Fig 5C**). This temporally ordered activation of Chrim$^+ \rightarrow$ ChR2$^+$ neurons suggested differential training-dependent changes in the synaptic connectivity of Chrim$^+$ and ChR2$^+$ neurons. This was further supported by the smaller difference in peak pairwise cross-correlation of Chrim$^+$ x ChR2$^+$ spontaneous events (U = 74, $n_{Untrained}$ = *13,* n_{Late} = 22, $p < 0.02$, Mann–Whitney test; Fig 5D) compared to the pairwise correlation of Chrim$^+$ x ChR2$^+$ in late-trained slices.

3.3.4 Asymmetric connectivity between different ensembles of excitatory neurons

In order to understand the temporal asymmetry between the different subpopulations of excitatory neurons, we next analyzed the monosynaptic connectivity between different populations. Due to the relatively sparse transduction, Chrim$^+$ and ChR2$^+$ neurons were generally farther apart (>75 um), making it difficult to study synaptic connectivity which drops off dramatically with distance [264]. However, since the temporal profile of evoked activity in the ChR2$^+$ and Opsin$^-$ neurons was similar (see Supplement

Figure 1), we assessed connectivity between pairs of neighboring (<50 um) Chrim$^+$ and Opsin$^-$ neurons in Layer 2/3 (**Fig. 6A**). Following Late-training, we discovered a significant bias in the direction of synaptic strength, with the connections from Chrim$^+$ $\rightarrow$ Opsin$^-$ neurons being stronger than the connections from Opsin$^-$ $\rightarrow$ Chrim$^+$ neurons (**Fig. 6B**). This finding suggests that the ability to learn and predict temporal patterns may depend on the training-induced asymmetry in excitatory synaptic strength between distinct neuronal ensembles.

3.3.5 Prediction or temporal prediction errors?

The above results establish that neocortical microcircuits are autonomously capable of learning to not only predict external events, but also predict when those events are expected to occur. These results are broadly consistent with computational and *in vivo* studies suggesting that some forms of prediction and timing are computational primitives. In the Late-training group, our results demonstrate that, on average, the learned late response starts to emerge at approximately the time of the expected blue light onset during training, but only peaks after the expected offset of the blue light (**Fig. 2B**). Interestingly, this internally generated late response could be interpreted as either prediction/anticipation of the expected arrival of blue light, or as a prediction error generated by the absence of blue light. The distinction between prediction and prediction error interpretations can be determined by comparing the evoked red-alone (CS-only) and red + blue (CS-US) responses after 24-hours of training. Specifically, if the late responses represent prediction errors, the responses to red + blue light should actually be weaker

than the responses to red-alone. As expected from a simple feed-forward network, the majority of Opsin$^-$ neurons responded more or less equally to both red-alone and red + blue light (**Fig. 7C, D**). However, a fourth of the neurons exhibited responses consistent with prediction errors (**Fig 7A, B, E**).

3.4 Discussion

The ability to predict when events in the external world will occur is a fundamental component of animal intelligence, as it provides a means to anticipate and prepare for external events before they happen, efficiently encode expected information, and rapidly attend to surprising events. Because of the importance of prediction, a wide range of learning and neurocomputational theories, including classical and operant conditioning, reinforcement learning, predictive coding and Bayesian inference, are based on the ability to learn to make predictions based on previous experiences [148, 149, 265-268]. Because of their importance, it has been proposed that simple forms of prediction and timing are computational primitives [147-149, 158]. Consistent with this view, it has been shown that visual cortex circuits can learn to predict the timing of an expected reward [152, 153]. Similarly, in the barrel cortex it has been shown that neurons develop internally generated responses that peak at approximately the onset time of an expected sensory event [269]. Furthermore, in the same study, some neurons exhibited larger responses if the expected sensory event arrived late—a finding that can be interpreted as a prediction error.

It is often assumed that predictive responses and prediction errors in sensory areas rely on top-down signals. However, a few studies have also observed simple forms of

timed prediction in acute and organotypic slices [154, 161, 162]. Here, by using a dual-optical training approach, we were able to directly address whether individual neurons in “standalone” neocortical circuits were able to learn to generate predictive responses and prediction errors. Our approach also allowed for the explicit identification of subpopulations of neurons representing both sensory stimuli, and to perform paired intracellular recordings to analyze the connectivity patterns between these subpopulations.

Our results establish that neocortical circuits are autonomously able to learn the temporal structure of the stimuli to which they are exposed. Furthermore, we observed that during spontaneous activity, the temporal profile of network dynamics reproduced the temporal structure of the training protocol and post-training evoked activity. This resemblance in the temporal structure of evoked and spontaneous activity post-training implies that a large degree of overlap may exist between the participating neurons in either form of activity, as well as a similar spatiotemporal order of activation. To the best of our knowledge, this is the first report of a form of learned replay in *in vitro* or *ex vivo* cortical circuits.

3.4.1 Neural mechanisms underlying prediction and timing

The neural microcircuit mechanisms and synaptic learning rules underlying the ability of neocortical circuits to learn to predict the arrival and timing of external events remain unknown. A necessary step towards understanding the neural mechanisms underlying the training-specific learned responses observed here is to characterize the

differential dynamics of distinct subpopulations of neurons. Paired whole-cell recordings from Chrim$^+$ and ChR2$^+$ positive neurons from Late-trained slices revealed a clear temporal order in their firing patterns during spontaneous activity (**Fig. 5**). Specifically, the peak cross-correlation lag of both the subthreshold voltage and spikes revealed that Chrim$^+$ neurons were active before ChR2$^+$ neurons. This observation is consistent with the notion that training resulted in the emergence of “red” and “blue” neuronal ensembles, and that the “red” ensemble drove activity in the “blue” ensemble.

While the temporal profile of activity in the Chrim$^+$ and ChR2$^+$ neurons were distinct, we did not observe any significant differences in the temporal profile between ChR2$^+$ and Opsin$^-$ neurons (**Fig. S1**) during either evoked or spontaneous activity. Thus, suggesting that Chrim$^+$ neurons may also drive Opsin$^-$ neurons. To address this question, we performed connectivity analyses between Chrim$^+$ and Opsin$^-$ negative neurons—as mentioned it was not possible to obtain connectivity data between Chrim$^+$ $\leftrightarrow$ ChR2$^+$ neurons because of the distance between sparsely transduced neurons—revealing that the strength of synaptic connections was stronger in the Chrim$^+$ $\rightarrow$ Opsin$^-$ direction compared to the Opsin$^-$ $\rightarrow$ Chrim$^+$ direction (**Fig. 6**).

We propose that these changes in excitatory connections between different neuronal ensembles contribute to learning and timed prediction. However, based on previous experimental and computational work we also suggest that internally generated dynamics require orchestrated plasticity operating at both excitatory and inhibitory synapses [162, 249]. Indeed, because learning requires the presence of internally generated neural dynamics that rely on positive excitation held in check by inhibition, we

hypothesize that the learned dynamics operate in an inhibition stabilized regime [199, 251, 270]. Thus, future studies should be aimed at studying the reciprocal connectivity between excitatory and inhibitory neurons, as well as training-specific and dynamic changes in the balance of excitation and inhibition.

3.5 Materials and Methods

Organotypic cultures

Cortical organotypic slice cultures were prepared as described previously [143, 162, 236]. Slices were obtained from postnatal day 5-7 wildtype FVB mice of either sex. Organotypic cultures were prepared using the interface method [226]. Coronal slices (400 µm thickness) containing primary auditory and somatosensory cortex were sectioned using a vibratome (Leica VT1200) and bisected before being individually placed onto Millicell cell culture inserts (MilliporeSigma) in a 6-well plate with 1mL of culture media per well. Culture media was changed at 1 and 24 hours after initial plating and every 2 days thereafter. Cutting media consisted of MEM (Corning 15-010-CV) plus (final concentration in mM): $MgCl_2$, 3; glucose, 10; HEPES, 25; and Tris-base, 10. Culture media consisted of MEM (Corning 15-010-CV) plus (final concentration in mM): glutamine, 1; CaCl2, 2.6; MgSO4, 2.6; glucose, 30; HEPES, 30; ascorbic acid, 0.5; 20% horse serum, 10 units/L penicillin, and 10 µg/L streptomycin. Slices were incubated in 5% CO2 at 35°C.

Viral transduction

For the double sparse transduction, slices were transduced with a total of 4 viruses: AAV9-CamKII(0.4)-Cre (Addgene plasmid #105558), AAV9-EF1a-DIO-hChR2(H134R)-EYFP (Addgene plasmid #20298), AAV8-CAG-FLPX-ChrimsonR-tdTomato (Addgene plasmid #130909), and AAV9-CamKII(0.4)-FLPo (Vector biolabs). All 4 viruses had a starting titer of approximately [1x1013] and were diluted/combined into a viral cocktail before delivery to the slices. First, the two recombinase-expressing viruses CamKII-Cre and CamKII-FLPo were individually diluted with nuclease-free water to a concentration of approximately [1x1011]. The two diluted recombinase viruses were then combined in a 1:1 ratio by volume. The two undiluted opsin viruses DIO-hChR2 and FLPx-ChrimsonR were also combined in a 1:1 ratio by volume. The combined diluted recombinase viruses were then further diluted by adding the combined opsin viruses in a 1:3 ratio by volume. The resulting final concentrations for all 4 viruses were approximately: [1x1010] AAV9-CamKII-Cre, [1x1010] AAV9-CamKII-FLPo, [8x1012] AAV9-DIO-hChR2, [8x1012] AAV8-FLPx-ChrimsonR. Each hemi-slice received a total of 0.8 µL of viral cocktail gently delivered via a sterilized pipette above the cortex. All viral transductions were performed at day-in-vitro (DIV) 6-7 and recordings were performed between DIV 22 – 30 to allow sufficient time for viral expression.

Chronic optogenetic stimulation

To minimize variability, experiments relied on “sister” slices, i.e. experimental batches were derived on the same day from the same litter of animals, maintained with the same culture medium/serum, placed in the same incubator, and virally transduced in

the same session. For the interval-training experiments, both Early/Late-trained and Untrained control slices received equal amounts of virus and were simultaneously placed into the training incubator to ensure identical environments and experimental conditions. In addition, experiments were balanced by training and recording an equal number of sister slices from each experimental condition (Early, Late, Untrained) per day. For chronic optical training, individual cell culture inserts containing one hemi-slice were placed in 6-well plates and quickly transferred along with their sister slices from the culture incubator to an identical “training incubator”, where each individual slice is aligned with a dual-channel RGB LED (Vollong part #: VL-H01RGB00302).

Both Early and Late training protocols consisted of a 440 ms train of red light pulses (625nm, 12 pulses, 5 ms each, 25 Hz, 0.2 mW/mm2,) paired with an 80 ms train of blue light pulses (455nm, 5 pulses, 5 ms each, 50 Hz, 0.15 mW/mm2) at two different temporal relationships. In the Early training case, the train of red light pulses preceded the train of blue light pulses by 10 ms, while in the Late training case, red preceded blue by 370 ms. In both training cases, patterned optical stimulation was delivered every 20 seconds for approximately 24 hours (± 2 hours). Following 24-hours of training, slices were individually transferred from the training incubator to the whole-cell patch clamp rig for recordings between 1 – 6 hours after the cessation of patterned stimulation.

Electrophysiology

Cell culture inserts were transferred to the recording rig and perfused with oxygenated ACSF composed of (mM): 125 NaCl, 5 KCl, 2.5 MgSO4, 25 NaHCO3, 1 NaH2PO4, 25 glucose, 2.5 CaCl2 (ACSF was formulated to match the standard culture

media). Temperature was maintained at 32-33□C and perfused at 5 mL/min. Whole-cell solution was composed of (mM): 100 K-gluconate, 20 KCl, 4 ATP-Mg, 10 phosphocreatine, 0.3 GTP, 10 HEPES (adjusted to pH 7.3 and 300 mOsm). All recordings were sampled at 10 kHz.

Pharmacology

For measurement of the direct optical response of ChR2+ and Chrim+ pyramidal neurons to their respective target wavelengths, glutamatergic synaptic blockers CNQX (HelloBio HB0205) and D-AP5 (HelloBio HB0225) were used at concentrations of [40 μM] and [80 μM] respectively.

Connectivity

Connectivity between Chrim+ and Opsin- pyramidal neurons was assessed through simultaneous current-clamp recordings where alternating trains of current was applied to each cell. A connection was considered to exist if the average excitatory post-synaptic potential (EPSP) amplitude was at least 3 times the baseline standard deviation. The first EPSP amplitude was calculated as the peak voltage of the EPSP subtracted by the baseline, subsequent EPSP amplitudes were calculated as the peak to the fitted decay of the previous EPSP.

Dual-targeted Recordings

For simultaneous current-clamp recordings of $ChR2^+$ and $Chrim^+$ pyramidal neurons, neurons were identified by either the individual presence of EYFP for $ChR2^+$ or tdTomato for $Chrim^+$ neurons, and additionally confirmed by the presence of a direct light-evoked

response. Opsin-negative pyramidal neurons were identified by morphology, electrophysiological properties, and the lack of a direct optical response.

Testing of Learned Dynamics with Optogenetics

Following training, whole-cell current-clamp recordings were obtained from both $ChR2^+$ and $Opsin^-$ pyramidal neurons in slices from Early- and Late-trained groups. Optical stimulation during testing was administered using a dual-channel RGB LED (Vollong part #: VL-H01RGB00302), which projected red (625 nm) and blue (455 nm) light through the base of the recording chamber covering approximately a 1 mm diameter at the location of the recorded neurons. Trains of red and blue light pulses delivered during testing were identical in both structure and intensity as light delivered during training in the incubator. During testing, red light trains (625 nm, 12 pulses, 5 ms duration, at 25 Hz, intensity 0.2 mW/mm^2) were delivered every 20 seconds, preceded by a 1-second baseline recording period per sweep. Evoked neuronal responses were analyzed in the 1-second window following the onset of red light stimulation. Recorded sweeps exhibiting spontaneous network activity during the baseline period were systematically excluded due to contamination of the light-evoked responses from spontaneous network activity.

Evoked neuronal activity was analyzed using spike-filtered voltage data, smoothed with a 10 ms moving average to reduce noise and improve the detection of voltage peaks and slopes. For each neuron, the median peak time of evoked activity was determined across a minimum of ten evoked sweeps and was calculated as the time point at which the peak voltage occurred during each sweep. The median event time of evoked activity

was defined by identifying when the slope of the recorded voltage exceeded a threshold set at three times the standard deviation of the slopes derived from a temporally shifted (circular shift of 10 ms) version of the voltage data. The significance threshold for slope detection was established based on the variability of the baseline voltage, quantified as three times the standard deviation of all recorded slopes across all evoked sweeps within a single cell. The center of gravity for each evoked trace was computed based on the midpoint of the integrated trace area. Cumulative distribution functions of evoked peak times were generated using the first 5 evoked sweeps from each neuron within both Early- and Late-training conditions. Analyses were performed blind to the training-condition to prevent bias in the evaluation of evoked activity.

Spontaneous event quantification/analysis

A minimum of 5 minutes of spontaneous activity was recorded for each neuron. Spontaneous network events were quantified based on previously defined criteria [143, 187, 213]. Spontaneous events were detected with a 5 mV voltage threshold above the resting membrane potential. However, during network events, the membrane potential would often make multiple crossings above and below the 5 mV threshold before returning to resting potential. Thus, we defined spontaneous events as activity that remained above threshold for at least 100 ms, allowing for drops below threshold that lasted less than 25 ms. Baseline was defined as a 100 ms period preceding the onset of a spontaneous event and the analysis window was defined as 1 second following the detected onset of a spontaneous event. Detected spontaneous events were down-sampled by a factor of 10 to filter out spikes and reduce computational load without compromising the integrity of the temporal dynamics. Spontaneous median peak time,

median event time, and mean center of gravity were computed in the same fashion as the evoked activity analysis. Cumulative distribution functions of evoked and spontaneous peak times were generated using the first 5 evoked sweeps or first 5 spontaneous events from each neuron within both Early- and Late-training conditions.

Correlation Analysis of Evoked and Spontaneous Activity

To assess the correlation between mean evoked and mean spontaneous activity within and between Early- and Late-training conditions, evoked and spontaneous activity data were detected based on the same criterium as above. For each neuron, evoked activity data was temporally shifted by adjusting for the lag time observed before a 5 mV threshold crossing during evocation, ensuring the alignment of evoked neuronal responses across sweeps (this is the same threshold criterium used spontaneous event detection). Importantly, this time shift of the evoked activity was only used for the correlation between evoked and spontaneous activity, and was not used to align evoked events for any other analyses used in this study.

Correlations between mean evoked and mean spontaneous activity was calculated to determine the degree of similarity in neural activity patterns within (intra-condition) and between (inter-condition) training conditions (Early and Late). The correlation matrices were populated by computing the Pearson correlation coefficient between mean traces of each combination of evoked and spontaneous activity. Each matrix element thus represented the correlation between a specific pair of mean evoked and mean spontaneous activity traces. Diagonal elements of the intra-condition matrices, which represented self-correlations (mean evoked vs mean spontaneous within the same cell),

were excluded to focus analysis on inter-slice correlations. The mean correlations were calculated for each comparison, emphasizing the generalized response pattern within each training condition compared to between training conditions.

Pairwise Correlation and Cross-Correlation Analysis

Spontaneous events for pairwise correlations of activity dynamics between simultaneously recorded ChR2+ and Chrim+ pyramidal neurons were detected using the same method described earlier in the Methods. Spontaneous events were down-sampled by a factor of 50 to filter out spikes without compromising the integrity of the temporal dynamics. Since detected event durations were not exactly the same between two simultaneously recorded neurons, we used a segment of the combined detected event index to compute the pairwise correlations of spontaneous event dynamics. Each segment spanned 1100 ms, including 100 ms of baseline activity before the start of the detected event.

The cross-correlations of spontaneous event bouts were computed using the same spike-filtered data as the pairwise correlations. However, to exclude transitions between active and inactive states, the analyzed voltage data were specifically sampled from 50 ms after the detected onset to 50 ms before the detected offset of each event.

Prediction Error Analysis:

To identify neurons exhibiting timed prediction error responses, we quantified the mean difference between responses to the conditioned stimulus (red light alone) and conditioned + unconditioned stimulus (red + blue light). For each neuron, the mean

response to CS and CSUS was extracted, and the difference between these mean responses (CS - CSUS) was computed. This subtraction represents the neuron's differential response when exposed to CS alone versus CS paired with US. Neurons were classified as exhibiting a timed prediction error response based on the area under the curve of the mean CS - CSUS subtraction. Specifically, neurons for which this measure exceeded three standard errors of the mean above the average were identified as exhibiting timed prediction error, indicating a significant difference in their response to CS alone versus CS paired with US.

3.6 Figures

Figure 1

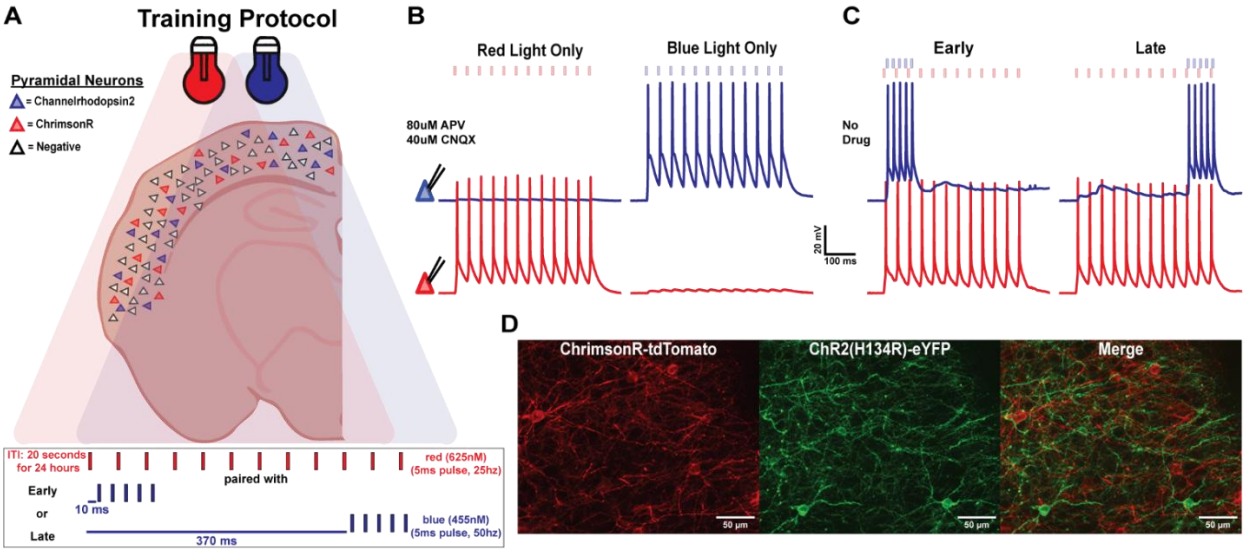

A sparse dual-opsin approach for interval learning in *ex vivo* cortical circuits. A, Schematic of cortical pyramidal neurons in an organotypic slice culture sparsely transduced with either ChR2 or Chrim (top) and Early vs Late chronic optogenetic training paradigm (bottom). **B,** Sample simultaneous whole-cell patch clamp recordings from two cortical pyramidal neurons expressing ChR2 (blue) or Chrim (red) during presentation of red or blue light (5 ms, 12 pulses, 25 Hz) in the presence of synaptic blockers [80 µM APV, 40 µM CNQX]. **C,** Sample simultaneous recording from ChR2^{+} (blue) and Chrim^{+} (red) neurons during presentation of the Early (left) and Late (right) training paradigms. **D,** Image showing non-overlapping expression of ChR2 and Chrim in Layer 2/3 pyramidal neurons in auditory cortex.

Figure 2

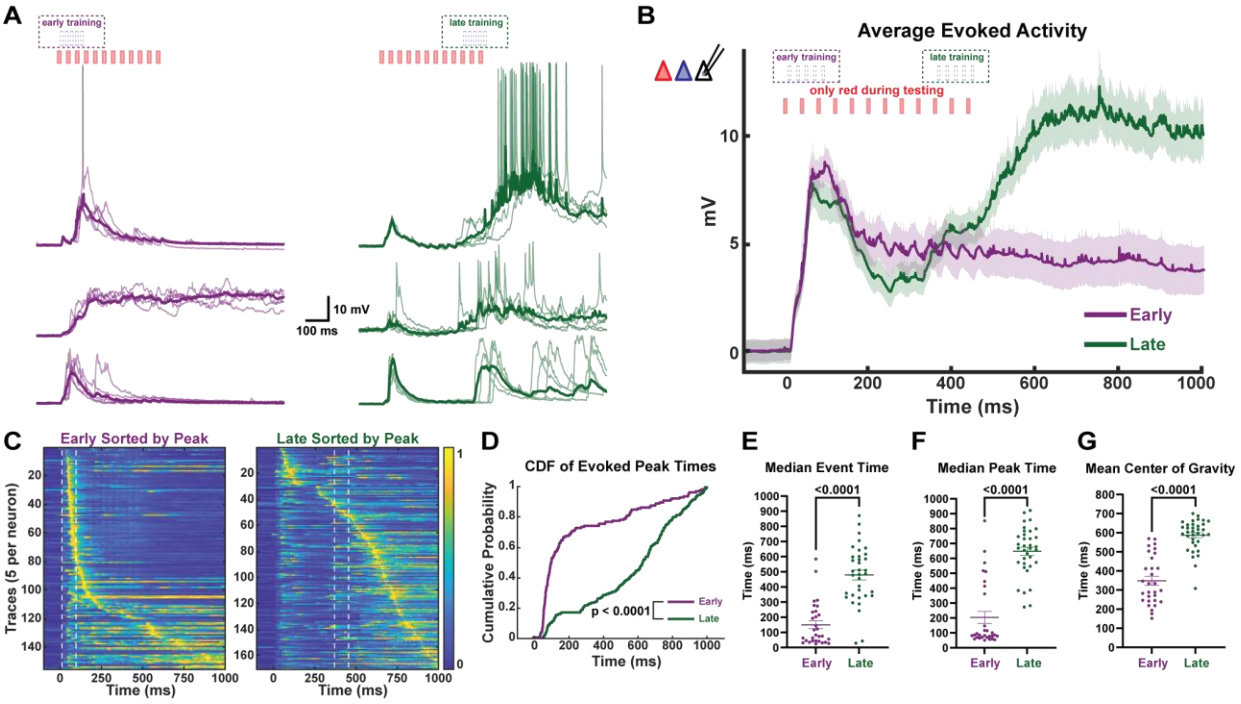

The temporal profile of network dynamics is dependent on training interval. A, Sample traces of evoked polysynaptic activity (5 traces per cell and mean (bold)) from Opsin$^-$ pyramidal neurons in response to red-alone in slices trained on the Early (left) vs Late (right) paradigm. **B,** Comparison of the mean ± SEM (shading) of evoked activity in pyramidal neurons from Early (Opsin$^-$: 19, ChR2$^+$: 11) vs Late (Opsin$^-$: 24, ChR2$^+$: 11) trained slices. **C,** Normalized voltagegram of red light evoked responses from ChR2$^+$ and Opsin$^-$ pyramidal neurons sorted by peak time in Early (left) vs Late (right) trained slices. Dashed white lines indicate when blue light stimulation occurred during training **D,** Cumulative distribution of evoked peak times was significantly different in recorded neurons from Early vs Late trained slices. **E,** Average median event time of evoked network activity was significantly lower in neurons from Early (Opsin$^-$(dark purple), ChR2$^+$(light purple)) vs Late (Opsin$^-$(dark green), ChR2$^+$(light green)) trained slices. **F,** Average median peak time of evoked network activity was significantly lower in neurons from Early vs Late trained slices. **G,** Mean center of gravity of evoked network activity was significantly lower in neurons from Early vs Late trained slices.

Figure 3

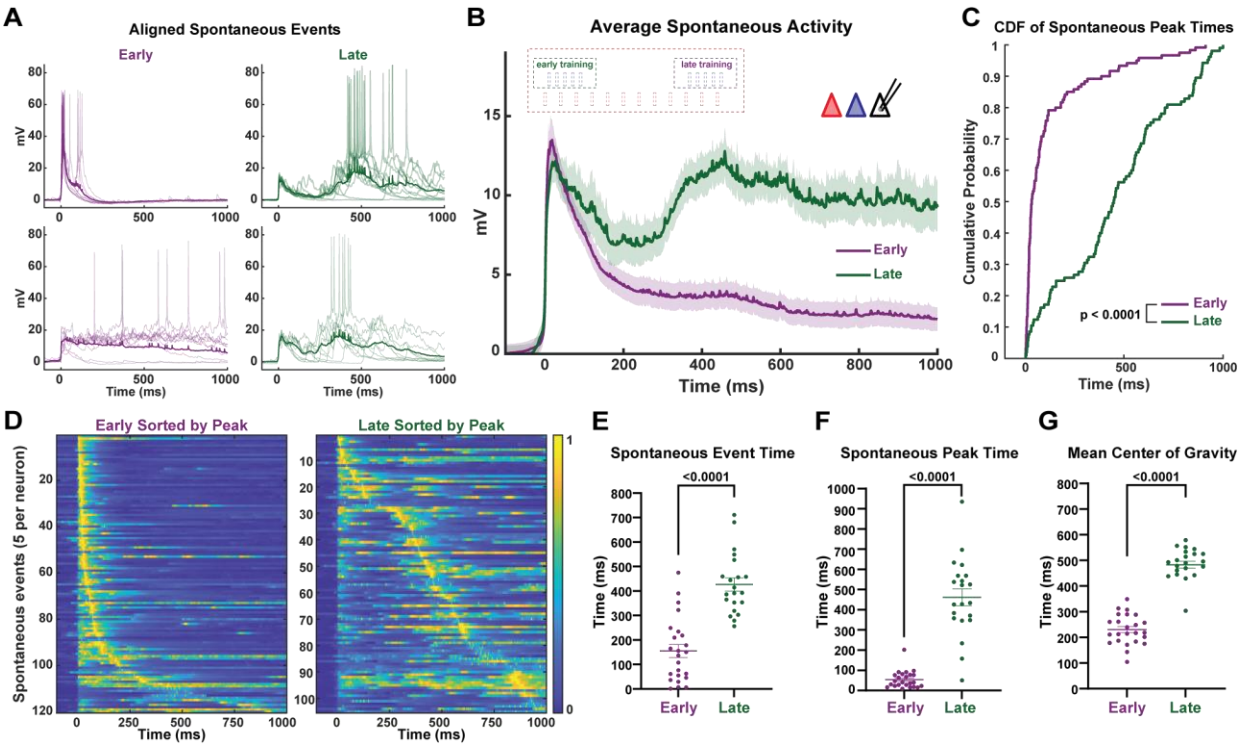

Spontaneous network activity mirrors the learned interval-specific network dynamics. A, Sample traces of aligned spontaneous network activity (10 spontaneous events per cell and mean (bold)) from Opsin$^-$ pyramidal neurons in Early (left) and Late (right) trained slices. **B,** Comparison of the mean ± SEM (shading) of spontaneous activity in pyramidal neurons from Early (Opsin$^-$: 18, ChR2$^+$: 6) vs Late (Opsin$^-$: 18, ChR2$^+$: 3) trained slices. **C,** Cumulative distribution of the spontaneous event peak times in ChR2$^+$ and Opsin$^-$ pyramidal neurons from Early vs Late trained slices. **D,** Normalized voltagegram of spontaneous events from recorded pyramidal neurons sorted by peak time in Early (left) vs Late (right) trained slices. **E,** Average median event times of spontaneous events was significantly lower in neurons from Early vs Late trained slices. **F,** Average median peak times of spontaneous events was significantly lower in neurons from Early vs Late trained slices. **G,** Mean center of gravity of spontaneous events was significantly lower in neurons from Early vs Late trained slices.

Figure 4

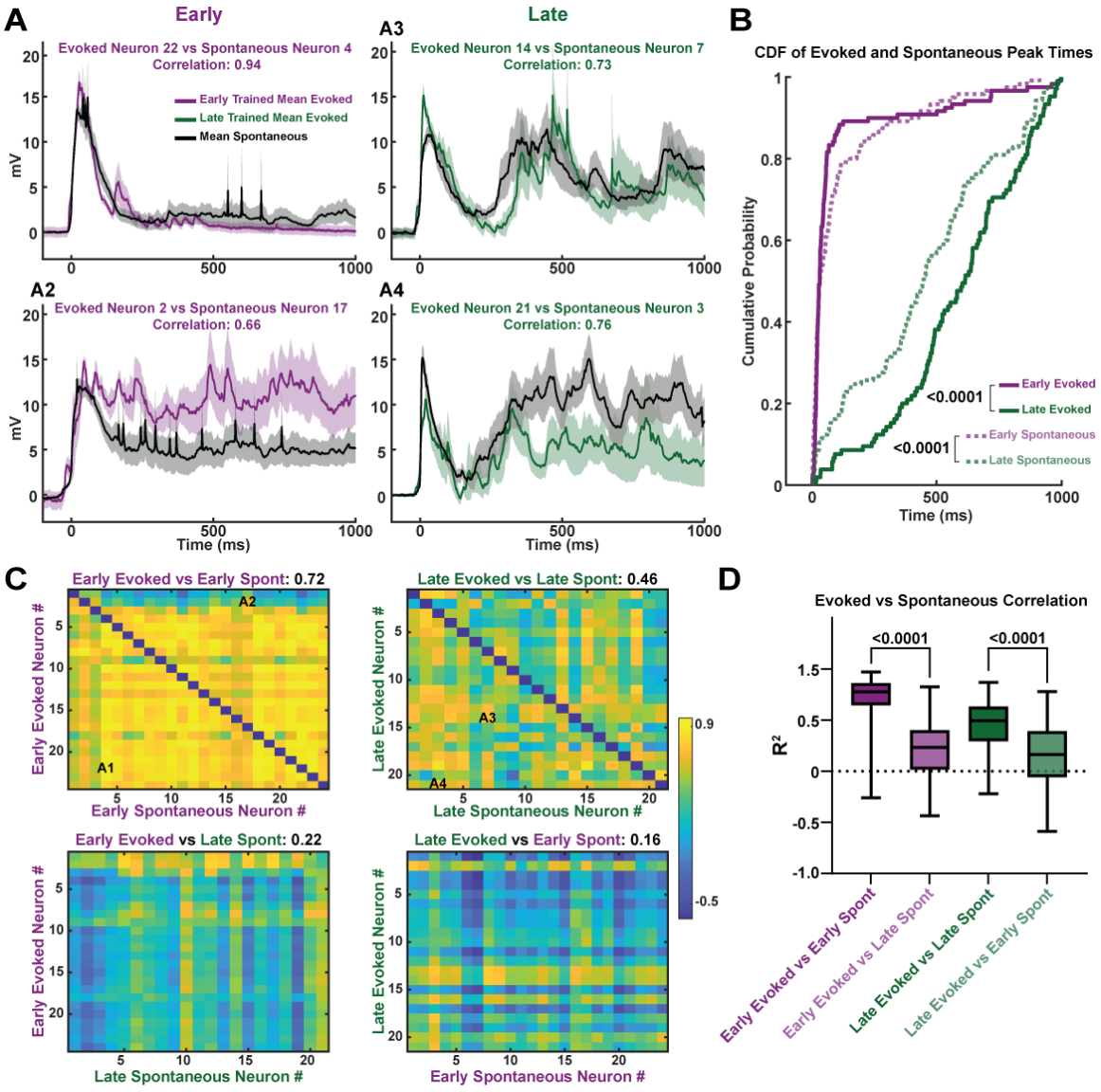

Training-specific replay demonstrated by the higher correlation between evoked and spontaneous network activity across slices. A, Example mean ± SEM (shading) of evoked (Early: purple, Late: green) vs spontaneous (black) network activity from pyramidal neurons in different slices within the same training group. **B,** Comparison of the cumulative distribution of evoked and spontaneous activity peak times across slices both within (e.g., Early evoked vs Early spontaneous) and across (e.g., Early evoked vs Late spontaneous) training groups. **C,** Correlation matrix of mean evoked vs mean spontaneous activity across neurons within the same training group (top) and across training groups (bottom). **D,** Box plot of correlation values for mean evoked vs mean spontaneous activity across neurons both within and across training groups.

Figure 5

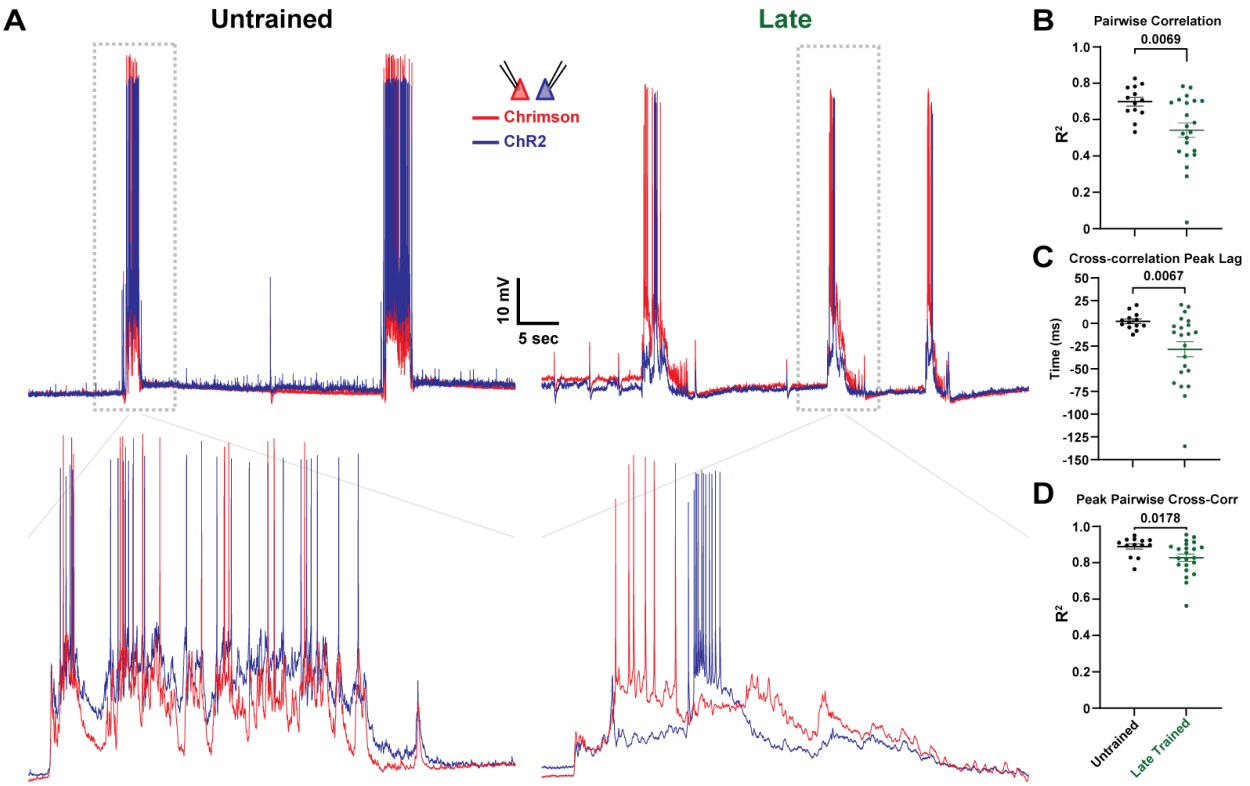

Training-dependent emergence of distinct neuronal ensembles as indicated by the decorrelation and temporal lag between Chrim⁺ and ChR2⁺ neurons. A, Sample 60 second trace of spontaneous network activity from simultaneously recorded ChR2⁺ and Chrim⁺ neurons (top). Dashed box is magnified in the traces below (2.5 second window, bottom). **B,** Significant decrease in the average pairwise voltage correlation of spontaneous events in simultaneously recorded ChR2⁺ and Chrim⁺ neurons in Late-trained compared to Untrained slices. **C,** Cross-correlation of spontaneous events in simultaneously recorded ChR2⁺ and Chrim⁺ neurons revealed a consistent temporal lag in ChR2⁺ compared to Chrim⁺ neurons. Sample spontaneous event with temporal lag in simultaneously recorded ChR2⁺ and Chrim⁺ neurons from a Late trained slice (Panel A, bottom right). **D,** Average peak pairwise cross-correlation of spontaneous events is less significantly different than average pairwise correlation of spontaneous events in simultaneously recorded ChR2⁺ and Chrim⁺ neurons.

Figure 6

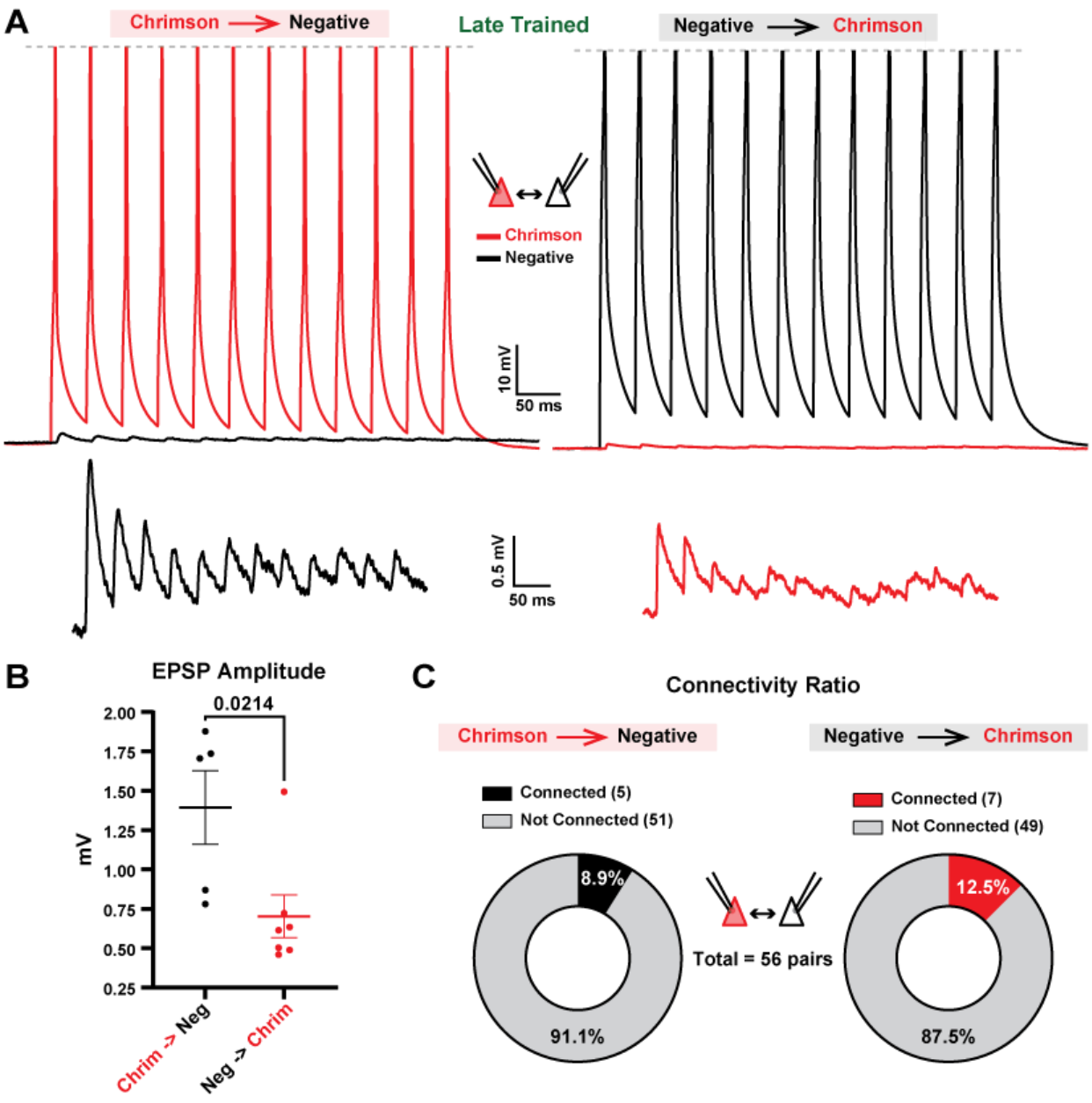

Asymmetric connectivity between different subpopulations of excitatory neurons. A, Averaged sample trace of a paired recording between connected Chrim$^+$→Opsin$^-$ pyramidal neurons (top) and enlarged view of the EPSPs (bottom). **B,** Averaged sample trace of a paired recording between connected Opsin$^-$→Chrim$^+$ pyramidal neurons (top) and enlarged view of the EPSPs (bottom). **C,** EPSP amplitudes of synaptic connections (<50 µm apart) were significantly stronger in the direction of Chrim$^+$→Opsin$^-$ connections compared to Opsin$^-$→Chrim$^+$ connections. **D,** Probability of connection was not significantly different in the Chrim$^+$→Opsin$^-$ direction compared to the Opsin$^-$→Chrim$^+$ direction.

Figure 7

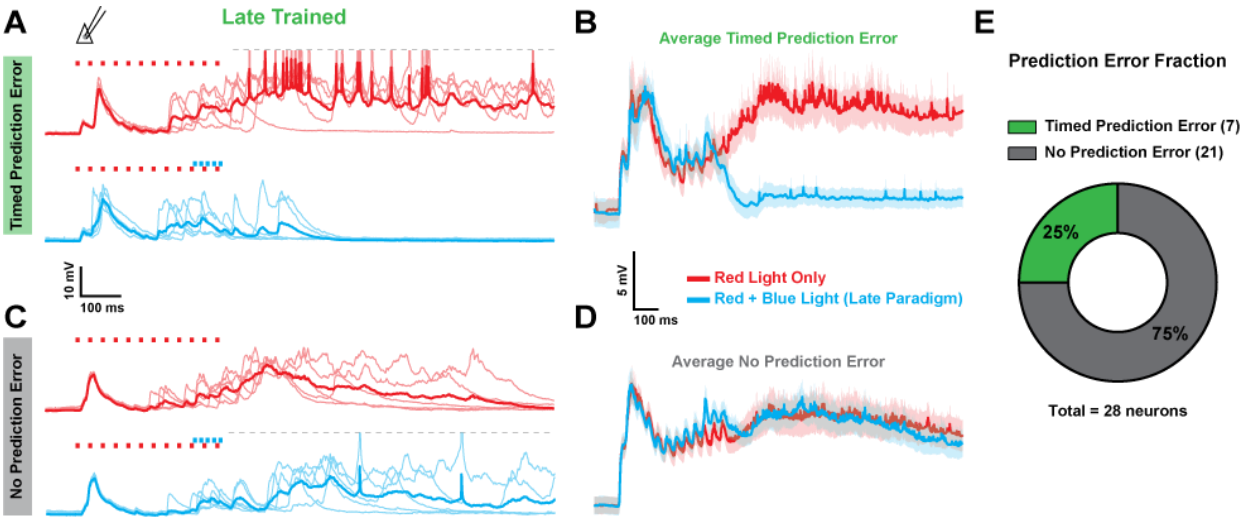

Following Late-training a subpopulation of Opsin$^-$ pyramidal neurons showed responses consistent with a timed prediction error. A, Five sample traces and mean (bold) from an Opsin$^-$ pyramidal neuron with larger responses to red-alone compared to red + blue light (Late-training protocol). **B,** Average responses from Opsin$^-$ pyramidal neurons expressing timed prediction error responses (n = 7). **C,** Five sample traces and mean trace (bold) from an Opsin$^-$ pyramidal neuron with similar responses to both red-alone and red+blue. **D,** Average responses from Opsin$^-$ pyramidal neurons that did not express timed prediction error responses (n = 21). **E,** Ratio of pyramidal neurons with timed prediction error responses (25%) vs no prediction error responses (75%).

Supplementary Figure 1

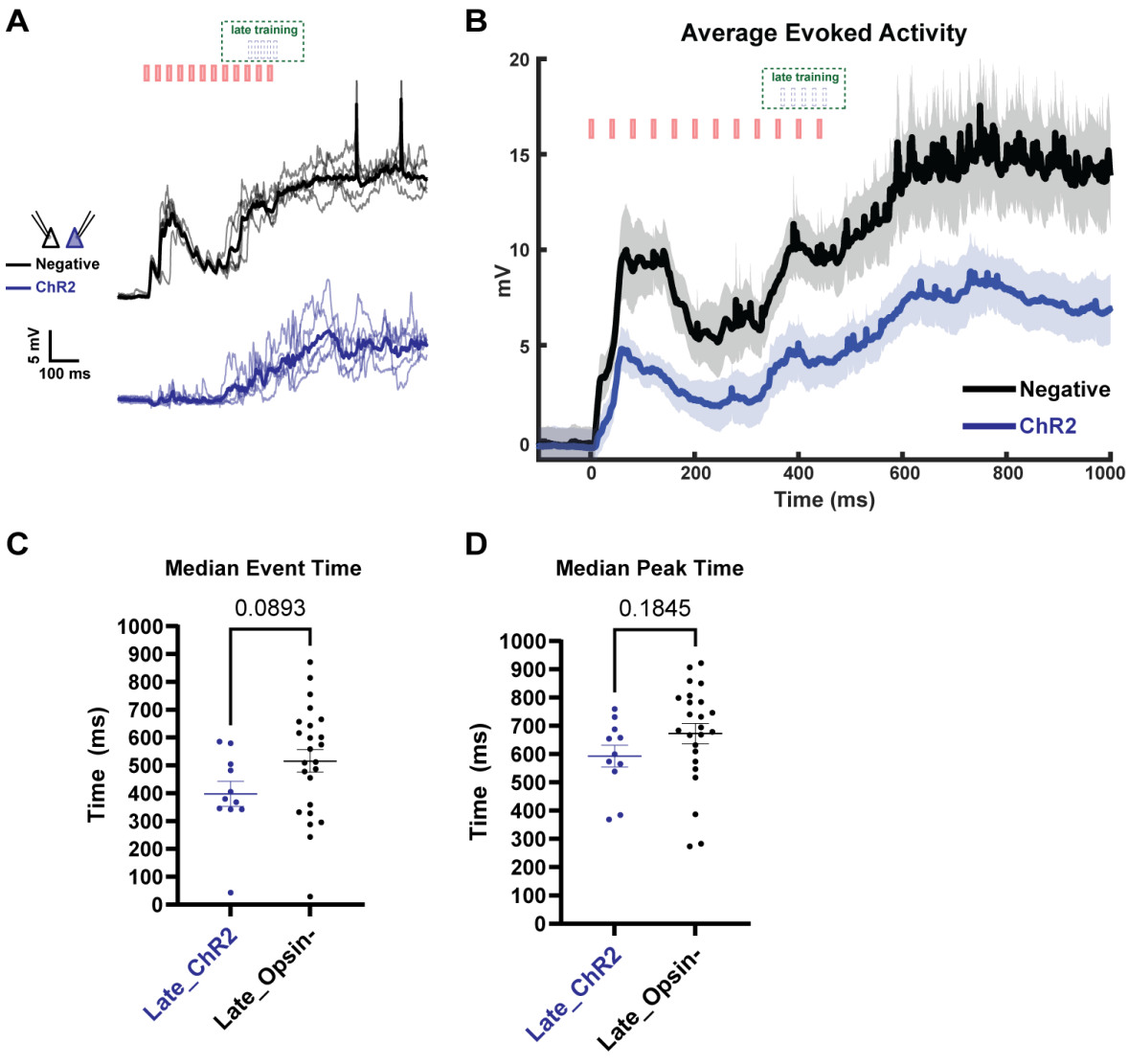

Following Late-training the temporal profile of evoked activity was not significantly different between simultaneously recorded ChR2$^+$ and opsin-negative neurons. A, Sample traces of evoked polysynaptic activity (5 traces per cell and mean (bold)) from a simultaneously recorded pair of ChR2$^+$ and Opsin$^-$ pyramidal neurons in response to red-alone. **B,** Comparison of the mean ± SEM (shading) of evoked activity in simultaneously recorded ChR2$^+$ and Opsin$^-$ pyramidal neurons from Late-trained slices (Opsin$^-$: 8, ChR2$^+$: 8).**C,** Average median event time of evoked network activity was not significantly different in ChR2$^+$ and Opsin$^-$ neurons from Late trained slices. **D,** Average median peak time of evoked network activity was not significantly different in ChR2$^+$ and Opsin$^-$ neurons from Late trained slices.

3.7 References Cited

136. MacLean, J.N., et al., *Internal Dynamics Determine the Cortical Response to Thalamic Stimulation.* Neuron, 2005. **48**(5): p. 811-823.

137. Luczak, A., P. Barthó, and K.D. Harris, *Spontaneous Events Outline the Realm of Possible Sensory Responses in Neocortical Populations.* Neuron, 2009. **62**(3): p. 413-425.

138. Luczak, A., et al., *Sequential structure of neocortical spontaneous activity in vivo.* PNAS, 2007. **104**(1): p. 347-52.

143. Liu, B., M.J. Seay, and D.V. Buonomano, *Creation of Neuronal Ensembles and Cell-Specific Homeostatic Plasticity through Chronic Sparse Optogenetic Stimulation.* The Journal of Neuroscience, 2023. **43**(1): p. 82-92.

146. Mauk, M.D. and D.V. Buonomano, *The Neural Basis of Temporal Processing.* Ann. Rev. Neurosci., 2004. **27**: p. 307-340.

147. Paton, J.J. and D.V. Buonomano, *The Neural Basis of Timing: Distributed Mechanisms for Diverse Functions.* Neuron, 2018. **98**(4): p. 687-705.

148. Keller, G.B. and T.D. Mrsic-Flogel, *Predictive Processing: A Canonical Cortical Computation.* Neuron, 2018. **100**(2): p. 424-435.

149. Rao, R.P. and D.H. Ballard, *Predictive coding in the visual cortex: a functional interpretation of some extra-classical receptive-field effects.* Nat Neurosci, 1999. **2**(1): p. 79-87.

152. Shuler, M.G. and M.F. Bear, *Reward timing in the primary visual cortex.* Science, 2006. **311**(5767): p. 1606-9.

153. Namboodiri, V., et al., *Visually Cued Action Timing in the Primary Visual Cortex.* Neuron, 2015. **86**(1): p. 319-330.

154. Chubykin, A.A., et al., *A Cholinergic Mechanism for Reward Timing within Primary Visual Cortex.* Neuron, 2013. **77**(4): p. 723-735.

158. Buonomano, D.V. and M.M. Merzenich, *Temporal information transformed into a spatial code by a neural network with realistic properties.* Science, 1995. **267**: p. 1028–30.

161. Johnson, H.A., A. Goel, and D.V. Buonomano, *Neural dynamics of in vitro cortical networks reflects experienced temporal patterns.* Nat Neurosci, 2010. **13**(8): p. 917-919.

162. Goel, A. and D.V. Buonomano, *Temporal Interval Learning in Cortical Cultures Is*

Encoded in Intrinsic Network Dynamics. Neuron, 2016. **91**: p. 320-327.

185. Plenz, D. and S.T. Kitai, *Up and down states in striatal medium spiny neurons simultaneously recorded with spontaneous activity in fast-spiking interneurons studied in cortex-striatum-substantia nigra organotypic cultures.* J Neurosci, 1998. **18**(1): p. 266-83.

187. Johnson, H.A. and D.V. Buonomano, *Development and Plasticity of Spontaneous Activity and Up States in Cortical Organotypic Slices.* J. Neurosci., 2007. **27**(22): p. 5915-5925.

196. Romero-Sosa, J.L., H. Motanis, and D.V. Buonomano, *Differential Excitability of PV and SST Neurons Results in Distinct Functional Roles in Inhibition Stabilization of Up States.* The Journal of Neuroscience, 2021. **41**(34): p. 7182-7196.

198. Tsodyks, M.V., et al., *Paradoxical Effects of External Modulation of Inhibitory Interneurons.* The Journal of Neuroscience, 1997. **17**(11): p. 4382-4388.

199. Ozeki, H., et al., *Inhibitory Stabilization of the Cortical Network Underlies Visual Surround Suppression.* Neuron, 2009. **62**(4): p. 578-592.

213. Goel, A. and D.V. Buonomano, *Chronic electrical stimulation homeostatically decreases spontaneous activity, but paradoxically increases evoked network activity.* Journal of Neurophysiology, 2013. **109**(7): p. 1824-1836.

215. Sugden, A.U., et al., *Cortical reactivations of recent sensory experiences predict bidirectional network changes during learning.* Nature Neuroscience, 2020. **23**(8): p. 981-991.

226. Stoppini, L., P.A. Buchs, and D. Muller, *A simple method for organotypic cultures of nervous tissue.* J Neurosci Methods, 1991. **37**(2): p. 173-82.

231. Zhang, X., et al., *Familiarity Detection and Memory Consolidation in Cortical Assemblies.* eneuro, 2020. **7**(3): p. ENEURO.0006-19.2020.

232. Dranias, M.R., et al., *Short-Term Memory in Networks of Dissociated Cortical Neurons.* The Journal of Neuroscience, 2013. **33**(5): p. 1940-1953.

233. Lamberti, M., et al., *Prediction in cultured cortical neural networks.* PNAS Nexus, 2023. **2**(6).

234. Hyde, R.A. and B.W. Strowbridge, *Mnemonic representations of transient stimuli and temporal sequences in the rodent hippocampus in vitro.* Nat Neurosci, 2012. **15**(10): p. 1430-1438.

235. Gähwiler, B.H., et al., *Organotypic slice cultures: a technique has come of age.* Trends Neurosci., 1997. **20**: p. 471-477.

236. Motanis, H. and D.V. Buonomano, *Delayed in vitro Development of Up States but Normal Network Plasticity in Fragile X Circuits.* Eur J Neurosci, 2015. **42**(6): p. 2312-21.

237. Bolz, J., *Cortical circuitry in a dish.* Curr. Opinion Neurobio, 1994. **4**: p. 545-549.

238. Echevarria, D. and K. Albus, *Activity-dependent development of spontaneous bioelectric activity in organotypic cultures of rat occipital cortex.* Brain Res Dev Brain Res, 2000. **123**(2): p. 151-64.

239. De Simoni, A., C.B. Griesinger, and F.A. Edwards, *Development of rat CA1 neurones in acute versus organotypic slices: role of experience in synaptic morphology and activity.* J Physiol, 2003. **550**(Pt 1): p. 135-47.

240. Humpel, C., *Organotypic brain slice cultures: A review.* Neuroscience, 2015. **305**: p. 86-98.

241. Debanne, D., B.H. Gahwiler, and S.M. Thompson, *Asynchronous pre- and postsynaptic activity induces associative long-term depression in area CA1 of the rat hippocampus in vitro.* Proc Natl Acad Sci U S A, 1994. **91**(3): p. 1148-52.

242. Anisimova, M., et al., *Spike-timing-dependent plasticity rewards synchrony rather than causality.* Cerebral Cortex, 2022: p. bhac050.

243. Musleh, W., et al., *Glycine-induced long-term potentiation is associated with structural and functional modifications of alpha-amino-3-hydroxyl-5-methyl-4-isoxazolepropionic acid receptors.* Proc Natl Acad Sci U S A, 1997. **94**(17): p. 9451-6.

244. Barria, A. and R. Malinow, *Subunit-Specific NMDA Receptor Trafficking to Synapses.* Neuron, 2002. **35**(2): p. 345-353.

245. Hayashi, Y., et al., *Driving AMPA receptors into synapses by LTP and CaMKII: requirement for GluR1 and PDZ domain interaction.* Science, 2000. **287**(5461): p. 2262-7.

246. Letellier, M., et al., *Differential role of pre- and postsynaptic neurons in the activity-dependent control of synaptic strengths across dendrites.* PLOS Biology, 2019. **17**(6): p. e2006223.

247. Yamada, A., et al., *Role of pre- and postsynaptic activity in thalamocortical axon branching.* Proceedings of the National Academy of Sciences, 2010. **107**(16): p. 7562-7567.

248. Goold, C.P. and R.A. Nicoll, *Single-Cell Optogenetic Excitation Drives Homeostatic Synaptic Depression.* Neuron, 2010. **68**(3): p. 512-528.

249. Soldado-Magraner, S., et al., *Paradoxical self-sustained dynamics emerge from*

orchestrated excitatory and inhibitory homeostatic plasticity rules. Proc Natl Acad Sci U S A, 2022. **119**(43): p. e2200621119.

250. Beggs, J.M. and D. Plenz, *Neuronal avalanches are diverse and precise activity patterns that are stable for many hours in cortical slice cultures.* J Neurosci, 2004. **24**: p. 5216-5229.

251. Sadeh, S. and C. Clopath, *Inhibitory stabilization and cortical computation.* Nature Reviews Neuroscience, 2021. **22**(1): p. 21-37.

252. Goto, A., et al., *Stepwise synaptic plasticity events drive the early phase of memory consolidation.* Science, 2021. **374**(6569): p. 857-863.

253. Ji, D. and M.A. Wilson, *Coordinated memory replay in the visual cortex and hippocampus during sleep.* Nat Neurosci, 2007. **10**(1): p. 100-107.

254. Euston, D.R., M. Tatsuno, and B.L. McNaughton, *Fast-Forward Playback of Recent Memory Sequences in Prefrontal Cortex During Sleep.* Science, 2007. **318**(5853): p. 1147-1150.

255. Dave, A.S. and D. Margoliash, *Song replay during sleep and computational rules for sensorimotor learning.* Science., 2000. **290**: p. 812-816.

256. Hoffman, K.L. and B.L. McNaughton, *Coordinated reactivation of distributed memory traces in primate neocortex.* Science, 2002. **297**(5589): p. 2070-3.

257. Walker, M.P. and R. Stickgold, *Sleep, memory, and plasticity.* Annu Rev Psychol, 2006. **57**: p. 139-66.

258. Diba, K. and G. Buzsáki, *Forward and reverse hippocampal place-cell sequences during ripples.* Nat Neurosci, 2007. **10**(10): p. 1241-2.

259. Pfeiffer, B.E. and D.J. Foster, *Hippocampal place-cell sequences depict future paths to remembered goals.* Nature, 2013. **497**(7447): p. 74-79.

260. Káli, S. and P. Dayan, *Off-line replay maintains declarative memories in a model of hippocampal-neocortical interactions.* Nat Neurosci, 2004. **7**(3): p. 286-94.

261. Siapas, A.G. and M.A. Wilson, *Coordinated interactions between hippocampal ripples and cortical spindles during slow-wave sleep.* Neuron, 1998. **21**(5): p. 1123-8.

262. Hooks, B.M., *Dual-Channel Photostimulation for Independent Excitation of Two Populations.* Curr Protoc Neurosci, 2018. **85**(1): p. e52.

263. Stamatakis, A.M., et al., *Simultaneous Optogenetics and Cellular Resolution Calcium Imaging During Active Behavior Using a Miniaturized Microscope.* Frontiers in Neuroscience, 2018. **12**(496): p. 496.

264. Holmgren, C., et al., *Pyramidal cell communication within local networks in layer 2/3 of rat neocortex.* J Physiol, 2003. **551**(Pt 1): p. 139-53.

265. Friston, K., *A theory of cortical responses.* Philosophical Transactions of the Royal Society B: Biological Sciences, 2005. **360**(1456): p. 815-836.

266. Suri, R.E. and W. Schultz, *Temporal Difference Model Reproduces Anticipatory Neural Activity.* Neural Computation, 2001. **13**(4): p. 841-862.

267. Sutton, R.S. and A.G. Barto, *Toward a modern theory of adaptive networks: Expectation and prediction.* Psychological Review, 1981. **88**(2): p. 135-170.

268. Hawkins, J. and S. Blakeslee, *On intelligence*. 2004, New York: Time Books.

269. Rabinovich, R.J., D.D. Kato, and R.M. Bruno, *Learning enhances encoding of time and temporal surprise in mouse primary sensory cortex.* Nature Communications, 2022. **13**(1): p. 5504.

270. Zhou, S., et al., *Multiplexing working memory and time in the trajectories of neural networks.* Nature Human Behaviour, 2023.

Chapter 4: Novel Kv3.1b Allosteric Modulator Increases Parvalbumin Interneuron Excitability and Improves Cortical Circuit Function in Fragile X mice

Published as: Kourdougli, N., Suresh, A., **Liu, B.**, Juarez, P., Lin, A., Chung, D. T., Graven Sams, A., Gandal, M. J., Martínez-Cerdeño, V., Buonomano, D. V., Hall, B. J., Mombereau, C., & Portera-Cailliau, C. (2023). Improvement of sensory deficits in fragile X mice by increasing cortical interneuron activity after the critical period. *Neuron*

I was a collaborator in this study that was led by Dr. Nazim Kourdougli in the Portera-Cailliau lab at UCLA. My contributions to this work were the intracellular recordings used to test the efficacy of a novel Kv3.1b allosteric modulator on increasing parvalbumin interneuron excitability. The data is presented in Figure 8 and Supplementary Figure 13. The text has been appropriately modified to include just the relevant background/data to understand the justification for my contribution. The full version is published in Neuron.

4.1 Summary

Changes in the function of inhibitory interneurons (INs) during cortical development could contribute to the pathophysiology of neurodevelopmental disorders. Using all-optical in vivo approaches, we find that parvalbumin (PV) IN and their immature precursors are hypoactive and transiently decoupled from excitatory neurons in postnatal mouse somatosensory cortex (S1) of *Fmr1* KO mice, a model of Fragile X Syndrome (FXS). This leads to a loss of parvalbumin interneurons (PV-INs) in both mice and humans

with FXS. Increasing the activity of future PV-INs in neonatal *Fmr1* KO mice restores PV density and ameliorates transcriptional dysregulation in S1, but not circuit dysfunction. Critically, administering an allosteric modulator of Kv3.1 channels after the S1 critical period does rescue circuit dynamics and tactile defensiveness. Symptoms in FXS and related disorders could be mitigated by targeting PV-INs.

4.2 Introduction

Neurodevelopmental disorders (NDDs) arise due to changes in developmental trajectories of neurons during the early stages of circuit assembly in the brain. Although symptoms of NDDs, such as intellectual disability and autism, are first recognized in the toddler stage, circuit differences are likely present at birth and may begin even earlier.[1] From a therapeutic perspective identifying the earliest circuit changes in NDDs is critical because early interventions are more likely to redirect the trajectory of neural development before it is irreversibly changed as a consequence of genetic and/or environmental factors.

Differences in GABAergic inhibition and excitability have been implicated in the origins of NDDs and autism, and proposed as targets for therapy.[2–5] However, the prevalent notion that an imbalance in excitatory and inhibitory signaling is associated with NDDs is principally based on observations in adulthood. In the last decade, as our understanding of cortical development grew significantly, there has been increased awareness about the important developmental role of inhibitory interneurons (INs) in shaping neuronal circuits.[6,7] The typical density, function, and integration of INs into

cortical networks all depend on genetic and activity-dependent programs.[8] Deviations from the usual trajectory of these developmental programs in NDDs could have an impact on functional circuit assembly.[4,5] For example, hypofunction of cortical INs has been described in multiple models of autism and other psychiatric conditions,[4,9–11] but the nature of GABAergic population dynamics throughout neonatal development in NDDs remains an unexplored territory. To investigate this, we focused on Fragile X Syndrome (FXS) because it is the most common single gene cause of intellectual disability and autism,[12] and because hypoactivity of fast-spiking PV-INs has been observed repeatedly in *Fmr1* knockout mice (*Fmr1* KO, referring to both male *Fmr1*$^{-/y}$ and females *Fmr1*$^{-/-}$ mice) the principal animal model of FXS.[13–16]

In this study, we examined the developmental origins of PV-IN hypoactivity in L2/3 of S1 in vivo because we previously identified early postnatal circuit changes in *Fmr1* mice (excessive network synchrony and reduced adaptation to repetitive tactile stimulation) that could be associated with reduced PV-IN activity.[19,20] We show that PV-INs and their immature counterparts from the medial ganglionic eminence (MGE), which express the transcription factor Nkx2.1, are hypoactive in S1 as early as postnatal day (P) 6 and fail to modulate excitatory neurons in *Fmr1* mice before P15. Interestingly, an early chemogenetic intervention to increase Nkx2.1-IN firing in *Fmr1* KO mice at P5-P9 failed to restore circuit dysfunction despite partially correcting the FXS S1 transcriptome, whereas a delayed intervention at P15-P20 (post S1 critical period) was more successful. Finally, boosting PV-IN activity more globally with a Kv3.1 channel modulator at P15-P20 significantly improved both circuit and behavioral sensory phenotypes of *Fmr1* KO mice. Thus, circuit changes in FXS (and perhaps in other NDDs) can be reversed by targeting

PV-INs, but the timing of circuit interventions may be critical.

4.3 Results

4.3.1 Reduced activity of cortical PV- INs and MGE-derived INs in early postnatal Fmr1 KO mice

Several in vivo studies have shown that the activity of cortical PV-INs is reduced in adult *Fmr1* KO mice.[14,21] Moreover, we previously discovered pronounced circuit changes in S1 during the critical period at P14-P16 that could be due to reduced inhibition, including fewer whisker-responsive excitatory pyramidal (Pyr) neurons and lack of neuronal adaptation to repeated stimulation. To assess whether PV-INs were also hypoactive in S1 earlier in development, we used in vivo two-photon calcium imaging at P15 to record from them in S1 of PV-Cre;WT or *Fmr1* KO mice injected with AAV1-CAG-Flex-GCaMP6s at P10 (Fig 1A-C). This approach led to GCaMP6s expression in ~80% of PV-INs in L2/3 of the transfected region (Fig. S1A,B). We found that both spontaneous and whisker-evoked activity of PV-INs were significantly reduced by ~35% in *Fmr1* KO mice (n=7) compared to WT mice (n=6) (Fig. 1D-F). The percentage of PV-INs that were spontaneously active was also significantly reduced (Fig. 1E), though the percentage of whisker-responsive PV-INs was not different from controls (Fig. 1F).

During the period that spans from the establishment of barrels to the closure of S1 critical period, GABAergic assemblies display synchronous dynamics that help shape developing circuits.[25,26] We next investigated whether differences in MGE-IN activity during the first postnatal week contributes to previously reported signs of early cortical

circuit dysfunction.[19,27,28]Cortical PV-INs do not express PVALB before P10,[24,29,30] but their immature precursors from the MGE can be identified through their expression of the transcription factor *Nkx2.1*. We used in vivo calcium imaging to record from MGE-INs at P6 in Nkx2.1-Cre mice injected with AAV1-CAG-Flex-GCaMP6s into S1 at P1 (Fig. 1G-I), which led to 43% of Nkx2.1-INs expressing the indicator in the transfected region (Fig. S1C,D); a small fraction of Nkx2.1-INs also express SST at P6 (Fig. S1E-H). Early cortical network activity is dominated by large and infrequent synchronous network events that propagate as waves.[31-32] We confirmed that MGE-INs participated in synchronous cortical activity, as previously reported.[33] However, we found a significantly lower proportion of active Nkx2.1-INs and a lower frequency of synchronous MGE-IN network events in *Fmr1* KO mice (n=8) compared to WT controls (n=9), even though the amplitude of these events was similar (Fig. 1J-L). Hence, Nkx2.1-INs (which give rise to PV- and SST-INs) are hypoactive at P6 and less likely to participate in synchronous network activity.

4.3.2 Future PV-INs within the Nkx2.1-IN population fail to modulate Pyr cells in neonatal Fmr1 KO mice

The hypoactivity of Nkx2.1-INs could account for the previously reported hypersynchrony and hyperactivity of Pyr neurons in early postnatal *Fmr1* KO mice.[19,27,28] Indeed, the maturation of cortical networks depends on the proper integration and function of GABAergic INs[7,34] and co-activation of MGE-INs and Pyr cells during the first postnatal week is thought to restrict the spread of spontaneous synchronous network events.[33,35] However, even though GABAergic perisomatic axons are observed in the first

postnatal days, functional synaptic inhibition in S1 does not emerge until P8-10.[36,37] Because fast-spiking INs in S1 of *Fmr1* KO mice seem significantly immature relative to those in WT controls,[15] we sought to determine whether or not Nkx2.1-INs in developing *Fmr1* KO mice are properly integrated into the S1 network. We used an all-optical two-photon optogenetic approach in vivo[38,39] to specifically increase the firing of putative future PV-INs within this population, since SST-INs are not hypoactive at P15 (Fig. S2). Taken together, these optogenetic results showed that putative future PV-INs in *Fmr1* KO mice at P10 are functionally decoupled from Pyr cells and fail to properly modulate network activity.

4.3.3 Post critical period, but not neonatal, chemogenetic activation of Nkx2.1-INs partially rescues S1 circuit deficits in Fmr1 KO mice

Several aspects of cortical maturation are known to be transiently delayed in Fmr1 KO mice, but eventually catch up to WT levels.[19,67,68] Knowing that PV-INs are capable of modulating Pyr cells in Fmr1 KO mice by P15, we tested the effect of chronic chemogenetic activation of Nkx2.1-INs from P15 to 20 on S1 circuit deficits (Fig. 7E). Post critical period DREADD activation of Nkx2.1-INs significantly increased the proportion of whisker-responsive neurons (Fig. 7F) and modestly increased their adaptation to repetitive whisker stimulation, though this did not reach significance (Fig. 7G). Similarly, using an acute chemogenetic approach at P15 but targeting PV-INs (instead of Nkx2.1-INs) in PV-Cre;Fmr1 KO mice at P15, we observed that a single dose of C21 also caused a significant increase in the percentage of whisker-responsive Pyr cells in the hM3Dq

group compared to vehicle injection, but no change to their adaptation (Fig. S12G-I). Altogether, these results suggest that by the end of second postnatal week, putative future PV-INs within the Nkx2.1 population in Fmr1 KO mice are finally functionally integrated in S1 and that boosting their firing at this age (but not earlier) can lessen whisker-evoked circuit deficits.

4.3.4 Boosting PV-IN activity using a Kv3.1 modulator ameliorates S1 circuit deficits and tactile defensiveness in juvenile Fmr1 KO mice

Our chronic chemogenetic activation of Nkx2.1-INs from P15 to P20 only partially restored S1 circuit dysfunction in *Fmr1* KO mice. One possibility is that, because the local viral injection only infects a subset of our targeted neurons (Fig. S8A,B), we could not drive the activity of a sufficient number of Nkx2.1-INs with DREADDs. We therefore tested a chronic pharmacologic approach to achieve a more global and longer-lasting increase of PV cell activity in *Fmr1* KO mice after the critical period. After ~P10, cortical PV-INs assume their fast-spiking characteristics due to their expression of Kv3.1b channels. This subclass of voltage-gated potassium channels, responsible for rapid repolarization that enables their fast-spiking behavior, is almost exclusively expressed in PV-INs.[69,70] We reasoned that targeting Kv3.1b channels pharmacologically could be used to modulate the firing of PV-INs as a potential treatment for various NDDs. We used the compound AG00563 (1-(4-methylbenzene-1-sulfonyl)-N-[(1,3-oxazol-2-yl)methyl]-1H-pyrrole-3-carboxamide), a Kv3.1 positive allosteric modulator (Fig. 8A). Patch-clamp recordings of identified PV-INs in acute slices from P14-P16 PV-Cre;tdTom*;Fmr1* KO mice (see

Methods), showed that bath application of AG00563 (10 µM) significantly increased their excitability (Fig. 8B,C). Of note, AG000563 did not affect the membrane potential or excitability of Pyr cells, nor the input resistance of PV-INs or Pyr cells (Fig. S13A-E).

Using in vivo calcium imaging, we found that acute administration of AG00563 (3 mg/kg, s.c.) at P15 significantly increased the fraction of whisker-responsive Pyr cells but did not change their adaptation index (Fig. S13F-H), which matches our results with acute excitatory DREADDs in PV-INs (Fig. S12G-I). We next administered AG00563 (or vehicle) chronically (3 mg/kg, s.c., twice daily) to *Fmr1* KO mice from P15 to P20, and then performed calcium imaging the following day (Fig. 8D,E). We found that compared to vehicle controls (n=11 mice) the proportion of whisker-responsive Pyr cells in S1 was significantly higher in AG00563-treated mice (n=13 mice) (Fig. 8F), reaching near WT levels.[20] Moreover, the adaptation index of Pyr cells was also significantly increased by AG00563 (Fig. 8G).

The absence of neuronal adaptation in certain brain circuits is one potential reason why children with NDDs/autism exhibit sensory hypersensitivity, because they are unable to 'tune out' non-threatening or non-salient stimuli.[71] We used a tactile defensiveness assay based on repetitive whisker stimulation[20] (see Methods; Fig. 8H) to test whether AG006563 might lessen the maladaptive avoidance/defensive behaviors previously observed in *Fmr1* KO mice. We found that mice chronically treated with AG00563 from P15 to P20 manifested significantly less grabbing of the stimulator than vehicle-treated *Fmr1* KO controls, and they also spent more time demonstrating healthy adaptive behaviors, such as grooming (Fig. 8I). Overall, more AG00563-treated juvenile *Fmr1* KO mice displayed grooming and fewer showed grabbing during whisker stimulation, while

the opposite was true in vehicle-treated *Fmr1* KO mice (Fig. S13I). To determine whether this pharmacologic approach could also be beneficial in older animals, we also treated young adult *Fmr1* KO mice with AG00563 (from P45 to P50) and found a significant reduction in the proportion of time spent grabbing the stimulator (Fig. 8J). Therefore, chronic pharmacological activation of PV-INs any time after P15 can ameliorate S1 sensory circuit deficits and rescue behavioral manifestations of tactile defensiveness in *Fmr1* KO mice.

4.4 Discussion

We set out to identify when IN hypofunction first begins in *Fmr1* KO mice to better understand how developmental trajectories of cortical circuits are changed in FXS and in other NDDs that share a cortical IN hypofunction phenotype.[4] We used an intersectional strategy to express chemo- and optogenetic tools to manipulate Nkx2.1-INs, as well as in vivo calcium imaging to record from them and their excitatory Pyr cell partners. We discovered that: 1. PV-INs and their immature precursors from the MGE in *Fmr1* KO mice are hypoactive as early as P6 and functionally decoupled from Pyr cells in S1 cortical circuits. Boosting PV-IN activity after the S1 critical period (P15-P20) does restore network activity in S1, especially when using a Kv3.1 allosteric modulator, which also ameliorated tactile defensiveness in *Fmr1* KO mice.

4.4.1 Critical developmental role of Nkx2.1-INs in sensory circuits in FXS

GABAergic INs govern crucial steps in the maturation of brain circuits and have been hypothesized to play a key role in NDDs.[4,5] We confirm previous observations that, during the early postnatal period, spontaneous Pyr cell activity is hypersynchronous in *Fmr1* KO mice.[19,28] Additionally, we now demonstrate that Nkx2.1-INs are hypoactive in neonatal *Fmr1* KO mice during a time that coincides with the emergence of perisomatic GABAergic inhibition onto Pyr cells.[37] Considering the emerging knowledge about IN-Pyr connectivity in neonatal cortex,[23,72] this hypoactivity likely has drastic consequences for both structural and functional connectivity,[73] and sensory processing. Inhibition is likely necessary for the desynchronization of network activity at around P12.[31] Indeed, our all-optical two-photon optogenetic approach demonstrated that activation of Nkx2.1-INs can drive the decorrelation of Pyr cells in WT mice at P10 (**Fig. 2F**). The previously reported developmental delay in this desynchronization in *Fmr1* KO mice[19,28] is probably due to the fact that Nkx2.1-INs are hypoactive and functionally decoupled from Pyr cells. Thus, early changes in cortical connectivity could have profound effects on the developmental trajectory of PV-INs.

4.4.2 Why did chronic chemogenetic activation of Nkx2.1-INs at P5-P9 fail to fully rescue S1 circuit dynamics in Fmr1 KO mice

One of our most striking observations was that raising the excitability of INs in neonatal *Fmr1* KO mice was not sufficient to restore sensory-evoked network function in S1. Our data provide strong evidence that the reason is that MGE-INs are decoupled from

their Pyr cell partners during neonatal development (**Fig. 2**). This could reflect changes in INs themselves (e.g., a delay in synaptogenesis) or in post-synaptic Pyr cells (e.g., changes in post-synaptic GABA receptor expression). We also find that eventually PV-IN → Pyr cell connectivity is established (Fig. S12), which is consistent with the known delayed maturation PV-INs in *Fmr1* KO mice.[15,18] This likely explains why we could restore circuit dynamics in S1 and ameliorate sensory avoidance behaviors in *Fmr1* KO mice by boosting PV-IN firing after P15, but not earlier.

4.4.3 Implications for treatment of FXS

Because symptoms of NDDs are first recognized in toddlers, it is generally understood that they arise because of changes in the brain that likely occur in utero. This makes sense for FXS because expression of FMRP in the brain starts prenatally, so its absence could change the typical developmental trajectory of brain maturation in the third trimester of gestation or earlier. Therapeutic interventions for intellectual disability or autism that begin at the earliest stages of brain development should therefore be the most effective.[84,85] However, we found that increasing the activity of Nkx2.1-INs in neonatal mice did not fully rescue *Fmr1* KO circuit phenotypes in S1, whereas increasing PV-IN firing after P15 did and also mitigated tactile defensiveness. This offers hope in FXS, because it means that interventions to boost IN activity need not start at birth (this may not be in fact desirable), but could be efficacious if started in childhood, adolescence, or even adulthood.[14] Atypical sensory perception is present in toddlers with FXS and other NDDs and is believed to contribute to social communication differences, repetitive

behaviors and learning disability in adulthood.[86,87] Our encouraging preclinical results with the Kv3.1 activator AG00563 suggest that increasing activity of PV-INs is a plausible strategy to lessen certain symptoms in children and adults with NDDs.

4.5 Materials and Methods

Brain slice electrophysiology

PV-Cre_Ai14_Fmr1_KO mice at P15 were deeply anesthetized using 5% isoflurane prior to decapitation and 400 µm-thick coronal slices were prepared with a vibratome (Leica VT1200S, Germany). Slices were prepared in ice-cold oxygenated (95% O_2 and 5% CO_2) modified artificial cerebrospinal fluid (ACSF) containing (in mM): 92 NMDG, 5 Na^+-ascorbate, 3 Na^+-Pyruvate 2.5 KCl, 10 $MgSO_4$, 2 $CaCl_2$, 1.2 Na2HPO_4, 24 $NaHCO_3$, 5 HEPES, 25 Glucose. Slices were then left to recover in the modified ACSF at ~33°C for 30 min before being transferred to oxygenated regular ACSF at room temperature (RT) for storage for at least 1 h prior to recording. Recordings were made at 32-33°C in oxygenated ACSF containing (in mM) 124 NaCl, 2.5 KCl, 2 $MgSO_4$, 2 $CaCl_2$, 1.2 Na2HPO_4, 24 $NaHCO_3$, 5 HEPES, 13 Glucose, and the perfusion rate was set to 5 mL/min. Whole-cell patch-clamp recordings were performed in cortical L2/3 PV-Cre-tdTom$^+$ cells. Recordings relied on fluorescence visualization using a Zeiss AxioSKOp FS+ microscope and additional verification by their intrinsic electrophysiological properties. For current-clamp recordings, the intracellular solution consisted of (in mM) 100 K-gluconate, 20 KCl, 4 ATP-Mg, 10 phosphocreatine, 0.3 GTP-Na, 10 HEPES (adjusted to pH 7.3 and 300 mOsm). Intrinsic excitability was measured as the number of

action potentials evoked during a 250 ms current step at intensities of 0.05, 0.1, 0.15, 0.2, 0.25, 0.3, 0.35, 0.4, 0.45, 0.5 nA. Wash-on of AG00563 (10 µM) was performed at 32-33°C for a minimum of 5 min before assessing PV-IN intrinsic excitability. Series resistance was monitored, and recordings were discarded if series resistance changed by more than 15%, or if apparent loss of current clamp control occurred as reflected by a sudden change in the recording stability.

4.6 Figures

Figure 1

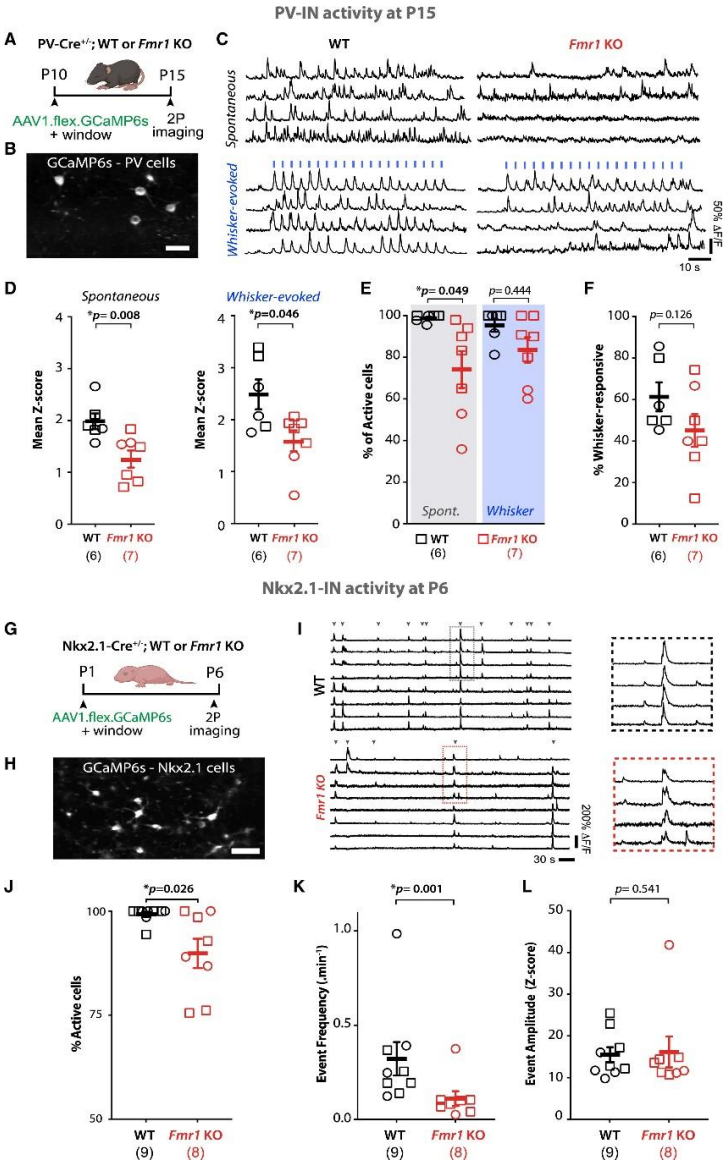

PV-INs and their MGE-derived immature INs are hypoactive in S1 of developing Fmr1 KO mice. A. Cartoon of experimental design. **B.** Example field of view of PV-INs expressing AAV1-flex-GCaMP6s in S1 cortex of PV-Cre mice (scale=25um). **C.** Representative traces of PV-IN calcium transients in WT and Fmr1 KO mice. Whisker stimulation (blue bars, 1s at 10 Hz, 3 s I.S.I). **D.** Mean Z-scores of PV-INs at P15 are significantly lower in Fmr1 KO than in WT mice. In panels D-F and J-L, symbols represent individual mice (sample size in parenthesis, females=circles, males=squares. (spontaneous: 1.98±0.15 for WT vs. 1.28±0.17 for Fmr1 KO; whisker-evoked: 2.49±0.29 for WT vs. 1.61±0.21 for Fmr1 KO, respectively; p=0.008 and p=0.046, M-W t-test, n=6 WT and n=7 Fmr1 KO mice). **E.** Percentage of active PV-INs in WT and Fmr1 KO mice (spontaneous: 98.9±0.8% for WT vs. 74.2±8.9% for Fmr1 KO; p=0.049, whisker-evoked: 95.5±3.2% for WT vs. 83.6±6.1% for Fmr1 KO, p=0.444, M-W t-test). **F.** Percentage of stimulus-locked PV-INs (61.4±6.9% for WT vs. 45.2±7.9% for Fmr1 KO; p=0.126, M-W t-test). **G.** Experimental design for in vivo recordings at P6. **H.** Example field of view of Nkx2.1-INs expressing AAV1-flex-GcaMP6s in S1 cortex Nkx2.1-Cre mice (scale =25um). **I.** Example calcium traces of Nkx2.1-INs in WT and Fmr1 KO mice. Inset shows expanded traces for representative synchronous network events. **J.** The percentage of active Nkx2.1-INs at P6 was significantly lower in Fmr1 KO mice than in WT controls. (99.2±0.6% for WT and 89.8±3.5% for Fmr1 KO, n=9 and 8, respectively; p=0.026, MW t-test). **K.** The frequency of synchronous network events for Nkx2.1-INs was significantly lower in Fmr1 KO mice. (0.32±0.09 events per min for WT vs. 0.11±0.04 for Fmr1 KO, n=9 WT and n=8 Fmr1 KO, p=1.4x10-3, MW t-test). **L.** The amplitude of calcium transient events of Nkx2.1-INs was not different between genotypes (15.5±1.8 for WT vs. 16.2±3.7 for Fmr1 KO, p=0.541, MW t-test).

Figure 2

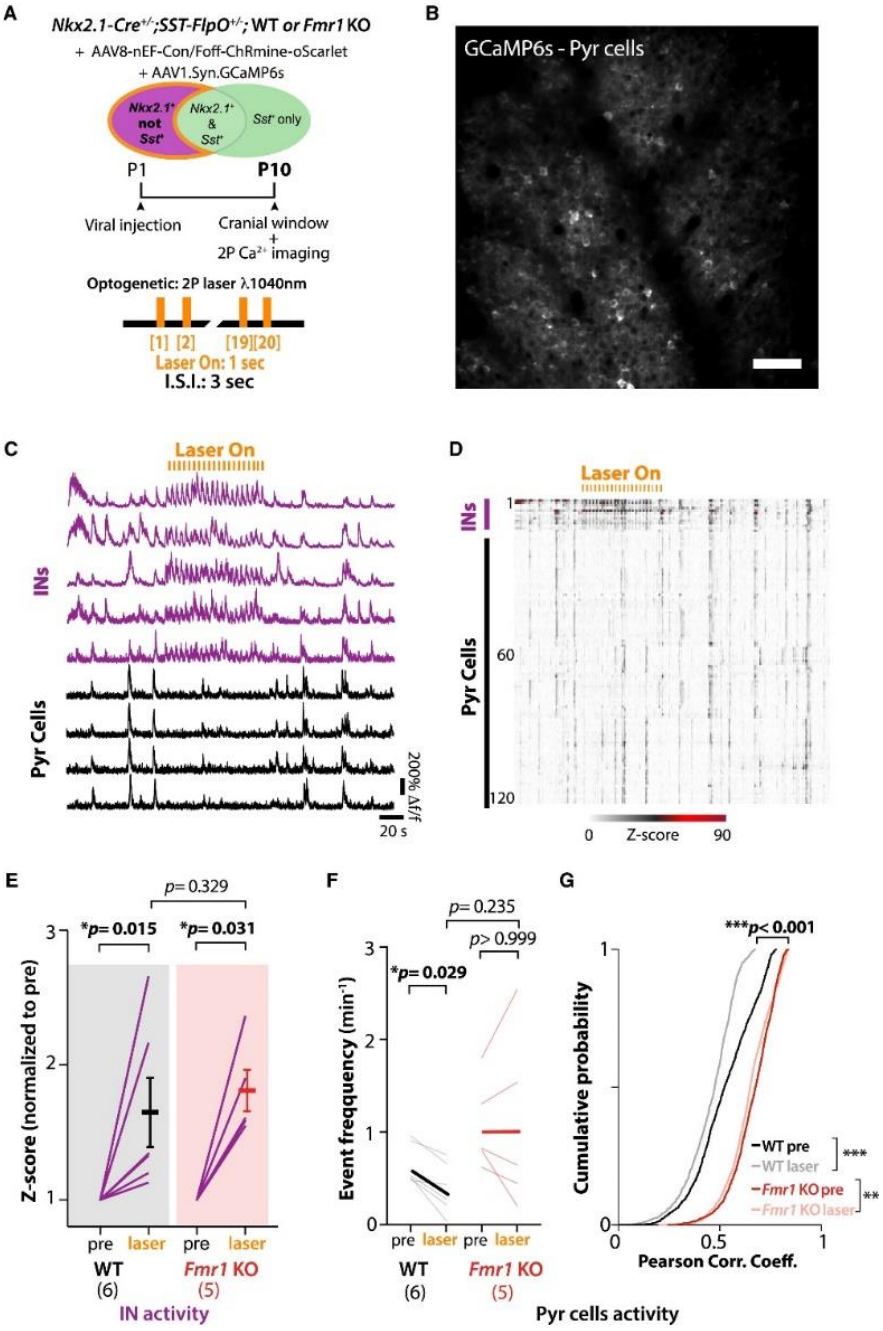

Nkx2.1-INs form a weak functional network with Pyr cells in neonatal Fmr1 KO mice. A. Experimental design for optogenetic experiments. **B.** Example field of view of Pyr cells expressing GCaMP6s in Nkx2.1-Cre;SST-FlpO mice at P10. **C.** Representative calcium traces for 5 presumed Nkx2.1+/Sst--INs (magenta) and 4 Pyr cells (black). **D.** Raster plot of neuronal activity in a representative WT mouse. **E.** Mean z-score of activity in Nkx2.1+/SST--INs before (pre) and during optogenetic stimulation (laser). Each line represents an individual mouse (mean normalized z-score increased by 63.7%±25.5 for WT, p=0.015, and 79.9%±15.3, p=0.031, for Fmr1 KO mice upon laser-on stimulation; Wilcoxon matched-pairs signed rank test; n=6 and 5, respectively). **F.** Mean frequency of Pyr cell calcium transients was significantly lower during optogenetic stimulation in WT mice but was unchanged in Fmr1 KO mice. (0.63±0.09 events.min-1 pre vs. 0.38±0.11 with laser; p=0.029 in WT; 1.06±0.21 events.min-1 pre vs. 1.06±0.43 with laser for Fmr1 KO, p> 0.99; two-way ANOVA, post-hoc Tukey). **G.** Pair-wise correlation coefficients of Pyr cells were significantly modulated by optogenetic stimulation in both WT and Fmr1 KO mice but the magnitude of the effect was greater in WT (mean Corr. Coeff. WT: 0.52±0.0035 for pre vs. 0.45±0.0044 for laser; p=2.2x10-16; Fmr1 KO: 0.66±0.0024 for pre vs. 0.64±0.0025 for laser, p=3.3x10-9; and p<0.001 for WT pre vs. Fmr1 KO pre; Kolmogorov-Smirnov test).

Figure 7

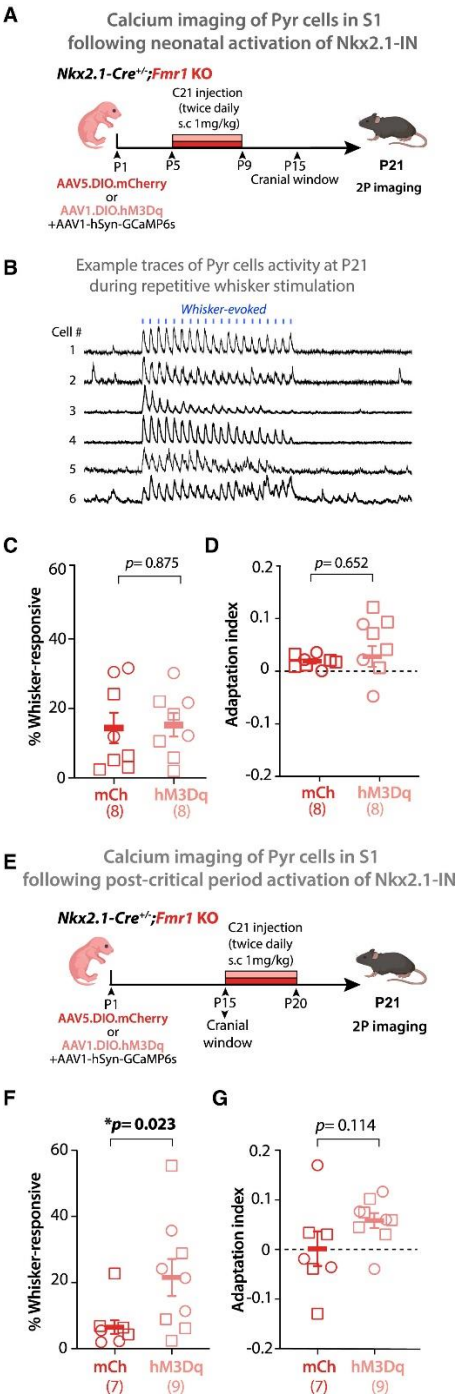

Post-critical period but not neonatal chronic chemogenetic activation of Nkx2.1-INs improves S1 circuit deficits. A. Experimental design for chronic chemogenetic activation of Nkx2.1-INs in neonatal Fmr1 KO mice from P5 to P9 to assess circuit deficits using in vivo two-photon calcium imaging at P21. **B.** The proportion of whisker-responsive Pyr cells was not changed by DREADDs in Fmr1 KO mice. (14.4±4.4% vs. 15.3±3.3%, p=0.875, unpaired t-test). **C.** The neuronal adaptation index of Pyr cells to repetitive whisker stimulation was not changed by chemogenetics (0.02±0.004 for Fmr1 KO mCherry vs. 0.03±0.01 for Fmr1 KO; p=0.652, unpaired t-test). **D.** Experimental design for chronic chemogenetic activation of Nkx2.1-INs in juvenile (post-critical period) Fmr1 KO mice. **E.** The proportion of whisker-responsive Pyr cells was significantly changed by DREADDs in Fmr1 KO mice. (10.4±3.35% vs. 21.6±6.37%, p=0.0229, MW t-test) **F.** The neuronal adaptation index of Pyr cells to repetitive whisker stimulation was ~340% higher in the Fmr1 KO-hM3Dq group compared to Fmr1 KO-mCherry controls, though the difference was not significant (0.0016±0.03 for Fmr1 KO-mCherry vs. 0.058±0.015 for Fmr1 KO; p=0.114, MW test).

Figure 8

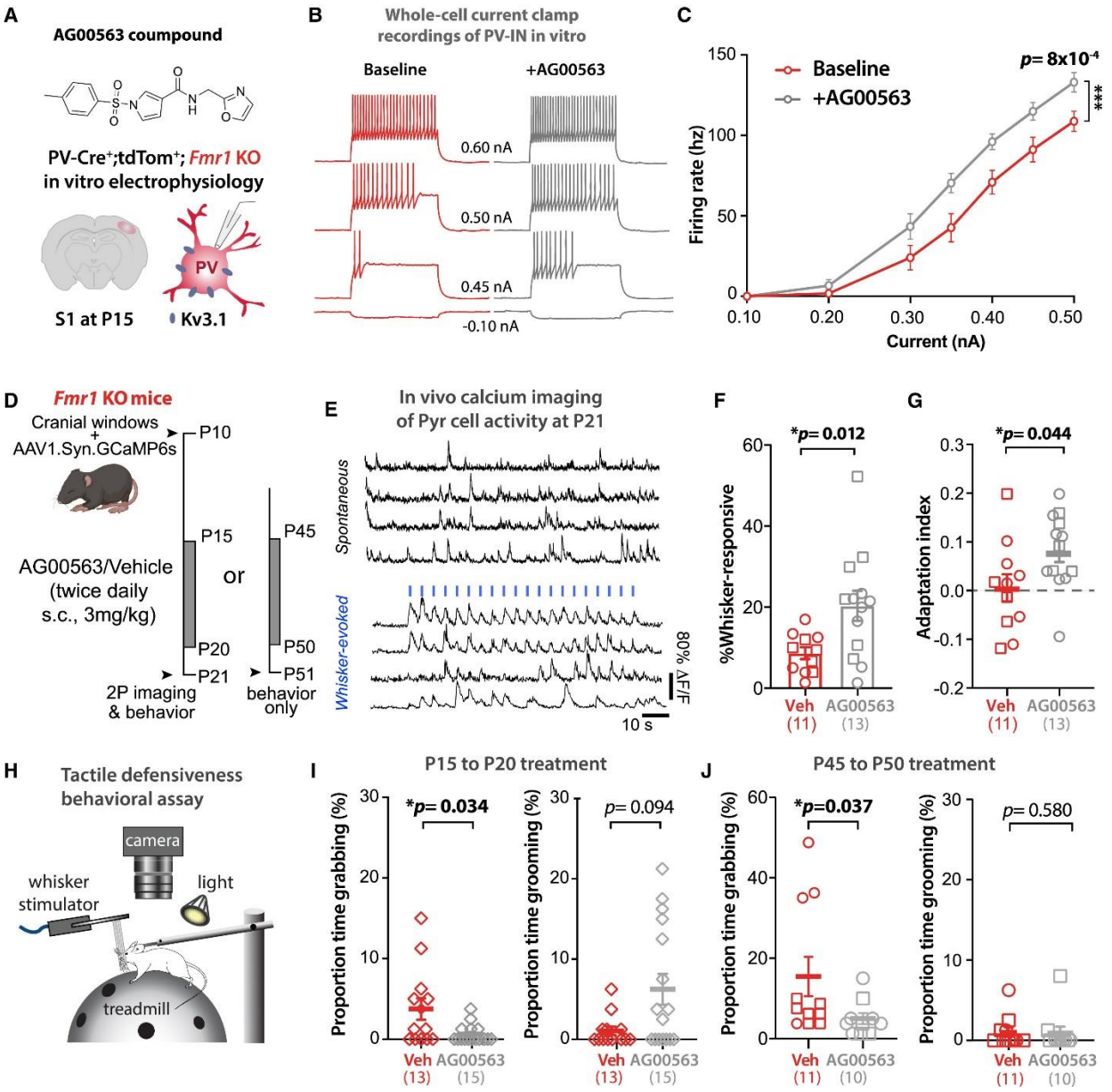

A Kv3.1 allosteric modulator, AG00563, ameliorates circuit function and tactile defensiveness in juvenile and young adult Fmr1 KO mice. A. Chemical structure of the AG00563 compound and experimental design for the in vitro patch-clamp recordings of PV-INs. **B.** Example traces of action potential trains evoked by 250 ms current injection in a PV-Cre-tdTom+ cell from a Fmr1 KO mouse at P15 in S1. **C.** Cumulative input-output curves during baseline (red) or AG00563 (gray) (n=15 cells from 6 PV-Cre;tdTom;Fmr1 KO mice, two-way RM ANOVA). **D.** Experimental design for chronic AG00563 vs. vehicle treatment (3 mg/kg, s.c, twice daily) from P15-20 or P45-50 in Fmr1 KO mice. **E.** Example traces of L2/3 Pyr cell calcium transients in Fmr1 KO mouse. Whisker stimulation (1 s at 10 Hz, 3 s I.S.I, blue bars). **F.** The percentage of whisker-responsive Pyr cells was significantly higher in Fmr1 KO mice treated with AG00563 than in vehicle controls. (20.3±3.7% vs. 8.7±1.5%, p=0.012; unpaired t-test, n=10 and 13 mice, respectively). **G.** The adaptation index of Pyr cells was also significantly higher in Fmr1 KO mice treated with AG00563- compared to vehicle controls. (0.01±0.03 vs. 0.08±0.03; p=0.0438; unpaired t-test). **H.** Cartoon of tactile defensiveness behavioral assay. **I.** Left: The proportion of time spent grabbing the stimulator was significantly lower in AG00563-treated mice than in vehicle controls (0.62%±0.28 s vs. 3.75%±1.33 s, p=0.0343, MW t-test, n=15 and 13 Fmr1 KO mice, respectively). Right: The proportion of time spent grooming was higher in AG00563-treated group, but not significant (6.25%±1.9 s vs. 1.06%±0.53 s, p=0.094, MW t-test). **J.** Left: The proportion of time spent grabbing the stimulator was significantly lower in AG00563-treated mice than in controls (5.0%±1.38 s vs. 15.45%±4.9 s, p=0.037, MW t-test, n=10 and 11 mice, respectively). Right: The proportion of time spent grooming (1.02%±0.57 s vs. 0.92%±0.79 s, p=0.58, MW t-test).

Supplementary Figure 13

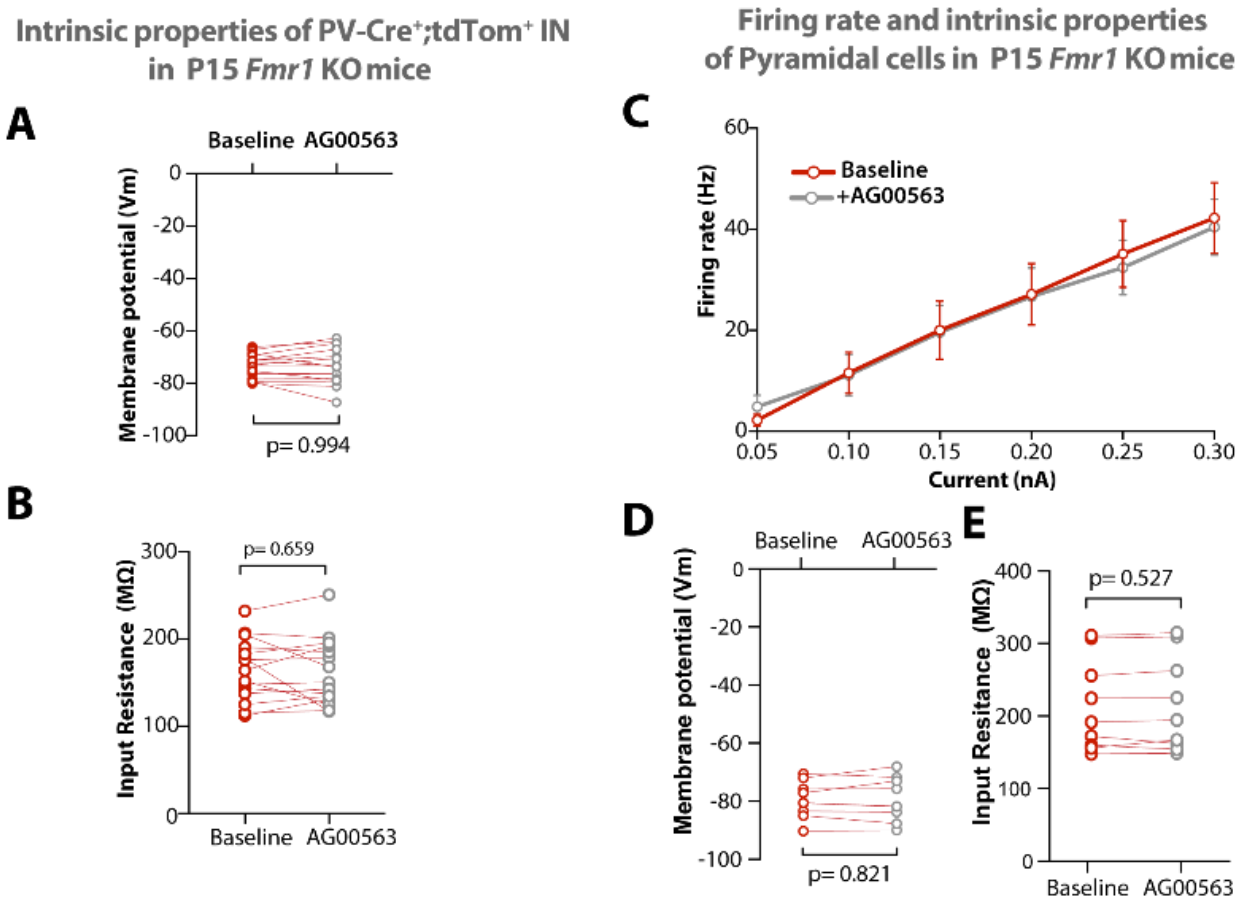

Intrinsic properties of PV-INs and Pyr cells are unchanged by AG00563 (Related to Fig. 8) **A.** Resting membrane potential (Vm) of PV-INs is unchanged by bath application of AG00563 during current clamp recordings of PV-tdTom+ cells (-73.4± 1.2 mV vs. -73.2± 1.8 mV, p= 0.805, paired t-test, n=15 cells from 6 Fmr1 KO mice at P15-16). **B.** Input resistance (Rm) of PV-INs is unchanged by AG00563 (164.6± 9.2 MΩ vs. 161.2± 10.1 MΩ, p= 0.608, paired t-test). **C.** Cumulative input-output curves during baseline (red) or bath application of AG00563 (gray) (n=9 Pyr cells from 6 PV-Cre;tdTom+/-;Fmr1 KO mice, two-way RM ANOVA). **D.** Vm of Pyr cells is unchanged by AG00563 (-79.5± 2.1 mV vs -79.3± 2.5 mV, p=0.805, paired t-test). **E.** Rm of Pyr cells is unchanged by AG00563 (214.0± 21.4 MΩ vs. 215.4± 22.0 MΩ, p=0.608, paired t-test). **F.** Experimental design for the acute administration of AG00563 (3 mg/kg, s.c.) and calcium imaging at P15, before and 30 min after injection. **G.** The percentage of whisker-responsive Pyr cells in Fmr1 KO mice was significantly higher after AG00563 injection compared to baseline (17.1± 4.3% baseline vs. 21.9± 5.1% ~30-40 min after AG00563, p=0.033; paired t-test, n=8 mice). **H.** The neuronal adaptation index of Pyr cells was not changed by AG00563 (0.05± 0.01 baseline vs. 0.01± 0.03 after AG00563, p=0.033; paired t-test, n=8 mice). **I.** A smaller percentage of mice showed defensive behavior (grabbing) at least once during whisker stimulation in the AG00563-treated group than among vehicle controls (5/15 mice vs. 8/13, respectively). The opposite was true for adaptive healthy behavior (grooming) (9/15 mice vs. 5/13, respectively).

4.4 References Cited

1. Robertson, C.E., and Baron-Cohen, S. (2017). Sensory perception in autism. Nat Rev Neurosci *18*.

2. Rubenstein, J.L.R., and Merzenich, M.M. (2003). Model of autism: increased ratio of excitation/inhibition in key neural systems. Genes Brain Behav *2*, 255–267. 10.1034/j.1601-183x.2003.00037.x.

3. Contractor, A., and Klyachko, V.A. (2015). Altered neuronal and circuit excitability in Fragile X syndrome. Neuron *87*.

4. Contractor, A., Ethell, I.M., and Portera-Cailliau, C. (2021). Cortical interneurons in autism. Nat Neurosci *24*, 1648–1659. 10.1038/s41593-021-00967-6.

5. Marín, O. (2016). Developmental timing and critical windows for the treatment of psychiatric disorders. Nat. Medicine *22*, 1229–1238. 10.1038/nm.4225.

6. Dorrn, A.L., Yuan, K., Barker, A.J., Schreiner, C.E., and Froemke, R.C. (2010). Developmental sensory experience balances cortical excitation and inhibition. Nature *465*, 932–936. 10.1038/nature09119.

7. Fishell, G., and Kepecs, A. (2020). Interneuron Types as Attractors and Controllers. Annu Rev Neurosci *43*, 1–30. 10.1146/annurev-neuro-070918-050421.

8. Wamsley, B., and Fishell, G. (2017). Genetic and activity-dependent mechanisms underlying interneuron diversity. Nature Reviews Neuroscience *18*, 299–309. 10.1038/nrn.2017.30.

9. Salazar, R.F., Bertollini, C., Mutel, S., Roo, M., and Muller, D. (2018). Restoring wild-type-like CA1 network dynamics and behavior during adulthood in a mouse model of schizophrenia. Nat Neurosci *21*, 1–14. 10.1038/s41593-018-0225-y.

10. Chen, Q., Deister, C.A., Gao, X., Guo, B., Lynn-Jones, T., Chen, N., Wells, M.F., Liu, R., Goard, M.J., Feng, S., et al. (2020). Dysfunction of cortical GABAergic neurons leads to sensory hyper-reactivity in a Shank3 mouse model of ASD. Nat Neurosci *23*, 1–18. 10.1038/s41593-020-0598-6.

11. Marín, O. (2012). Interneuron dysfunction in psychiatric disorders. Nature Reviews Neuroscience *13*, 107–120. 10.1038/nrn3155.

12. Rifé, M., Badenas, C., Mallolas, J., Jiménez, L., Cervera, R., Maya, A., Glover, G., Rivera, F., and Milà, M. (2003). Incidence of fragile X in 5,000 consecutive newborn males. Genet. Test. *7*, 339–343. 10.1089/109065703322783725.

13. Antoine, M.W., Langberg, T., Schnepel, P., and Feldman, D.E. (2019). Increased Excitation-Inhibition Ratio Stabilizes Synapse and Circuit Excitability in Four Autism Mouse Models. Neuron *101*, 648-661.e4. 10.1016/j.neuron.2018.12.026.

14. Goel, A., Cantu, D.A., Guilfoyle, J., Chaudhari, G.R., Newadkar, A., Todisco, B., Alba, D., NAZIM, K., Schmitt, L.M., Pedapati, E., et al. (2018). Impaired perceptual learning in a mouse model of Fragile X syndrome is mediated by parvalbumin neuron dysfunction and is reversible. Nat Neurosci *21*, 1–14. 10.1038/s41593-018-0231-0.

18. Domanski, A.P.F., Booker, S.A., Wyllie, D.J.A., Isaac, J.T.R., and Kind, P.C. (2019). Cellular and synaptic phenotypes lead to disrupted information processing in Fmr1-KO mouse layer 4 barrel cortex. Nature Communications *10*, 4814–4818. 10.1038/s41467-019-12736-y.

19. Gonçalves, J.T., Anstey, J.E., Golshani, P., and Portera-Cailliau, C. (2013). Circuit level defects in the developing neocortex of Fragile X mice. Nat. Neurosci. *16*, 903–909. 10.1038/nn.3415.

20. He, C.X., Cantu, D.A., Mantri, S.S., Zeiger, W.A., Goel, A., and Portera-Cailliau, C. (2017). Tactile Defensiveness and Impaired Adaptation of Neuronal Activity in the Fmr1 Knock-Out Mouse Model of Autism. The J. Neurosci. *37*, 6475–6487. 10.1523/jneurosci.0651-17.2017.

21. Antoine, M.W., Schnepel, P., Langberg, T., and Feldman, D.E. (2018). Increased excitation-inhibition ratio stabilizes synapse and circuit excitability in four autism mouse models. 1–33. 10.1101/317693.

22. Tuncdemir, S.N., Wamsley, B., Stam, F.J., Osakada, F., Goulding, M., and Rudy, B. (2016). Early Somatostatin Interneuron Connectivity Mediates the Maturation of Deep Layer Cortical Circuits. Neuron *89*, 521–535. 10.1016/j.neuron.2015.11.020.

23. Marques-Smith, A., Lyngholm, D., Kaufmann, A.-K., Stacey, J.A., Hoerder-Suabedissen, A., Becker, E.B.E., and Wilson, M.C. (2016). A Transient Translaminar GABAergic Interneuron Circuit Connects Thalamocortical Recipient Layers in Neonatal Somatosensory Cortex. Neuron *89*, 536–549. 10.1016/j.neuron.2016.01.015.

24. Pouchelon, G., Dwivedi, D., Bollmann, Y., Agba, C.K., Xu, Q., Mirow, A.M.C., Kim, S., Qiu, Y., Sevier, E., Ritola, K.D., et al. (2021). The organization and development of cortical interneuron presynaptic circuits are area specific. CellReports *37*, 109993. 10.1016/j.celrep.2021.109993.

25. Mòdol, L., Bollmann, Y., Tressard, T., Baude, A., Che, A., Duan, Z.R.S., Babij, R., García, N.V.D.M., and Cossart, R. (2020). Assemblies of Perisomatic GABAergic Neurons in the Developing Barrel Cortex. Neuron *105*, 93-105.e4. 10.1016/j.neuron.2019.10.007.

26. Stern, E.A., Maravall, M., and Svoboda, K. (2001). Rapid development and plasticity of layer 2/3 maps in rat barrel cortex in vivo. Neuron *31*, 305–315. 10.1016/s0896-6273(01)00360-9.

27. Fata, G.L., Gärtner, A., Domínguez-Iturza, N., Dresselaers, T., Dawitz, J., Poorthuis, R.B., Averna, M., Himmelreich, U., Meredith, R.M., Achsel, T., et al. (2014). FMRP regulates multipolar to bipolar transition affecting neuronal migration and cortical circuitry. *17*, 1693–1700. 10.1038/nn.3870.

28. Cheyne, J.E., Zabouri, N., Baddeley, D., and Lohmann, C. (2019). Spontaneous Activity Patterns Are Altered in the Developing Visual Cortex of the Fmr1 Knockout Mouse. Front Neural Circuits *13*, 57. 10.3389/fncir.2019.00057.

30. Butt, S.J.B., Sousa, V.H., Fuccillo, M.V., Hjerling-Leffler, J., Miyoshi, G., Kimura, S., and Fishell, G. (2008). The requirement of Nkx2-1 in the temporal specification of cortical interneuron subtypes. Neuron *59*, 722–732. 10.1016/j.neuron.2008.07.031.

31. Rochefort, N.L., Garaschuk, O., Milos, R.-I., Narushima, M., Marandi, N., Pichler, B., Kovalchuk, Y., and Konnerth, A. (2009). Sparsification of neuronal activity in the visual cortex at eye-opening. Proceedings of the National Academy of Sciences *106*, 15049–15054. 10.1073/pnas.0907660106.

32. Golshani,Peyman, Gonçalves, and Tiago, J. (2009). Internally Mediated Developmental Desynchronization of Neocortical Network Activity. J. Neurosci. *29*, 10890–10899. 10.1523/jneurosci.2012-09.2009.

33. Duan, Z.R.S., Che, A., Chu, P., Mòdol, L., Bollmann, Y., Babij, R., Fetcho, R.N., Otsuka, T., Fuccillo, M.V., Liston, C., et al. (2020). GABAergic Restriction of Network Dynamics Regulates Interneuron Survival in the Developing Cortex. Neuron *105*, 75-92.e5. 10.1016/j.neuron.2019.10.008.

34. García, N.V.D.M., Karayannis, T., and Fishell, G. (2011). Neuronal activity is required for the development of specific cortical interneuron subtypes. Nature *472*, 351–355. 10.1038/nature09865.

36. Favuzzi, E., Marques-Smith, A., Deogracias, R., Winterflood, C.M., Sánchez-Aguilera, A., Maeso, P., Fernandes, C., and Ewers, H. (2017). Activity-Dependent Gating of Parvalbumin Interneuron Function by the Perineuronal Net Protein Brevican. Neuron *95*, 639-655.e10. 10.1016/j.neuron.2017.06.028.

37. Gour, A., Boergens, K.M., Heike, N., Hua, Y., Laserstein, P., Song, K., and Helmstaedter, M. (2021). Postnatal connectomic development of inhibition in mouse barrel cortex. Science *371*. 10.1126/science.abb4534.

38. Rickgauer, J.P., Deisseroth, K., and Tank, D.W. (2014). Simultaneous cellular-resolution optical perturbation and imaging of place cell firing fields. Nat. Neurosci. *17*, 1816–1824. 10.1038/nn.3866.

39. Packer, A.M., Russell, L.E., Dalgleish, H.W.P., and Häusser, M. (2015). Simultaneous all-optical manipulation and recording of neural circuit activity with cellular resolution in vivo. Nat Meth *12*, 140–146. 10.1038/nmeth.3217.

67. Cruz-Martín, A., Crespo, M., and Portera-Cailliau, C. (2010). Delayed stabilization of dendritic spines in fragile X mice. Journal of Neuroscience *30*, 7793–7803. 10.1523/jneurosci.0577-10.2010.

68. He, Q., Nomura, T., Xu, J., and Contractor, A. (2014). The Developmental Switch in GABA Polarity Is Delayed in Fragile X Mice. Journal of Neuroscience *34*, 446–450. 10.1523/jneurosci.4447-13.2014.

69. Du, J., Zhang, L., Weiser, M., Rudy, B., and McBain, C.J. (1996). Developmental expression and functional characterization of the potassium-channel subunit Kv3.1b in parvalbumin-containing interneurons of the rat hippocampus. J. Neurosci. *16*, 506–518. 10.1523/jneurosci.16-02-00506.1996.

70. Rudy, B., and McBain, C.J. (2001). Kv3 channels: voltage-gated K+ channels designed for high-frequency repetitive firing. Trends in Neurosciences *24*, 517–526. 10.1016/s0166-2236(00)01892-0.

71. Green, S.A., Hernandez, L., Tottenham, N., Krasileva, K., Bookheimer, S.Y., and Dapretto, M. (2015). Neurobiology of Sensory Overresponsivity in Youth With Autism Spectrum Disorders. JAMA Psychiatry *72*, 778–786. 10.1001/jamapsychiatry.2015.0737.

72. Anastasiades, P.G., Marques-Smith, A., Lyngholm, D., Lickiss, T., Raffiq, S., Kätzel, D., Miesenböck, G., and Butt, S.J.B. (2016). GABAergic interneurons form transient layer-specific circuits in early postnatal neocortex. Nature Communications *7*, 10584–13. 10.1038/ncomms10584.

84. Veenstra-VanderWeele, J., and Warren, Z. (2015). Intervention in the context of development: pathways toward new treatments. *40*, 225–237. 10.1038/npp.2014.232.

85. Robertson, C.E., and Baron-Cohen, S. (2017). Sensory perception in autism. Nat Rev Neurosci *18*.

86. Rogers, S.J., Hepburn, S., and Wehner, E. (2003). Parent reports of sensory symptoms in toddlers with autism and those with other developmental disorders. J Autism Dev Disord *33*, 631–642. 10.1023/b:jadd.0000006000.38991.a7.

87. Robertson, C.E., and Baron-Cohen, S. (2017). Sensory perception in autism. Nature Reviews Neuroscience *18*, 671–684. 10.1038/nrn.2017.112.

Chapter 5: Conclusions

In the current work, I examine how neocortical circuits learn by engaging various interacting forms of plasticity. First, Chapter 2 demonstrates the ability of cortical circuits *in vitro* to undergo experience-dependent reorganization and form functional subnetworks known as neuronal ensembles. Next, Chapter 3 reveals that isolated cortical circuits can learn different temporal intervals and generate timed predictions. Finally, Chapter 4 presents a pharmacological rescue strategy for neocortical circuit dysfunction *in vivo* in Fragile X mice. The major findings discussed in this dissertation support that: 1. neural mechanisms are in place to allow isolated neocortical microcircuits to autonomously learn the temporal structure of external stimuli and generate internal predictions, and 2. irregular development of neocortical circuitry, in disorders such as Fragile X Syndrome, can drive aberrant network dynamics that cause deficits in behavior, but be functionally rescued by interventions that selectively boost circuit function. In conclusion, though the principles linking the characteristics of cortical circuitry to the nature of cortical processing in normal and pathological conditions remain to be fully understood, this work advances our understanding of learning and temporal processing in neocortical microcircuits and provides inspiration for future work.

It is an exciting time to be a neuroscientist, and I eagerly await the advancements our field will achieve in the upcoming years.